Investigating the Function and Pharmacology of Human Induced Pluripotent Stem Cell-Derived Atrial Cardiomyocytes (hiPSC-aCMs)

by

Marvin Gozal Gunawan

B.Sc. (Hons.), Simon Fraser University, 2015

Thesis Submitted in Partial Fulfillment of the
Requirements for the Degree of
Master of Science

in the
Department of Biomedical Physiology and Kinesiology
Faculty of Science

SIMON FRASER UNIVERSITY
Summer 2019

Approval

Name:	**Marvin Gozal Gunawan**
Degree:	**Master of Science**
Title:	**Investigating the Function and Pharmacology of Human Induced Pluripotent Stem Cell-Derived Atrial Cardiomyocytes (hiPSC-aCMs)**
Examining Committee:	**Chair:** **Dawn Mackey** Associate Professor
	Glen F. Tibbits Senior Supervisor Professor
	Thomas Claydon Supervisor Associate Professor
	Zachary Laksman Supervisor Clinical Assistant Professor University of British Columbia
	Damon Poburko External Examiner Associate Professor
Date Defended/Approved:	April 30, 2019

Ethics Statement

The author, whose name appears on the title page of this work, has obtained, for the research described in this work, either:

a. human research ethics approval from the Simon Fraser University Office of Research Ethics

or

b. advance approval of the animal care protocol from the University Animal Care Committee of Simon Fraser University

or has conducted the research

c. as a co-investigator, collaborator, or research assistant in a research project approved in advance.

A copy of the approval letter has been filed with the Theses Office of the University Library at the time of submission of this thesis or project.

The original application for approval and letter of approval are filed with the relevant offices. Inquiries may be directed to those authorities.

Simon Fraser University Library
Burnaby, British Columbia, Canada

Update Spring 2016

Abstract

Atrial fibrillation (AF) is the most common form of cardiac arrhythmia that causes the irregular and uncoordinated contractions of the atrial chambers. Current first-line pharmacological treatments are limited in efficacy with side effects including ventricular proarrhythmia. Thus, it is imperative to find novel treatments for better management of the disease. However, current preclinical assays such as heterologous expression and animal models do not recapitulate the entirety of human cardiac physiology. As such, the ability to generate hiPSC-derived atrial-like CMs (hiPSC-aCMs) and ventricular-like CMs (hiPSC-vCMs) can provide a more robust physiological system to assess drug effects for AF treatment *in vitro*. The objective of this thesis is to develop a preclinical assay system using optical mapping technique and human induced pluripotent stem cells (hiPSCs). Here, I characterized the function of hiPSC-aCMs and demonstrated the sensitivity and specificity of the assay system in capturing the effects of atrial-selective compounds.

Keywords: induced pluripotent stem cells; pharmacology; atrial fibrillation; optical mapping; cardiac differentiation; drug screening

To my parents, my sister, my nephew, and my hun bun

Acknowledgements

This thesis would not have been possible without the support of many people. First, I would like to express my gratitude towards my senior supervisor Dr. Glen Tibbits. Dr. Tibbits has been a great mentor – teaching me not only about cardiac physiology, grantsmanship, and scientific rigour, but also about life. He has enabled me to develop my scientific acuity by granting the freedom in pursuing interesting but challenging questions, generously giving funding support, encouraging me to learn new techniques, and guiding me every step of the way.

I would like to extend my gratitude to my committee supervisors Dr. Zachary Laksman and Dr. Thomas Claydon. Dr. Laksman has provided funding support, and his knowledge in developmental biology and clinical expertise gave assistance to the atrial differentiation project and provided the guidance for the translational aspect of my thesis. Dr. Claydon supported in council throughout this thesis, offering his expertise in electrophysiology and cardiac physiology.

I would like to give a special thanks to Dr. Sanam Shaffaattalab. Her knowledge and work ethic has inspired me to pursue this field. In addition, her patience in mentorship allowed me to have learned so much from her. It was also a pleasure working with her on numerous research projects. Thank you so much for your great mentorship and above all a friend for all these years.

To my friend and colleague Sarabjit Sangha, thank you for all your hard work. It has been a pleasure working with you. We tackled on a large project together, and after conducting countless experiments and troubleshooting, we saw it to completion. Also, thank you for all the fun we had trying different foods and scotch whisky.

Next, I would like to thank Dr. Eric Lin for his engineering prowess. He built the optical mapping instrument that is key in many of our projects. I learned the foundations of photonics, fluorescence imaging, electronics, and rapid prototyping from Dr. Lin.

I am grateful for many colleagues who have contributed to my training and stimulating graduate degree. In particular, Dr. Alison Li for showing me the ropes at the beginning of my degree and for her friendship, Dr. Kaveh Rayani for the discussions about science and life as well as for the great haircuts, Haruyo Kashihara for her lab

management support, Dr. Patrick Shi for our collaboration in the zebrafish project and his friendship, and BaRun Kim for her moral support and friendship. I would also like to thank everyone at the Tibbits Lab and the Molecular Cardiac Physiology Group. It was great sharing the laboratory with you all.

Finally, I would like to thank the staff at the Department of Biomedical Physiology and Kinesiology: Maggie Yeung, Brittney Nurmi, and Clare Zheng, for their administrative assistance.

Table of Contents

List of Tables

List of Figures

List of Acronyms

4AP	4-aminopyridine
AAV	Adeno-associated virus
AF	Atrial fibrillation
AP	Action potential
APD	Action potential duration
AV node	Atrial ventricular node
CaT	Calcium transient
CaTD	Calcium transient duration
CCh	Carbachol
CICR	Calcium induced calcium release
CMs	Cardiomyocytes
CRISPR	Clustered regularly interspaced short palindromic repeats
cTnT	Cardiac troponin T
CV	Conduction velocity
DAD	Delayed-after depolarization
EAD	Early-after depolarization
EB	Embryoid body
EC coupling	Excitation-contraction coupling
ERP	Effective refractory period
FACS	Fluorescence-activated cell sorting
hERG	Human ether ago-go
hESC	Human embryonic stem cells
hESC-CMs	Human embryonic stem cell-derived cardiomyocytes
hiPSC	Human induced pluripotent stem cells
hiPSC-aCMs	Human induced pluripotent stem cell-derived atrial cardiomyocytes
hiPSC-vCMs	Human induced pluripotent stem cell-derived ventricular cardiomyocytes
LQTS	Long QT syndrome
LTCC	L-type calcium channel
MACS	Magnetic-activated cell sorting
MLC-2v	Myosin light chain – ventricular isoform
NCX	Sodium/calcium exchanger

OM	Optical mapping
RA	Retinoic acid
RyR	Ryanodine receptor
SERCA	Sarco/endoplasmic reticulum calcium ATPase
SK channel	Small conductance calcium activated potassium channel
SR	Sarcoplasmic reticulum
TdP	Torsade de Pointes
V_m	Membrane voltage

Chapter 1.
Introduction

Atrial fibrillation (AF) is a cardiac arrhythmia that causes the irregular and uncoordinated contractions of the atrial chambers. AF is associated with increased risk of stroke, and in the long term dementia, and congestive heart failure (Lloyd-Jones et al., 2004) . AF is the most common form of cardiac arrhythmia that affects about 2% of the general population, with a prevalence that is expected to increase by three-fold in the coming three decades (Magnani et al., 2011). Thus, this disease is quickly becoming a high financial and resource burden on the healthcare system. In Canada, in-hospital treatment of AF is estimated to be $5,000 CDN per patient bringing the total estimate cost (not accounting for comorbidity) to $815 million (O'Reilly et al., 2013). Therefore, finding more efficacious treatments are crucial in improving therapy for the better management of the disease and prognosis of patients. Current drug development is hampered by the potential for co-incidental ventricular proarrhythmia. This thesis project aimed to address the combined use of human induced pluripotent stem cell-derived cardiomyocytes (hiPSC) and optical mapping technology as a sophisticated approach in preclinical testing for potential AF drug candidates.

1.1. Overview of Cardiac Physiology

1.1.1. Electrophysiology – Action Potential Characteristics

The cardiac action potential (AP) refers to the change in membrane potential (V_m) produced by the sum of inward and outward ionic currents. The AP is typically described as having four phases. Phase 4 of the AP is the resting membrane potential that is driven mainly by I_{K1} and maintained at -80 to 90 mV. The cardiac AP is initiated in Phase 0 by rapid influx of Na^+ through the fast Na^+ channels ($Na_V1.5$) depolarizing the membrane potential to around +30 mV. The cells then exhibit a transient outward K^+ current (I_{to}) through opening of K^+ channels in Phase 1. Phase 2, referred to as the plateau phase, is produced by opening of L-type Ca channels (LTCCs, Cav1.2) which causes an inward depolarizing Ca^{2+} current that is in balance with the repolarizing outward K^+ currents. The plateau phase is also maintained by decreased I_{K1}. Phase 1

and Phase 2 combined gives the spike-and-dome morphology of the AP. In the repolarizing phase 3, the LTCCs are inactivated and strong K^+ efflux through both the slow component (I_{Ks}) and the rapid component (I_{Kr}) of the delayed rectifier currents produced by the transmembrane proteins K_vLQT1 and human ether ago go (hERG), respectively. The large efflux of K^+ returns the membrane potential to -90mV (phase 4).

The general properties of the AP, such as upstroke kinetics, are shared between cardiomyocytes from the atria and the ventricles. The main differences in AP properties between the cardiomyocyte subtypes are found in the expression of atrial-specific K^+ currents such as the ultra-rapid outward potassium current (I_{Kur}) and the G-protein-activated K^+ current (I_{KAch}). There are also other K^+ channels contributing to background current that are preferentially expressed in the atria such as the small conductance Ca^{2+} activated K^+ current (I_{SK}) and weak inward rectifying two-pore domain K^+ (K_{2P}) channels.

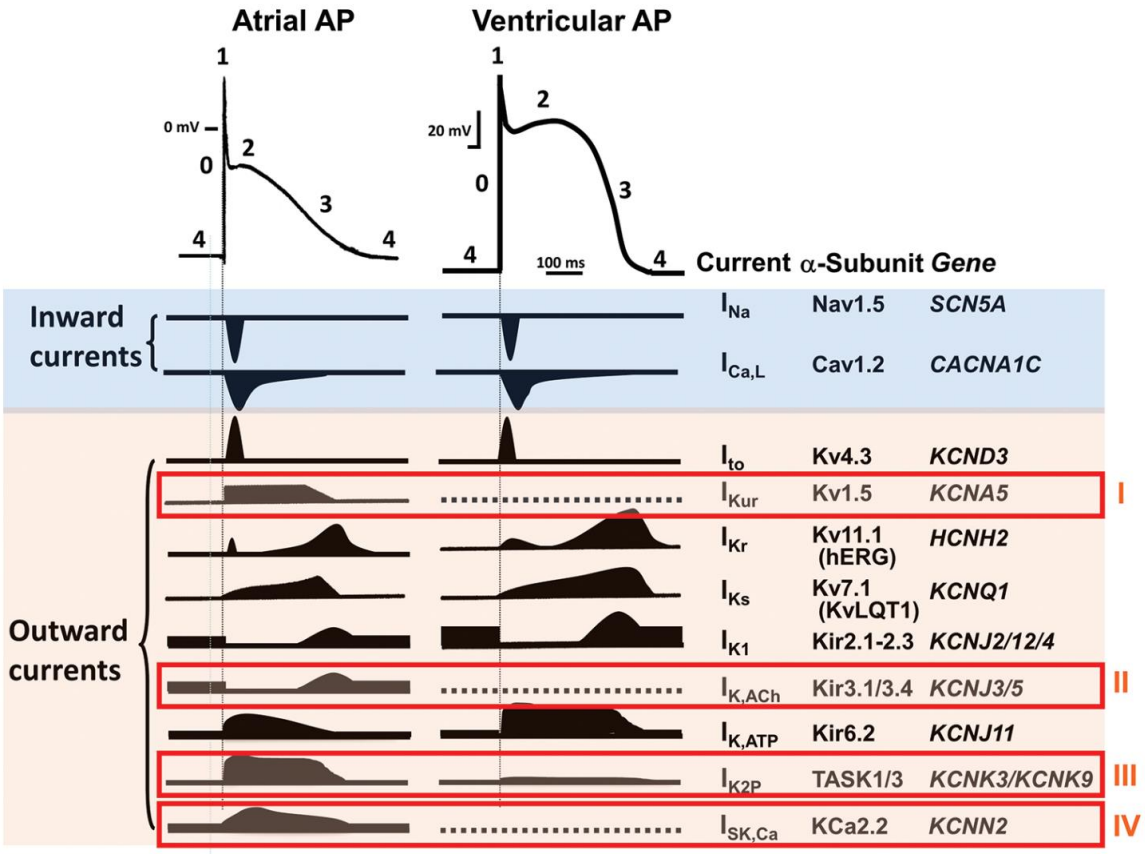

Figure 1.1. The action potential of human atrial and ventricular myocytes.
The currents present in atrial myocytes and absent in ventricular myocytes are highlighted in red boxes. Figure obtained from Ravens, 2017 and reproduced with permission.

The $K_v1.5$ channel encoded by the gene *KCNA5* produces the ultra-rapid K^+ current (I_{Kur}) (Fedida et al., 1993). $K_v1.5$ is predominantly found in the atrial chamber with minimal expression in the ventricular myocytes (Gaborit et al., 2007). $K_v1.5$ is activated before the LTCC, which explains why the plateau phase of the atrial AP occurs at a more negative potential than ventricular myocytes (Ravens, 2017). In addition to I_{to}, I_{Kur} is responsible for the rapid initial repolarization that contributes to the prominent notch of atrial AP morphology (Figure 1.1).

With parasympathetic activation, the neurotransmitter acetylcholine (ACh) is released resulting in multiple cardiac response including a decrease in pacemaker activity through cholinergic receptors (Campbell, S., & O'Shea, 1989). Acetylcholine affects the atrial cardiomyocytes through similar cholinergic receptors, shortening the APD upon vagal nerve stimulation (Kovacs & Bailey, 1985). The genes *KCNJ5* and *KCNJ3* encode for $K_{ir}3.1$/ $K_{ir}3.4$, respectively, forming a heteromeric channel that is gated by a G-protein (Zylbergold, Ramakrishnan, & Hébert, 2010). When activated, the $K_{ir}3.1$/ $K_{ir}3.4$ channel complex produces an outward K^+ current and shortens the APD (Verkerk, Geuzebroek, Veldkamp, & Wilders, 2012). Similarly, the cholinergic receptors can be activated by carbachol (CCh). In AF, $K_{ir}3.1$/ $K_{ir}3.4$ can be upregulated, which shortens the APD of the atrial tissue (Schmidt et al., 2015). Furthermore, the channels have been found to be constitutively active in patients with chronic atrial fibrillation in the absence of acetylcholine due to atrial remodelling (D. Dobrev et al., 2005).

As the name suggests, the small conductance Ca^{2+}-activated K^+ (SK) channel produces K^+ efflux with modulation through cytosolic Ca^{2+} levels and not changes in V_m (Tuteja et al., 2010). The SK channel family is formed by three paralogs (*KCNN1, KCNN2*, and *KCNN3*) and is expressed in numerous excitable tissues such as neurons, vascular endothelium, and cardiomyocytes (Tang et al., 2015; Tuteja et al., 2005; Wulff, Kolski-Andreaco, Sankaranarayanan, Sabatier, & Shakkottai, 2007). The three paralogs co-assemble to produce the inward K^+ current in response to Ca^{2+}(I_{SK}) which contributes to the cardiac background current (Wulff et al., 2007). However, there is differential expression between the two chambers. While both SK2 and SK3 are found in both chambers, the SK3 is preferentially expressed in the atria (Skibsbye et al., 2014; Tuteja et al., 2005) which suggest that the *KCNN3* is atrial specific and may provide a potential therapeutic target. Interestingly, the ventricles of humans and rabbits have increased expression of *KCNN2* in heart failure conditions (X.-D. Zhang, Lieu, & Chiamvimonvat,

2015). In a burst pacing-induced heart failure rabbit model, overall K^+ current was increased, with a component of the AP sensitive to apamin, a bee venom that blocks SK channels, indicating a possible role of SK channels in heart failure (Chua et al., 2011). Finally, the SK3 current is found to be upregulated in a rapid pacing AF canine model (Qi et al., 2013) and increased channel trafficking in burst-pacing AF rabbit model (Özgen et al., 2008).

The two-pore domain weak inward rectifying K^+ (K_{2P}) channel superfamily is comprised of tandem P domain weak inward-rectifying K^+ (TWIK) and TWIK-related acid-sensitive K^+ (TASK) channels (Goldstein, Bockenhauer, O'Kelly, & Zilberberg, 2001; González et al., 2013). The role of (K_{2P}) channels in cardiac function can be described as "leak channels" that contribute to background cardiac current (Backx & Marban, 2012; Decher, Kiper, Rolfes, Schulze-Bahr, & Rinné, 2015; Yue & Marban, 1988). Moreover, TWIK-1, TASK-1, TASK-3, and TASK-4 channels are predominantly expressed in the atria compared to ventricles (Decher et al., 2015; Gaborit et al., 2007). However, the role of K_{2P} channels in AF pathogenesis is still under debate, with reports of both upregulation of TASK-1 function in atrial tissue of permanent AF patients leading to shortening of AP duration (APD) (Schmidt et al., 2015) as well as loss-of-function in TASK-1 channel due to inhibition by channel phosphorylation (Harleton et al., 2015).

1.1.2. Calcium Handling Dynamics

The translation of electrical signals (excitation) to cardiac contraction is dependent on the intracellular Ca^{2+} signalling cascade referred to as the Ca^{2+} transient. Excitation-contraction (EC) coupling relies on Ca^{2+}-induced Ca^{2+} release (CICR). CICR creates a tight interaction between the inward Ca^{2+} gradient coming through the opening of LTCC and the opening of the ryanodine receptor 2 (RyR) to release Ca^{2+} from the sarcoplasmic reticulum (SR). In ventricular myocytes, LTCCs and RyR are spatially coupled which synchronizes the Ca^{2+} transient throughout the cytosol in the whole myocyte. LTCCs open in response to depolarization causing Ca^{2+} to flow into the dyadic space and inducing Ca^{2+} release from the SR via the RyR. The cytosolic Ca^{2+} then binds to the troponin complex inducing conformational change to the tropomyosin and exposes the binding site on the actin filament. Then, contraction occurs during cross-bridge cycling formation with the myosin head binding to the actin filament thereby shortening the cardiomyocyte and producing force. Cardiomyocyte relaxation occurs when ATPase

causes phosphorylation and the myosin head to disengage from the actin filament. Ca^{2+} is extruded from the cytosol through Na^{+}/Ca^{2+} exchanger (NCX) and SR reuptake is mediated by the sarco/endoplasmic reticulum Ca^{2+} ATPase (SERCA), thus ending a single Ca^{2+} transient cycle.

There are a few differences in Ca^{2+} handling between atrial and ventricular cardiomyocytes. Structurally, atrial myocytes possess more heterogeneous axial tubules and less developed T-tubules resulting in less organization in the coupling of LTCC and RyR (Dobromir Dobrev, 2017; Richards et al., 2011). This makes SR Ca^{2+} release more localized to the cell surface with the Ca^{2+} transient more slowly diffusing to the myocyte core (Greiser et al., 2014; Ishida et al., 2005). Mitochondrial Ca^{2+} buffering capacity is also larger in atrial myocytes (Ishida et al., 2005). Atrial myocytes also possess a different LTTC with $Ca_v1.3$ being predominantly expressed in the atria (Z. Zhang et al., 2005).

1.2. Factors of Cardiac Arrhythmia

1.2.1. Triggers and Re-entry

The mechanisms of cardiac arrhythmia at the cellular and tissue level are complex and multi-factorial. Factors that describe cardiac arrhythmia can be distilled into three models: 1) “triggers” for ectopic activity; 2) substrates promoting re-entry arrhythmia and its triggers; 3) the re-entrant arrhythmia itself. It is important to note that more complex models such as phase singularity of spiral waves in cardiac fibrillation are not covered in this thesis.

Ectopic activity can be caused by afterdepolarizations which produce extra-systolic activity and are generally classified into early afterdepolarization (EAD) and delayed afterdepolarization (DAD). EADs are defined as depolarizations before AP repolarization is complete, and typically occur in phase 2 and phase 3 of the AP (Burashnikov & Antzelevitch, 2003). The main causes of EADs are from the prolongation of the AP either related to increased opening of the Ca^{2+} channels (phase 2 EAD) or loss of function of K^{+} channels (phase 3 EAD) (Figure 1.2.B). In the ventricles, EADs can trigger Torsade de Pointes (TdP), a form of polymorphic ventricular tachycardia. Prolongation of the APD is common in long QT syndrome (LQTS) which can be

congenital due to various channel mutations or acquired through drug use. Many drug side effects have hERG binding component resulting in loss of function in I_{Kr}. Thus, drugs that bind to hERG and induce QTc (QT interval corrected for heart rate) prolongation are considered proarrhythmic and is mandated to be screened by the Food and Drug Administration (FDA).

DADs occur after repolarization is complete (phase 4 of the AP) (Figure 1.2.A). DADs are typically caused by elevated cytosolic Ca^{2+} during diastole that arises from several mechanisms, such as SR Ca^{2+} overload that leads to abnormal diastolic Ca^{2+} release, or mutations in the troponin complex that increases Ca^{2+} sensitivity which increases cytosolic Ca^{2+} concentration on the next beat. The increase in cytosolic Ca^{2+} induces the NCX in forward mode to extrude one Ca^{2+} ion and bring in three Na^{+} ions, producing a net positive current that depolarizes the cell leading to discharge of ectopic foci (Figure 1.2.A). These ectopic impulses are thought to be the initiating triggers of cardiac arrhythmia.

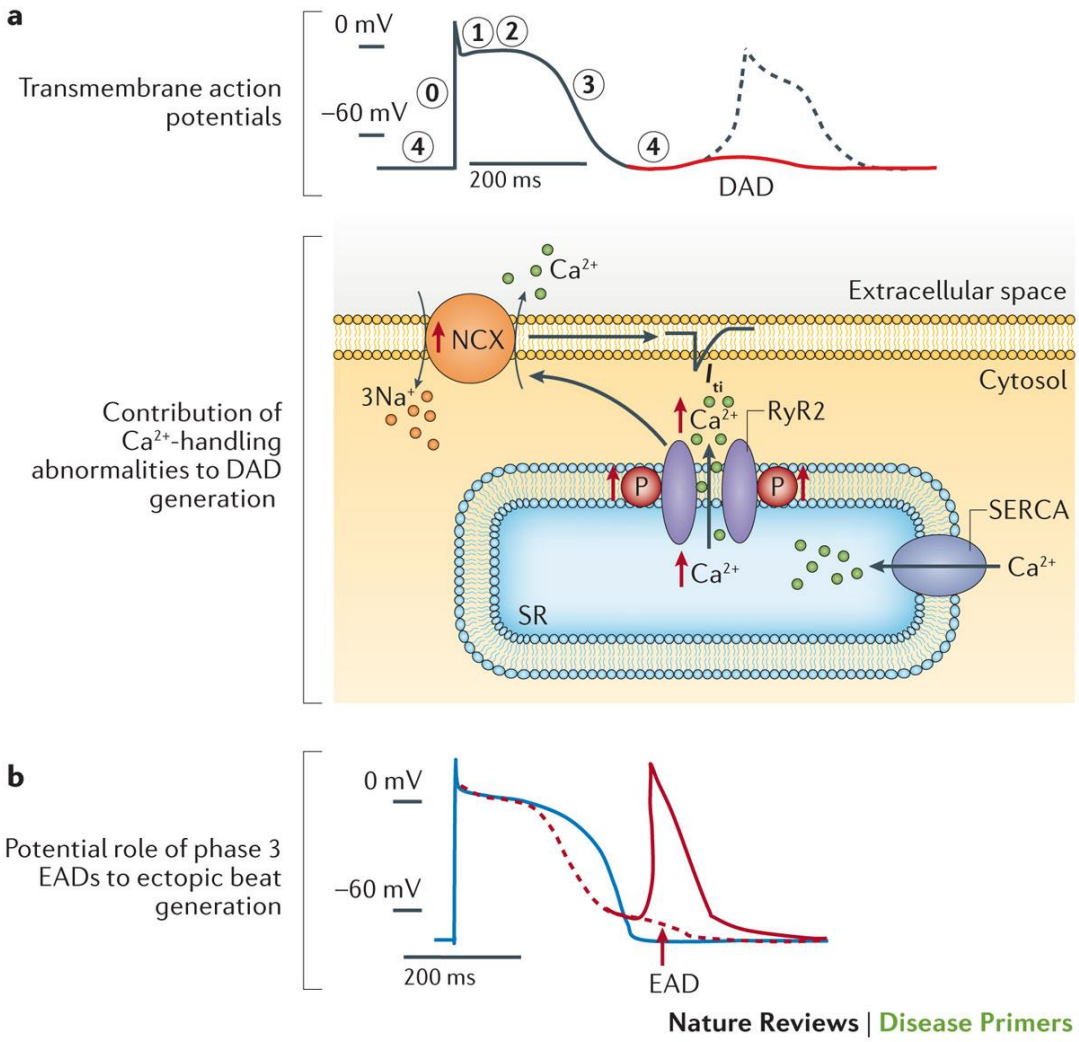

Figure 1.2. The triggers of ectopic foci in cardiac arrhythmia.
A) Top panel: Delayed after depolarization (DAD). Bottom panel: the mechanism of Ca^{2+} mishandling and its contribution to DAD. B) Phase 3 early after depolarization (EAD). Figure obtained from Lip et al., 2016 and reproduced with permission.

At the level of cardiac tissue, focal ectopic activities can trigger a cascading effect of excitable wave activation that is out of sync with normal propagation. Conceptually, electrical impulse travels along a normal electrical circuit and completes its propagation (Figure 1.3). However, in the instance of a unidirectional block, the impulse can travel in retrograde and exits to the next excitable tissue creating a loop in the circuitry (Figure 1.3). This mechanism, referred to as re-entry, is the predominant premise cardiac arrhythmias. Factors of re-entry include abnormal electrical circuit, slowed conduction velocity, and unidirectional block.

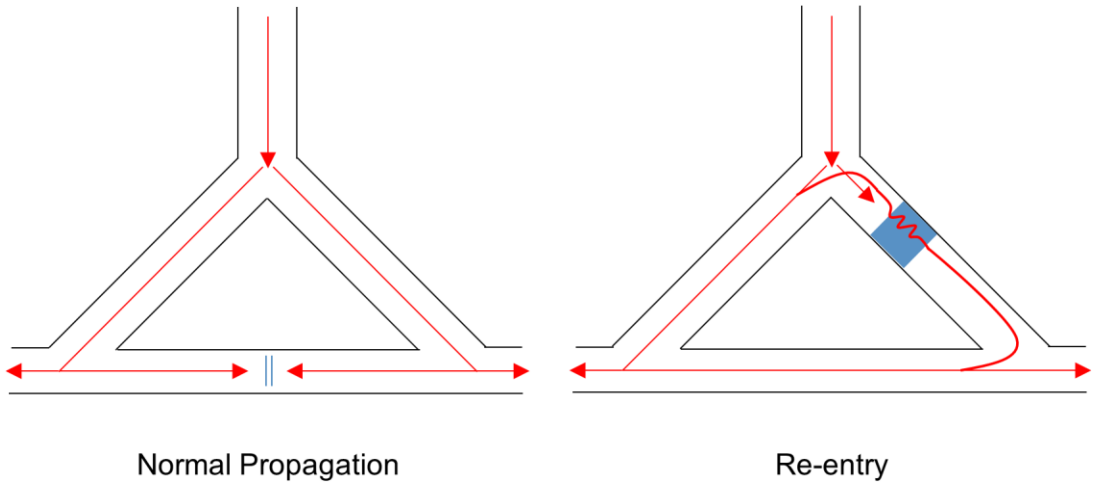

Figure 1.3. Electrical impulse propagation in cardiac tissue and re-entry.
Left panel: electrical impulse propagation under normal conditions. Right panel: re-entry arrhythmia caused by unidirectional block (as indicated in blue). A loop in the electrical circuit is created when an impulse travel in retrograde.

Electrical conduction through the cardiac tissue can be described by the equation $\lambda = ERP \times CV$ where λ is the wavelength, ERP is the effective refractory period, and CV is the conduction velocity (Wijffels, Kirchhof, Dorland, & Allessie, 1995). ERP reflects the time in repolarization in which a new AP cannot be formed and can be estimated using APD. The decrease in ERP governs the excitability of the cardiac tissue in which shortening in the ERP results in increased time for the next impulse generation. The spatial distribution and heterogeneity of the ERP also impacts on the probability of re-entrant formation (Comtois, Kneller, & Nattel, 2005). Meanwhile, slowed conduction velocity increases the spatial and temporal capacity for the next impulse generation to occur. Therefore, decreased cardiac wavelength through shortening of ERP and/or slowed conduction velocity contributes to the substrate of cardiac arrhythmias. For instance, a triggered ectopic impulse can travel around an area of slow conduction and excite tissue that has recently repolarized leading to the re-entrant arrhythmia.

For cardioversion and maintenance of sinus rhythm, many antiarrhythmic drugs aim to modify the substrate of arrhythmia by decreasing the excitability of the cardiac tissue such as through prolongation of the ERP. As such, spatial measurement of the ERP (or its closest marker APD) in a cardiac tissue layer is advantageous in a system that aims to screen for potential AF treatments.

1.2.2. Electrical Restitution and Alternans

The electrical restitution, the shortening of APD in response to increased heart rate, plays a role in accommodating high heart rates which allows the time for blood to refill the heart and allows for more rapid and forceful contract in an effort to maintain diastolic interval (Goldhaber et al., 2005). The electrical restitution is the result of activation and recovery kinetics of multiple ion channels. At high heart rates this restitution property may result in alternans or beat-to-beat variations (Franz, 2003; Goldhaber et al., 2005). In APD alternans, the APD is shorter in one cycle but can return to normal duration on the next beat. CaT alternans may occur as well (Carmeliet, 2004) in which shortening in the duration and/or decrease in the transient amplitude occur every other cycle due, in part, to recovery kinetics of RyR (Sun et al., 2018; Zhong et al., 2016, 2018). Ca^{2+} alternans is thought to be one of the drivers of re-entrant arrhythmias including AF pathogenesis (Chang & Trayanova, 2016; Tse et al., 2016). In addition to high heart rates, there are numerous factors in the provocation of alternans in the case of abnormal physiology. For instance, there is an increased propensity of Ca^{2+} driven alternans in atrial myocytes isolated from chronic AF patients which is attributed to an increased SR Ca^{2+} leak (Molina et al., 2016).

Traditionally, measuring the electrical restitution to determine the propensity of alternans is used in describing VF although the concept has been imported to describe AF propensity (Bode, Kilborn, Karasik, & Franz, 2001; Franz, Jamal, & Narayan, 2012; B.-S. Kim et al., 2002; Miyauchi et al., 2003). Electrical restitution is often presented as a best-fit curve, plotting APD as a function of the diastolic interval (DI), with the maximum slope of the curve as the quantified measurement. A maximum slope > 1 has been proposed to be arrhythmogenic, with an increased propensity and stability of a re-entrant arrhythmia (Qu, Weiss, & Garfinkel, 1999). A maximum slope > 1 indicates that the substrate is enhanced for alternans as alternating cycles result in a larger difference between APD and DI (Franz, 2003). Vice versa, a slope < 1 indicates dampening of the substrate for alternans (Franz, 2003). However, the validity of this parameter is controversial as the parameter serves as an index for increased propensity of arrhythmia but does not reliably predict fibrillation itself (Dorenkamp, Morguet, Sticherling, Behrens, & Zabel, 2013; R. Wu & Patwardhan, 2004). Furthermore, in the guinea pig model the restitution slope is primarily driven by steady-state APD and does not predict ventricular fibrillation by itself (Shattock et al., 2017). Nonetheless, electrical restitution is implicated

in arrhythmia as an important driver, and analysis of the restitution curve presents a convenient tool to investigate the propensity of cardiac tissue towards an arrhythmia under a given set of conditions.

1.3. Pathophysiology of Atrial Fibrillation

Atrial fibrillation (AF) tends to arise with other comorbidities such as hypertension, obesity, and cardiomyopathies (Lip et al., 2016). However, lone AF can occur in the absence of comorbidities (Wyse et al., 2014). Clinically, AF is classified further into paroxysmal, persistent, and permanent AF which refers primarily to the duration of AF events as well as the property of spontaneous conversion. In paroxysmal AF, patients can have spontaneous termination of the arrhythmia within 7 days of its onset (January et al., 2014). In contrast, persistent AF patients have sustained arrhythmia beyond 7 days, while permanent AF patients live with the arrhythmia for over 1 year (January et al., 2014), indicating that the arrhythmia is likely maintained for long periods of time via remodelling pathways. The rapid and irregular conduction patterns of AF in the atria can be conducted via the AV node to the ventricles resulting in tachycardia and possible substrate for ventricular fibrillation (Espinoza, Mehra, & DeAntonio, 2016; Santini & Ricci, 2001; Sarrias et al., 2015). It is important to note that AF itself can cause AF-promoting abnormalities and remodelling of the atria, a phenomenon often termed as “AF begets AF” (Wijffels et al., 1995). Atrial remodelling can include four properties: electrical (AP and conduction), Ca^{2+} handling, atrial structure, and the autonomic nervous system (Nattel, Burstein, & Dobrev, 2008). In turn, abnormalities in these 4 properties can provide and or re-enforce the substrate for AF. Long term atrial remodelling is believed to produce a persistent AF phenotype (Nattel et al., 2008). The pathophysiology of AF is complex involving multiple pathways and mechanisms as previously explained.

1.4. Treatment Strategies for Atrial Fibrillation

1.4.1. Current Treatment Modalities

The Canadian Cardiovascular Society guidelines outline current management strategies for AF. After AF is diagnosed, the first priority is to assess and manage thrombotic risk with antiplatelet and anticoagulants agents as indicated to combat the

risk of embolic stroke (Andrade et al., 2018). The current treatment strategies to combat AF mechanisms and reverse the AF substrate remain limited. The main methods to treat and manage the underlying arrhythmia are pharmacological or surgical interventions (Andrade et al., 2018).

In surgical catheter ablation, the principal strategy is to isolate the pulmonary vein (PVI procedure), a common area of ectopic foci origin, and functionally separate the atrial chamber from spontaneous discharging ectopic excitations (Haïssaguerre et al., 1998). Catheter ablation is effective in terminating paroxysmal AF and was found to decrease AF burden leading to the improvement in patients' quality of life (Pappone et al., 2006; Stabile et al., 2006; Wazni et al., 2005). In the **C**atheter **Ab**lation vs. **An**ti-Arrhythmic Drug Therapy for **A**trial Fibrillation (CABANA) trial, catheter ablation was found to decrease cardiac-related hospitalization rate while not improving overall composite score of death, disabling stroke, serious bleeding, or cardiac arrest (Packer et al., 2019). Catheter ablation is effective in treating paroxysmal AF with success rate of up to 63% (Ganesan et al., 2013). However, the long-term efficacy of ablations for persistent AF can be limited with an average success rate of 20% on a single procedure and an average success rate of 56% on multiple procedures after a five-year follow-up (Schreiber et al., 2015). Furthermore, ablations are relatively expensive and may lead to complications such as cardiac tamponade, transient ischemia, phrenic nerve injuries, and the highly-lethal atrio-esophageal fistula (Baman, Latchamsetty, & Oral, 2011; Sorgente et al., 2011). As ablations are invasive, patients must be able to withstand multiple procedures if necessary and as patients tend to be much older with other comorbidities, surgical ablation is recommended to be second-line therapy for most patients (Andrade et al., 2018). As such, alternative strategies must be employed.

Pharmacological treatment of AF typically aims to control cardiac rate and/or rhythm. In a rate control strategy, the aim is to pharmacologically suppress the high heart rates of AF through modification of the AV node by using drugs such as blockers of the beta-adrenergic pathways and of the LTCCs in the form dihydropyridines (Lip et al., 2016). In a rhythm control strategy, drugs target the underlying arrhythmia with cardioversion and maintenance of sinus rhythm as the desired outcome. Cardioversion can be carried out both electrically or pharmacologically, while anti-arrhythmic drugs are utilized principally for the maintenance of sinus rhythm (Lip et al., 2016).

Pharmacological agents are traditionally categorized based on the main drug target according to the Vaughan-Williams classification, though a recent attempt has modernized and expanded the classification system to reflect up-to-date mechanisms of action (Lei, Wu, Terrar, & Huang, 2018). The Vaughan-Williams system categorizes Class I agents as Na^+ channel blockers, Class II agents as beta-blockers, Class III agents as K^+ channel blockers, and Class IV agents as Ca^{2+} channel blockers and those that affect the AV node. Many of the currently approved antiarrhythmic agents for AF have multiple effects, some of which can be associated with adverse drug events. For example, flecainide and propafenone, both Class IC agents, are commonly prescribed but carry increased risk of proarrhythmia (C.-Y. Lin et al., 2015). Sotalol, a Class II and III agent for rhythm control, is associated with increased mortality (C.-Y. Lin et al., 2015). Amiodarone, classified as Class III agent that also blocks Na^+ and Ca^{2+} channels, has been found to be the most efficacious antiarrythmic in sinus rhythm maintenance but carries a large risk of toxicity due to the dissociation of iodine moiety in the bloodstream (Narayana, Woods, & Boos, 2011). Class III agents ibutilide and dofetilide are effective in cardioversion but the use has fallen out of favour due to the risk of proarrhythmia and the intensive monitoring required to avoid pre-arrhythmia in the form of Torsade de pointe related to QT prolongation (Lip et al., 2016).

Currently, it is unclear which pharmacological strategy (Rate vs Rhythm) presents the best outcome. Two of the largest randomized clinical trials thus far that compared the two treatment strategies found no differences in improving mortality (Investigators, 2002; Roy, Talajic, et al., 2008). It is important to note that rate control strategy manages the risk of polymorphic ventricular tachycardia but do not address the underlying arrhythmia. In a cohort of 682 patients, amiodarone was found to decrease AF prevalence from 54% to 17% in 4 months (Roy, Talajic, et al., 2008). Effective antiarrhythmic administration that results in maintenance of sinus rhythm is associated with improved quality of life such as exercise tolerance, lower risk of stroke, and improved left ventricular function (Dorian & Mangat, 2003; Hohnloser, Kuck, & Lilienthal, 2000; Opolski et al., 2004; Singh et al., 2006). The difficulty in pharmacological maintenance of sinus rhythm is that antiarrhythmic drugs must demonstrate cardiac safety meaning that it displays atrial selectivity without grossly affecting the ventricular chamber as drug-induced arrhythmia is one of the most common drug side effects. This is increasingly difficult as rhythm control drugs typically target ion channels, many of

which are shared between the atria and the ventricles. Therefore, it is necessary to develop compounds that can treat AF in a selective manner.

1.4.2. Development in Atrial-Specific Pharmacology

Future drug interventions take advantage of the differences in cardiac-subtype specific electrophysiology (as discussed in Chapter 1.1.1.) and consequently aim to produce an atrial-selective pharmacological response. By targeting the ion channels that are preferentially expressed in the atria, these drugs have the potential to decrease AF burden while posing minimal risk of ventricular proarrhythmia. One of the main goals of atrial-selective compounds is to lengthen the ERP of the atrial-tissue, thus suppressing AF events and protecting the atrial tissue from re-entrant substrate.

Blockers of $K_v1.5$

$K_v1.5$ or I_{Kur} has been a drug target since it was the first discovered as an atrial-selective K^+ channel (Fedida et al., 1993). Amongst the potential atrial-selective drug candidates, $K_v1.5$ experimental blockers are perhaps the most well characterized *in vitro*, *in vivo*, and in clinical setting. Experimental $K_v1.5$ blockers include S9947, MK0448, XEN-D0101, DPO-1, and AVE0118.

S9947 blocks $K_v1.5$ with IC_{50} 0.42 μM and suppressed I_{Kur} in human right atrial appendage (Bachmann et al., 2001). MK0448 prolonged atrial refractoriness in a canine model but did not show an effect on atrial refractoriness in healthy human participants (Pavri et al., 2012). XEN-D0101, developed by Xention, prolonged repolarization in human atrial trabaculae and in hESC-derived atrial cardiomyocytes (Devalla et al., 2015; J. Ford et al., 2013). XEN-D0103, the derivative of XEN-D0101, displayed frequency-dependent prolongation of APD and ERP in right atrial trabaculae of chronic AF patients (J. Ford et al., 2016) but did not reduce AF burden in a double-blind randomized trial (Shunmugam et al., 2018). DPO-1 is a potent $K_v1.5$ blocker with an IC_{50} of 0.78 μM in an heterologous expression system (Du et al., 2010) and selectively prolonged APD in isolated human atrial myocytes (Lagrutta, Wang, Fermini, & Salata, 2006). AVE0118 is a relatively specific I_{to}/I_{Kur} blocker with IC_{50} of 3.4 and 6.2 μM as tested in heterologous expression systems, though it also inhibits I_{KACh} and I_{kr} with IC_{50} values of 4.5, and 10 μM, respectively (Gogelein et al., 2004). In a rapid paced AF goat model, AVE0118

terminated AF more effectively than dofetilide and ibutilide (Blaauw et al., 2004). AVE0118 was found to have a dose-dependent effect on prolonging early-repolarization in atrial appendages isolated from sinus rhythm and chronic AF patients (Christ et al., 2009). AVE0118 has undergone phase 2 clinical trials in Germany, however, this agent has failed to proceed in further clinical trials (J. W. Ford & Milnes, 2008). Furthermore, DPO-1 and AVE0118 share similarities in binding sites of the pore domain and S6 helix of $K_v1.5$ indicating similar mode of action among $K_v1.5$ blockers (Decher, Kumar, Gonzalez, Pirard, & Sanguinetti, 2006; Du et al., 2010).

Blockers of $K_{ir}3.1$/ $K_{ir}3.4$

As $K_{ir}3.1/K_{ir}3.4$ (I_{KAch}) is upregulated in AF remodelling, this channel complex presents a potential drug target of reducing I_{KAch} which may reverse the shortening of APD and suppress AF. There are several experimental drugs that block $K_{ir}3.1/K_{ir}3.4$ including NTC-801 – also known as BMS914392, XEN-R0703, XEN-R0706, A7071, and AZD2927. XEN-R0703 prolonged ERP and decreased AF inducibility in canine atrial tissue (Devalla et al., 2015), while XEN-R0706 prolonged APD in human atrial tissue (Milnes et al., 2011). Both AZD2927 and A7071 demonstrated the ability to prolong the atrial ERP in a canine model but not in human subjects (Walfridsson et al., 2015). NTC-801 (BMS914392) increased atrial ERP and suppressed AF induced both by acotinine and rapid atrial pacing in a canine model (Machida et al., 2011). However, a clinical study showed no evidence that BMS914392 decreased AF burden when compared to placebo control (Podd, Freemantle, Furniss, & Sulke, 2016). Even though there are several experimental drugs that block $K_{ir}3.1/K_{ir}3.4$, the efficacy of selective block of this channel complex to decrease AF burden in humans remains to be determined.

Blockers of SK Channels

It is thought that the blockade of SK channels decreases background current which limits re-entrant arrhythmias by decreasing the rotor wavelength of cardiac tissue (Jonas Goldin Diness et al., 2010; Qi et al., 2013). Small molecules that block or modulate SK channels have been developed in recent years. UCL1684 and NS8593 are the most well characterized small molecules of these compounds. UCL1684 is a highly potent SK channel pore blocker with SK1-3 IC_{50} values of 0.76, 0.36, and 5.8 nM, respectively (Hosseini, Benton, Dunn, Jenkinson, & Moss, 2001; D Strøbaek, Jørgensen, Christophersen, Ahring, & Olesen, 2000). Another SK channel pore blocker

is ICA with IC_{50} values of 0.3 µM (SK2) and 0.5 µM (SK3) as reported in an expression system (Gentles et al., 2008). NS 8593, on the other hand, is a negative allosteric modulator of the channel which acts by inhibiting the calmodulin (CaM) Ca^{2+} sensor through the binding of its activation site, and decreases the channel sensitivity to Ca^{2+} thereby increasing the required Ca^{2+} concentration to open the channel (Dorte Strøbaek et al., 2006). NS 8593 has SK1-3 IC_{50} values of 0.42, 0.60, and 0.73 µM, respectively (Dorte Strøbaek et al., 2006). Another negative allosteric modulator of the SK channel is AP 14145 with an IC_{50} of 1.1 µM and at 10 µM demonstrated a reduction in Ca^{2+} sensitivity of an SK3 variant by three-fold (Simó-Vicens et al., 2017).

The efficacy of these SK channel blockers in terminating AF has been demonstrated in several animal models. UCL1684 (1 µM), ICAGEN (1 µM), and NS 8593 (10 µM) terminated AF in a burst pacing model of guinea pig hearts (Jonas Goldin Diness et al., 2010). NS 8593 increased atrial repolarization resulting in AF termination in an equine model (Haugaard et al., 2015). NS 8593 was felt to have greater efficacy than ICAGEN in a study using isolated atrial myocytes from patients that found both compounds increased APD and ERP of sinus rhythm patients, but only NS 8593 had an effect in tissues from AF patients (Skibsbye et al., 2014). The negative allosteric inhibitor AP14145 was shown to elongate ERP and terminate vernakalant-resistant AF in a porcine model (Jonas Goldin Diness et al., 2017). Nonetheless, the effects of SK channel block on AF are still controversial. Hsueh et al. (2013) demonstrated increased proarrhythmia after SK channel block using apamin and UCL 1684 in a canine model (Hsueh et al., 2013). However, another negative allosteric CaM modulator, AP30663, has passed phase I clinical trials and is currently launching a phase II trial which suggests that SK channel block is a promising target in AF treatment (Frans Wuite, 2018).

Multi-ion Channel Blockers

Many multi-ion channel blockers are on the market and in clinical application for the treatment of AF. Newer analogues of amiodarone such as dronedarone have improved the safety profile due its lack of an iodine moiety, but ultimately was less efficacious in terminating AF (de Groot et al., 2010; Penugonda, Mohmand-Borkowski, & Burke, 2011). However, the amiodarone family is not atrial-selective and is utilized in other clinical applications as an antiarrhythmic such as for the treatment of ventricular

tachycardia. Other non-selective multi-ion channel blocking agents, including ranolazine and vanoxerine, have found off-label applications as possible AF treatments. Ranolazine is an antianginal medication that blocks peak and late I_{Na} as well as I_{Kr} (Gupta, Khera, Kolte, Aronow, & Iwai, 2015; Poulet et al., 2015). Clinically, ranolazine demonstrated decreased AF reoccurrence, and increased maintenance of sinus rhythm following electrical cardioversion (De Ferrari et al., 2015). However, ranolazine showed slight QTc prolongation (Hawwa & Menon, 2013) with a documented case of TdP (Z. Liu, Williams, & Rosen, 2013). Vanoxerine is a potent dopamine reuptake inhibitor that has a strong frequency-dependent block on I_{Kr} , I_{CaL} , and I_{Na} (Lacerda, Kuryshev, Yan, Waldo, & Brown, 2010). In a randomized clinical trial, vanoxerine demonstrated dose-dependent cardioversion of paroxysmal AF, but elongated QTc without resulting in ventricular proarrhythmia (Dittrich et al., 2015).

A clinically approved atrial-selective multi-ion channel blocker is vernakalant. Vernakalant was recently approved to be delivered intravenously for cardioversion of paroxysmal AF in Europe and Canada (European Medicines Agency, 2010; Health Canada, 2018). Clinically, vernakalant demonstrated efficacy in cardioversion through dose-dependent elongation of atrial ERP and AV nodal conduction while having no effect on ventricular ERP (Dorian et al., 2007; Roy et al., 2004; Roy, Pratt, et al., 2008). Vernakalant has selectivity to I_{Kur} with an IC_{50} of 13 μM (Wettwer et al., 2013). However, the drug also blocks other channels at varying doses including the I_{KACh}, I_{Kr}, I_{CaL}, and I_{Na} with IC_{50} values of 10, 21, 84, 95, respectively (Fedida et al., 2005; Wettwer et al., 2013). It is suggested that the AF reduction effect of vernakalant is due to its frequency-dependent I_{Na} blocking component which decreases the excitability of atrial tissue and suppresses the re-entrant wave propagation (Finnin, 2010).

Blockers of K_{2P} Channels

The two-pore-domain K^+ (K_{2P}) channels contribute to background cardiac current (Limberg et al., 2011). As K_{2P} isoforms TASK-1 and TASK-3 are more abundant in human atrial tissue (Gaborit et al., 2007; Limberg et al., 2011), this channel complex presents a potential novel drug target (Gaborit et al., 2007; Limberg et al., 2011). However, the current selection of TASK channel blockers is limited. ML365 is a novel potent and selective TASK-1 channel blocker with a reported IC_{50} of 16 nM (Zou et al., 2010). PK-THPP and A1899 are selective TASK-3 channel inhibitors with IC_{50} values of

42 nM and 1.6 μM, respectively (Cotten, 2013). Both ML365 and PK-THPP demonstrated increase in atrial refractoriness and AF suppression in a rapid pacing rabbit model (Veldkamp et al., 2018a). Furthermore, the TASK-1 channel is sensitive to many mixed channel blockers such as amiodarone and dronedarone as well as K_v1.5 blockers such as A293, AVE 0118, and S9947 (Gierten et al., 2010; Kiper et al., 2015; Schmidt et al., 2012). Interestingly, many of these blockers displayed a higher selectivity to TASK-1 channels than their primary target (Kiper et al., 2015). For instance, A293 demonstrated efficacy in APD prolongation to normal durations in isolated human atrial cardiomyocytes from chronic AF patients, which was attributed to TASK-1 blockade (Schmidt et al., 2015). Doxapram, a breathing stimulant, is also a known TASK-1/TASK-3 heterodimer blocker that has not yet been studied in the treatment of AF (Cotten, 2013; O'Donohoe, Huskens, Turner, Pandit, & Buckler, 2018).

1.5. Human Induced Pluripotent Stem Cell-derived Cardiomyocytes (hiPSC-CMs)

1.5.1. hiPSC-CMs in Disease Modelling and Drug Screening

Human induced pluripotent stem cells (hiPSCs) are somatic cells such as peripheral blood mononuclear cells (PBMC) or fibroblasts that are genetically reprogrammed into a cell state that is capable of differentiating into multiple cell types (Hirschi, Li, & Roy, 2014). This technology presents a robust model that mimics human physiology. hiPSCs circumvent possible ethical issues around the use of human embryonic stem cells (hESCs) as the source of hiPSCs come from readily available somatic cells (K. Takahashi et al., 2007). Furthermore, genome editing techniques such as clustered regularly interspaced short palindromic repeats (CRIPSR), allows for the introduction or correction of mutations, as well as the manipulation of gene regulation, thus enabling the creation of true isogenic controls in studying disease mechanisms (Shafaattalab et al., 2019). As such, hiPSC-derived cardiomyocytes (hiPSC-CMs) are continually being used in disease models to probe disease mechanisms as well as drug screening for efficacy and safety of pharmacological compounds (Himmel, 2013; Jans et al., 2017; Mathur et al., 2015). hiPSC-CMs retain human-specific ion channels and their physiological profiles.

1.5.2. Cardiac Differentiation Strategies and the Characteristics of hiPSC-CMs

The important aspects of a cardiac differentiation protocol are its ability to produce hiPSC-CMs efficiently and inexpensively, robust in use, scalable to satisfy large cell culture needs, and in a chemically defined environment to minimize sources of variability (Lian et al., 2012). In general, cells differentiate into terminal cell types from the pluripotent stage through the manipulation of gene regulators that upregulate and downregulate a series of transcription factors. As such, differentiation of cardiomyocytes from hPSCs is obtained from modulating the canonical Wnt signalling pathway as the Wnt pathways is one of the master regulators of cardiac cell fate (Flaherty, Kamerzell, & Dawn, 2012). The activation of Wnt signalling leads to cardiogenesis through the initial formation of mesoderm (Flaherty et al., 2012). However, further Wnt signalling after mesoderm formation decreases cardiogenesis and thus inhibition of the same pathway is necessary to promote cardiac differentiation (Flaherty et al., 2012).

Numerous methods to produce hPSC-CMs have been published with the two most widely used methodologies being embryoid bodies (EB) formation and monolayer-based differentiation (Smith, Macadangdang, Leung, Laflamme, & Kim, 2017). The EB methodology depends on cell aggregates with induction of differentiation using cytokines such as Activin A and BMP4 (Activin/BMP) (Elliott et al., 2011). The EB formation approach is laborious and costly as it requires expensive cytokines and suspended culture in large volumes of maintenance media (Burridge, Keller, Gold, & Wu, 2012). Additionally, the requirement of cytokines leads to extensive titration for differentiating multiple cell lines as endogenous BMP4 cannot be controlled. The monolayer format, in contrast, is simpler requiring less resources in terms of media and consumables as well as equipment infrastructure. The monolayer method consists of high-density culture with induction using small molecules making it chemically defined to reduce variability (Lian et al., 2012). The protocol that we use is based on the GiWi protocol developed by Lian et al. (2013) which was adapted for in-lab use by Dr. Sanam Shafaattalab during her PhD studies in our lab. This protocol is chemically defined and one is able to scale up production with the monolayer format (Lian et al., 2013). However, current differentiation protocols all produce a heterogenous pool of cardiac subtypes with predominance of the ventricular phenotype (Lian et al., 2012). Therefore, manipulating other gene regulatory

pathways such as the retinoic signaling pathway is necessary in producing hiPSC-derived atrial-like cardiomyocytes (hiPSC-aCMs).

Developmentally, the retinol signalling pathway is the regulator for chamber specification inducing atrial and nodal lineages (Protze et al., 2016; Q. Zhang et al., 2011). Several studies have successfully applied all-trans retinoic acid (RA) in differentiating hPSCs into atrial-like cardiomyocytes (Argenziano et al., 2018; Cyganek et al., 2018; Devalla et al., 2015; Laksman et al., 2017; Lee, Protze, Laksman, Backx, & Keller, 2017; Lemme et al., 2018; Zhang et al., 2011). Zhang et al (2011) introduced RA in hESC-CM differentiation and found that RA-treated cells expressed lower levels of MLC2-v and were nifedipine insensitive. However, as the study was focused on improving a ventricular differentiation protocol, the RA-treated CMs were not further characterized. In another study, Devalla et al. (2015) produced hiPSC-aCMs from hESCs using EB-based Activin/BMP protocol and introduced RA post-mesoderm formation. The study found that RA-treated CMs have increased expression of *COUPTFI/II* that seemed to affect the expression of *KCNA5* and *KCNJ3* (Devalla et al., 2015). Patch clamping also revealed that RA-treated CMs respond to the experimental compounds XEN-R0703 ($K_{ir}3.1$/ $K_{ir}3.4$ blocker) and XEN-D0101 ($K_v1.5$ blocker) (Devalla et al., 2015). The EB-based Activin/BMP protocol was further optimized and characterized by Lee et al. (2016) who found differential mesoderm lineages that arise by taking advantage of the tight control of Activin/BMP induction. Titrating the ratio of Activin/BMP produced differential mesoderm lineage as a high ratio of 12 ng / 5 ng appeared to push the hESCs into a ventricular fate with markedly higher expression of CD235a (J. H. Lee et al., 2017). In contrast, a slightly lower ratio of 2 ng / 3 ng of Activin/BMP increased the expression of retinaldehyde dehydrogenase (RALDH), the enzyme necessary to convert retinol into RA, in the mesoderm stage which subsequently produced a large proportion of cell fraction with increased expression of atrial markers (J. H. Lee et al., 2017). However, the use of all-trans RA circumvents the need for the tight regulation of Activin/BMP to preferentially produce RALDH expressing mesoderm as RA will push the cardiac mesoderm into an atrial lineage. A more recent study adapted a similar EB-based protocol to produce 3D engineered heart tissue (EHT) and found that in comparison to the control EHT, the RA-treated EHTs have upregulated atrial markers while having faster contraction kinetics, shortened APD, and were sensitive to 4-aminopyridine and carbachol (Lemme et al., 2018).

Argenziano et al. (2018) and Cyganek et al. (2018) both differentiated hiPSC-aCMs in a monolayer using similar protocols with simplified monolayer format (Argenziano et al., 2018; Cyganek et al., 2018). Argenziano et al. (2018) demonstrated that RA-treated hiPSC-CMs have faster Ca^{2+} uptake and release while decreasing LTCC availability with reduced $I_{Ca,L}$. Additionally, the CHIP-seq assay suggested that *COUPTFII* upregulates $Ca_v3.1$ expression while downregulating $Ca_v1.2$. Similarly, Cyganek et al. (2018) found that RA induced atrial-like genetic and proteomic patterns as well as having shorter APD and faster Ca^{2+} handling dynamics. This study also used 3D EHT and demonstrated similar findings to Lemme et al. (2018) in terms of faster and weaker contraction in RA-treated EHTs.

Although several lab groups have applied RA in differentiating aCMs from hPSCs, discrepancies still abound in the timeframe of RA addition. For example, Argenziano et al. (2018) introduced 1 μM RA in the cardiac progenitor formation phase or two days after the inhibition of the Wnt signalling pathway for a total exposure time of five days, while Cyganek et al. (2018) added 1 μM RA in post-mesoderm induction phase which corresponds to one day after inhibition of Wnt signalling pathway, for total exposure time of three days. The discrepancy in the time interval of RA addition in the literature indicates the limited characterization of the functional effect of RA addition in atrial phenotype. The determination of the ideal time point to introduce RA also arises. Nonetheless, we can deduce that RA is a strong regulator and the commitment to initial cardiac mesoderm stage is crucial in achieving atrial cardiomyocytes. Furthermore, gene expression assays from the studies mentioned above were well aligned in terms of factors that are upregulated by RA including the atrial specific genes *MLC2A, COUPTFI/II, PITX2, NPPA, KCNA5, KCNJ3, SLN, SK3* while downregulating ventricular markers *IRX4, MLC2V.* However, the signals of EC-coupling in the form of simultaneous measurement of V_m and Ca^{2+} transients have not been characterized. In this thesis, we aimed to develop an atrial differentiation protocol by altering the RA signalling in a defined timeframe after induction of cardiac progenitors to atrial specification.

1.6. Drug Screening Assay Systems

1.6.1. Current Technology Platforms

The patch clamp technique is considered to be the gold standard of electrophysiology. Patch clamp can measure absolute changes in membrane voltages and thus AP in its truest form at the cellular level (Verkerk et al., 2017). Additionally, the technique enables exploration of channel biophysics by characterizing channel currents which allows for the investigation of drug mechanisms and mode of action (Dunlop, Bowlby, Peri, Vasilyev, & Arias, 2008). Although patch clamping is the gold standard of electrophysiology, there are several critical caveats: 1) dissociation of a tissue into single cells with enzymes such as collagenase changes the properties of the gap junctions which may alter electrophysiology of the cell (Huang et al., 2010); 2) the technique involves highly variable cell preparation and readout (Horváth et al., 2018); 3) arrhythmias are multicellular in origin and an assay at the single cell level does not necessarily scale to tissue level making it difficult to study the underpinning mechanisms of the disease ; 4) manual patch clamp is low-throughput, which can lead to potential biases through sample selection and technically demanding requiring skilled experimentalists to conduct experiments (Dunlop et al., 2008); 5) current high-throughput patch clamp systems have low success rate (~31%) in assessing hiPSC-CMs (Rajamohan et al., 2016).

The second technology platform that records and quantifies cardiac electrophysiology is the Microelectrode Array (MEA) which measures field potentials as an estimate of AP (Blum, Ross, Brown, & Deweerth, 2007). The technology is being constantly updated with the new generations of MEA improving on the the capability to measure surrogates of local APs. MEA is an attractive technology due to the ease of use and potential integration of automation using liquid handling robotics and a programmable incubator for environmental control. Additionally, the MEA system is capable of mapping a propagating excitatory wave front and is also extensively used in the Comprehensive *in vitro* Proarrhythmia Assay (CiPA) Initiative that aims to create an *in vitro* model system for cardiac safety (Colatsky et al., 2016; Crumb, Vicente, Johannesen, & Strauss, 2016; Nozaki et al., 2016). The CiPA initiative aims to create a technology workflow for screening potential drug-induced QTc elongation before clinical trials (Colatsky et al., 2016).

The third technology platform for electrophysiology is fluorescence imaging. The advantages of imaging technology are the potential for multiplexing by using multiple fluorescent dyes and the ability to increase experimental throughput. Arguably, live cytosolic Ca^{2+} handling dynamics are best measured using fluorescent dyes (A. Takahashi, Camacho, Lechleiter, & Herman, 1999). Other techniques such as Ca^{2+}-selective electrodes are possible but are difficult to utilize (A. Takahashi et al., 1999). Fluorescence imaging has emerged because of its ease of use, relatively low cost, and scalability to high-throughput applications. Such systems that reliably measure the cytosolic Ca^{2+} transient include optical mapping, standard epifluorescence and confocal microscopy, or high-throughput Ca^{2+} flux assays such as the FLIPR Tetra system (Daily, Du, & Wakatsuki, 2017; Daily, Santos, Vecchi, Kemanli, & Wakatsuki, 2017). An example of an epifluorescence system is the CellOPTIQ that claims to be able to measure V_m, Ca^{2+} transients (CaTs), and contraction signatures in a 96-well plate format (Hortigon-Vinagre et al., 2017). In drug studies, however, the CellOPTIQ is limited to 48 wells due to limitations on the timing of dye and drug loading protocol (Hortigon-Vinagre et al., 2017; Lu et al., 2017). The CellOPTIQ system also became one of the technologies being tested in the CiPA initiative (Blinova et al., 2017). Another high-throughput system is the Hamamatsu FDSS/µCELL system that has been employed in quantifying the V_m and CaT of hiPSC-CMs to examine cardiac safety of pharmacological agents (Bedut et al., 2016; Zeng, Roman, Lis, Lagrutta, & Sannajust, 2016).

1.6.2. Principles of Multi-Well Optical Mapping

Optical mapping (OM) is perhaps the most suitable tool in studying cardiac arrhythmia (Herron, Lee, & Jalife, 2012). OM is a high-content, non-contact, live-cell imaging system that allows for detailed interrogation of key cardiomyocyte characteristics through simultaneous measurements of complex membrane voltage (V_m) activity and Ca^{2+} handling dynamics (E. Lin et al., 2015; Shafaattalab et al., 2019), representing the cellular coupling of excitation and contraction. OM has certain inherent advantages over the techniques discussed previously. As arrhythmias are multi-cellular events, OM at the tissue level presents allows for the study of pharmacological intervention on arrhythmias, as OM detects high-resolution spatial and temporal changes in the action potential duration (APD) and calcium cycling as reflected by the CaT (Herron et al., 2012). Historically, OM has been heavily utilized in assessing fibrillation

as rotor formations in 2D and 3D cardiac substrates. In the context of AF, one study using OM has successfully captured rotor formation in hESC-derived atrial-like CMs and observed the abolishment of re-entrant rhythms using pharmacological interventions (Laksman et al., 2017). Furthermore, our lab has previously published the application of hiPSC-CM and OM in disease modelling (Shafaattalab et al., 2019) and drug toxicity screening (Shafaattalab et al., 2019).

The Multi-well OM system with 24-well plate capability was designed and built by our Research Associate Dr. Eric Lin. The idea behind the Multi-Well OM system starts with the limitation of throughput or the number of experiments run for a given time. In a typical single well system, the experimenter can conduct a single experiment in 3 hours. The experimenter can stack the dye loading time of the next well for higher-throughput, but is still limited to 3 to 4 experiments per day. Thus, building a higher-throughput system was the next logical goal.

The fundamental goals for the medium-throughput assay with semi-automation were to reduce human error, improve reproducibility, increase the number of experimental replicates, and decrease the cost of a comprehensive assay. The 24-well plate presents a well-balanced solution to increasing experimental throughput while preserving image quality, as the field of view maintains a high resolution for spatiotemporal analysis. Higher throughput systems such as 96- or 384-well plate formats tend to sacrifice spatial resolution (ie. limiting spatial mapping of cardiac activity) and signal quality (ie. limited by photon density per sample) for throughput. The 24-well format also allows for quick prototyping and ease of implementation as the dimension of the wells makes it is easy to work with at the hardware prototyping stage. For instance, higher throughput format plates require microfabrication of plastic plates with built-in electrodes for stimulation, while quick prototyping of stimulation electrodes in a 24-well plate is straight-forward by machining an acrylic holder for the stimulation electrodes. The multi-well nature of the format allows for parallelization of experiments. The OM operator could stack experiments by starting dye incubation in the next well before the last experiment is finished. The next well is then ready for imaging upon the completion of the previous experiment. Depending on the length of the experiment and the number of conditions to be tested, the parallelization enables the operator to conduct anywhere from 4 up to the limit of 24 experiments using the automation features in a matter of 6 hours.

However, as with any technique, OM comes with several limitations. First is the reliance of measurement on fluorescent dyes that are prone to photobleaching, thus decreasing the overall time of recording/measurement and limiting the experimental study of drug effects. Second, fluorescent dye emissions reflect arbitrary units and while one can measure the duration and morphology of voltage and Ca^{2+} transients, one can only infer amplitude size from the relative measurements based on the arbitrary fluorescence units. Third, the data files generated from the high-resolution images are large with 8 MB generated for each frame captured by the Hamamatsu Orca 4 camera. The total file size including image processing is 17.6 GB per 20-second recording. Without the proper computational infrastructure in place, the data acquisition and processing can be challenging.

1.7. Overview and Objectives

Developing antiarrhythmics for AF treatment is exceedingly difficult due to cross reactivity between atrial and ventricular chambers which can lead to the undesired QTc prolongation and TdP risk. The overarching goal of establishing drug efficacy and safety before moving towards clinical trials is to save time, money, improve patients' quality of life, and save patient's lives. Considering this fact, hiPSCs provide a human relevant physiological model in a complex system to investigate atrial efficacy and potential ventricular proarrhythmia. Therefore, I hypothesized that hiPSC-derived atrial cardiomyocytes (hiPSC-aCMs) are responsive to atrial-selective pharmacology with high specificity and sensitivity, presenting a potential pre-clinical *in vitro* model for drug development of AF treatments. To address this hypothesis, there were three objectives: 1) To develop the process for production of highly pure hiPSC-aCMs and hiPSC-vCMs for subsequent assays; 2) To characterize the physiological differences in voltage and calcium handling dynamics between the two cardiac subtypes; 3) To establish proof of concept that the multi-well optical mapping and hiPSC-aCMs platform are capable of discerning atrial-specific pharmacology.

Chapter 2.

Materials and Methods

2.1. hiPSC Maintenance and Expansion

Commercially available hiPSCs (WiCell, IMR90-1) were maintained and expanded in feeder-free culture using 6-well plates coated with Matrigel (Corning; Cat: 354230) diluted with a solution containing 1 mg:12 mL DMEM/F12 and mTeSR1 medium (STEMCELL Technologies, Cat: 85850). Using Versene (EDTA) (Lonza, Cat: 17-711E), hiPSCs were passaged every 4 days or ~85% confluency at 1:15 ratio. Passaged hiPSCs were cultured with mTeSR1 supplemented with 10 µM Y27632, a ROCK inhibitor, (Biogems, Cat: 1293823) for the first 24 hours. mTeSR1 media was exchanged daily during cell culture maintenance.

2.2. Differentiation of hiPSC-derived Atrial and Ventricular Cardiomyocytes

hiPSCs were passaged using Versene (EDTA) (Lonza, Cat: 17-711E) and seeded at a density of ~8.5 x 10^3 per mm^2. Differentiation was conducted using either 12-well or 6-well plates depending on the required number of cells. Upon confluence (Day 0 of differentiation), hiPSC differentiation was induced via G3K inhibition using 12 µM CHIR99021 (Biogems, Cat: 2520691) for 24 hours followed by media exchange of RPMI-1640 medium supplemented by B27 minus insulin (Thermo Scientific, Cat: A1895601). At Day 3, the cells were induced into mesoderm lineage and cardiogenesis via WNT signalling inhibition using 12 µM IWP-4 (Biogems, Cat:6861787) for 48 hours. At Day 5, media were replaced with RPMI-1640 medium supplemented by B27 minus insulin. Starting on Day 7, hiPSC-CMs were maintained in culture using full CM medium which is comprised of RPMI-1640 medium (Thermo Scientific, Cat: 11875-085) supplemented with B27 (Thermo Scientific, Cat: 17504044). For subsequent cell culture maintenance, CM media were exchanged every 4 days.

hiPSC-aCMs were differentiated by modulating the retinoic signalling pathway. Briefly, hiPSCs were maintained until confluence and differentiated using CHIR99021

and IWP-4 as described above except for the daily addition of 0.75 µM all-trans retinoic acid (Sigma Aldrich, Cat: R2625) from Days 4 through Day 6 of differentiation. Both hiPSC-aCMs and hiPSC-vCMs were maintained in culture for about 40-50 days before optical mapping experimentation.

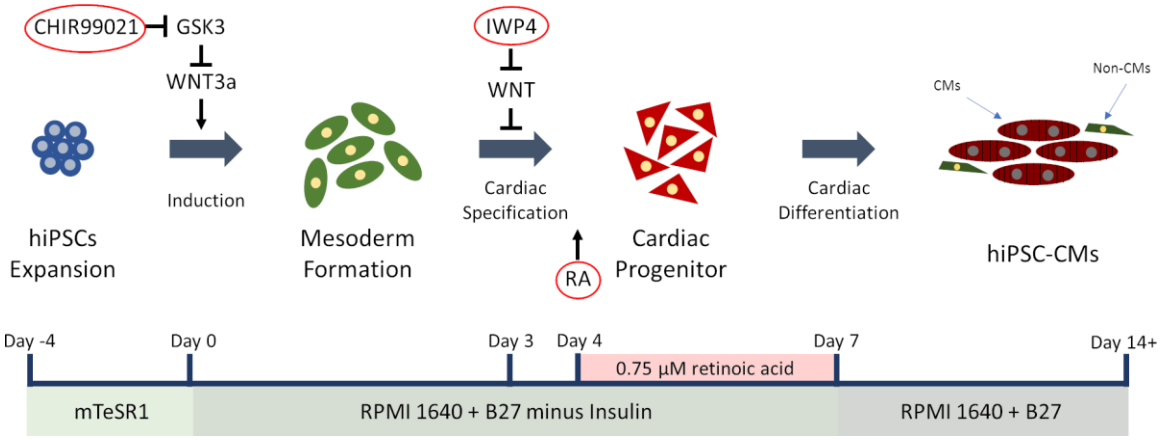

Figure 2.1. Directed differentiation of hiPSC-derived cardiomyocytes.
Atrial-lineage was induced by daily addition of 0.75 µM retinoic acid (RA) from Day 4 through 6 (total exposure from Day 4 to 7). Ventricular lineage was induced in the absence of RA.

2.3. Enrichment of hiPSC-CMs

For cardiac enrichment, hiPSC-aCMs and hiPSC-vCMs were dissociated into single cells with a 0.25% Trypsin-EDTA solution (Thermo Scientific, Cat: 25200072) at 37° C for 6-8 minutes, washed in DMEM medium containing 5% fetal bovine serum (FBS) (Thermo Scientific, Cat: 16000044, and filtered through a 70 µm filter (Miltenyi, Cat: 130-110-916). The single cell CMs were enriched using MidiMACS LS Magnet column setup (Miltenyi, Cat: 130-042-301) and the PSC-derived Cardiomyocyte Isolation Kit (Miltenyi, Cat: 130-110-188) according to the manufacturer's protocol. Briefly, hiPSC-derived non-cardiomyocytes such as fibroblasts, undifferentiated hiPSCs, and other cell types were labelled with non-cardiomyocyte binding antibodies and conjugated to magnetic nanobeads. The labelled non-cardiomyocytes were separated from the cell mixture after being bound in the magnetic column, leaving an enriched hiPSC-CM population (Figure 2.2). To test the efficacy of CD90-negative selection approach, non-hiPSC-CMs were incubated with CD90-APC antibodies (BD Biosciences; Cat: 8) which were then conjugated to anti-APC microbeads (Miltenyi; Cat: 130-090-855). The cells were then run through the MidiMACS LS Magnet columns as described above. Enriched

hiPSC-CMs were cultured on Matrigel-coated 24-well plates in full CM medium supplemented with 10 µM Y27632 for 24 hours. Medium was refreshed every 4 hours.

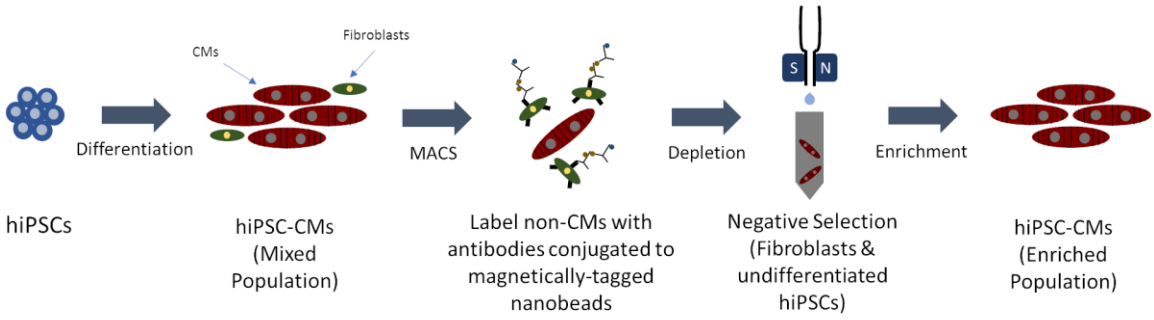

Figure 2.2. The hiPSC-CM enrichment strategy with non-cardiomyocyte depletion approach using Magnetic Activated Cell Sorting (MACS).

2.4. Gene Expression Analysis

Total RNA was isolated from hiPSC-CMs using RNeasy Mini Kit (Qiagen, Cat: 74104) and 1 mg of RNA were reverse transcribed to cDNA using QuantiTect Reverse Transcription Kit (Qiagen, Cat: 205311). Quantitative reverse transcriptase polymerase chain reaction (qRT-PCR) experiments were then performed in triplicate using SsoFast EvaGreen Supermix (Biorad, Cat: 1725201) and CFX9600 Real-Time PCR system (Biorad). For analysis, the expression of each gene was normalized to two housekeeping genes *GAPDH* and *ACTB* and analyzed using the ΔΔCt method (Livak & Schmittgen, 2001). The genes to be characterized included universal cardiac markers (*TNNT2*), pacemaker markers (*SHOX2, HCN4*), atrial markers (*SLN* and *GJA5*), and ventricular markers (*MYL2* and *IRX4*). The primer sequences and gene names are listed in Table 2.1.

Table 2.1. List of the primer sequences used in the qRT-PCR panel.

Subtype	Gene	Protein	Primer Sequences (5'– 3')
Housekeeping	*GAPDH*	Glyceraldehyde 3-phosphate dehydrogenase	F: CATGTTCCAATATGATTCCAC R: AGTCTTCTGGGTGGCAGTGAT
Housekeeping	*ACTB*	β-actin	F: ATTGCCGACAGGATGCAGAA R: GGGCCGGACTCGTCATACTC
Cardiac	*TNNT2*	Troponin T – cardiac isoform	F: TTCACCAAAGATCTGCTCCT R: TACTGGTGTGGAGTGGGTG
Cardiac	*NKX2.5*	NK2 Homeobox 5	F: CTCCCAACATGACCCTGAGT R: GACGGCGAGATAGCAAAGG
Pacemaker	*SHOX2*	Short stature homeobox 2	F: TAAAGGTGTTCTCATAGGGGC R: CCTGAACCTGCTGAAATGGC
Pacemaker	*HCN4*	Hyperpolarization-activated cyclic nucleotide-gated channel 4	F: GGAGTACCCCATGATGCGAA R: CTTCTTGCCAATGCGGTCCA
Atrial	*SLN*	Sarcolipin	F: GCTCAAGTTGGAGACAGCGAG R: GGCTTCTCCTCACCTCCTGAAG
Atrial	*GJA5*	Gap junction protein α-5 (connexin 40)	F: GGAGGAGGAAAAGAAGCAGA R: TATGAAGAGGACAGTGAGCC
Atrial	*KCNA5*	Voltage-gated K^+ channel, shaker-related subfamily member 5 ($K_V1.5$)	F: CGAGGATGAGGGCTTCATTA R: CTGAACTCAGGCAGGGTCTC
Atrial	*KCNJ3*	Inwardly rectifying K^+ channel 3, subfamily J member 3 ($K_{ir}3.1$)	F: CTGCTCAAAGGATGACTTGT R: CATGGAACTGGGAGTAATCA
Atrial	*NPPA*	Atrial Natriuretic Peptide	F: ACAGGATTGGAGCCCAGAG R: GGAGCCTCTTGCAGTCTGTC
Atrial	*KCNN3*	Small-conductance Ca^{2+} activated K^+ channel 3 (SK3)	F: CCTGTATGAGTCAGCCTTTC R: AGCTCTAGGGACTTCTAACC
Atrial/Ventricular	*KCNN2*	Small-conductance Ca^{2+} activated K^+ channel 2 (SK2)	F: TAAGCCAGACCATCAGGCAG R: GGGACCGCTCAGCATTGTAA
Ventricular	*MYL2*	Myosin regulatory light chain – ventricular isoform	F: ACAGGGATGGCTTCATTGAC R: CCGCTCCCTTAAGTTTCTCC
Ventricular	*IRX4*	Iroquois homeobox 4	F: TTCCGTTCTGAAGCGTGGTC R: TGAAGCAGGCAATTATTGGTGT

Subtype specific genes were based on the findings of Gaborit et al., 2007.

2.5. Flow Cytometry Analysis

hiPSC-CMs were dissociated into single cells using 0.25% Trypsin-EDTA solution (Thermo Scientific, Cat: 25200072) for 6-8 minutes at 37°C and fixed for 60 minutes at 4°C with 4% PFA in PBS (BD Biosciences, Cat: 554656). Then, the cells were stained in Perm/Wash buffer containing PBS, 5%FBS, and saponin (BD Biosciences, Cat: 554722). For cTnT analysis only, the harvested cells were stained with anti-cTnT

antibodies pre-conjugated to FITC (Miltenyi, Cat: 130-106-745) at a concentration of 1:100. For dual analysis of cTnT and MLC-2v, the cells are first stained with primary antibodies against cTnT (BD Biosciences, Cat: 565497) and MLC-2v (Abcam, Cat: ab79935) at a concentration of 1:2000 and 1:1000, respectively. The cells were then washed 2x in Perm/Wash buffer followed by incubation of secondary antibodies with goat anti-mouse IgG1 conjugated to Alexa-488 (Thermo Scientific, Cat: A21121) and goat anti-rabbit IgG (H+L) conjugated to Alexa-647 (Thermo Scientific, Cat: A21121, 21244) at concentrations of 1:1000 and 1:4000, respectively. Stained cells were washed 2x in Perm/Wash buffer and subsequently analyzed on a BD FACSJazz instrument (BD Biosiences). Data were analyzed using Flowing Software (Perttu Terho, Turku Centre for Biotechnology) and FlowJo Software (FlowJo LLC) (Figure 2.3).

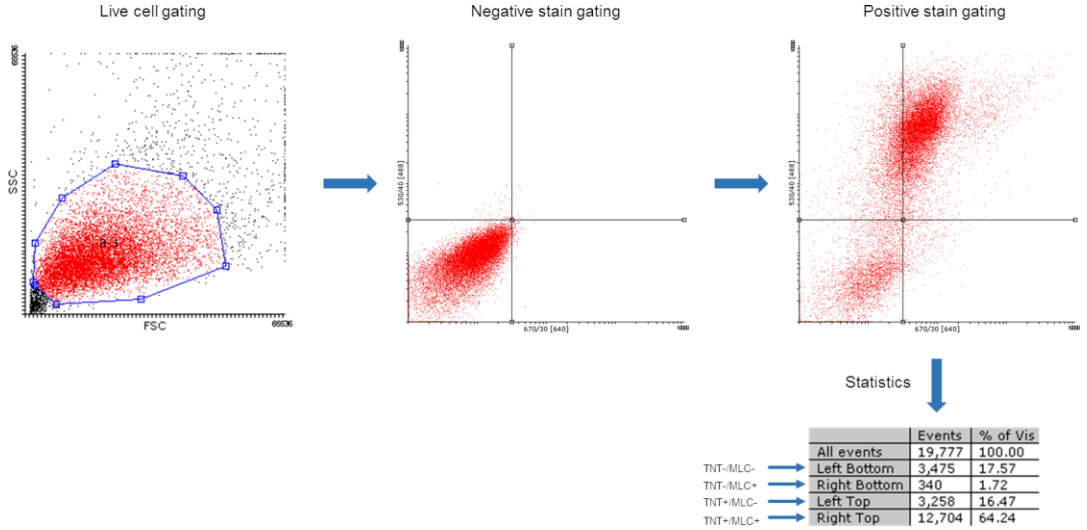

Figure 2.3. Example of the gating procedure in flow cytometric analysis of dual-stained cTnT and MLC2-v.

Analysis begins with gating the live cells of the experimental population as shown in red. The live cell population was then used in the negative and positive stain analyses. In negative-stain gating, unstained hiPSC-CMs were gated using a quadrant as shown in the middle panel to eliminate the background signal from cell autofluorescence. In positive-stain gating, population of dual-stained hiPSC-CMs were gated using the same quadrant as the negative-stain gating. The statistics of the quadrant were then generated by the software.

2.6. Optical Mapping

2.6.1. Optical Mapping Setup

The prototype Multi-well OM system includes custom-written software written in IDL (Harris Geospatial Solutions) and custom-engineered hardware. Briefly, one well of

the 24-well plate was illuminated with four 530 nm mounted LEDs (Thorlabs; Cat: M530L4) to excite both RH-237 and Rhod-2AM. Images were acquired by a scientific grade CMOS camera, Orca Flash 4.0 V2 (Hamamatsu; Cat: C11440-22CU), at 100 frames/second. The experimental chamber was maintained 37°C with thermal pads and controlled by PID controller (TE Technology; Cat: tc3625-rs232). The motorized imaging stage was controlled using custom-made programs through the Adruino platform. The custom software was also used for preliminary data analysis.

2.6.2. Experimental Protocol

hiPSC-CMs were seeded into 24-well plates and maintained according to protocol (Method 1.2). Optical mapping recordings were performed at Day 45-60 post-differentiation. Thirty minutes prior to recording, CM culture medium were exchanged to Ca^{2+} Tyrode's solution (in mM: 117 NaCl, 5.7 KCl, 4.4 $NaHCO_3$, 1.5 NaH_2PO_4-H_2O, 1.7 $MgCl_2$, 10 Na-HEPES ($C_8H_{18}N_2O_4S$), 5 glucose, 5 creatine, 5 Na-Pyruvic acid, 1.8 $CaCl_2$) and equilibrated in the incubator (37°C/5% CO_2). Then, the plate was transferred to the Multi-well OM instrument in which the temperature was maintained at 37°C and proceeded to the loading protocol (Figure A). The hiPSC-CMs were sequentially loaded with 5 µM RH-237 (Thermo Scientific, Cat: S1109) for 50 minutes, followed by co-incubation of 15 µM blebbistatin (Toronto Research Chemical, Cat: B592500) and 5 µM Rhod-2AM mixture for 40 minutes (Thermo Scientific, Cat: R1244). Blebbistatin was used to remove movement artefact. After dye incubation, a 20-second recording of spontaneous activity was conducted to collect data for the control condition. Drug effects were studied in serum-free conditions (i.e. Ca^{2+} Tyrode's and drug only) at four doses by increasing drug concentration in the same well with recordings at 20-minute time points. Dye and drug stocks were loaded in the tubing of individual pump channels for automated perfusion. Data collection, processing, and initial analysis were accomplished using software custom-written in IDL.

Figure 2.4. Optical mapping experimental procedure for drug characterization.

2.6.3. Stimulation Paradigm

The hiPSC-CMs were electrically driven by field stimulation through a pair of neighbouring stainless-steel electrodes that were placed in parallel 1 cm apart. The stimulation pulses were biphasic, rectangular, and 1 millisecond in duration. To mimic normal sinus rhythm of the human heart, hiPSC-CMs were paced at 60 bpm to establish baseline APD and CaTD in both hiPSC-aCMs and -vCMs. Restitution properties were assessed and compared with two different protocols: variable rate and standard S1S2. The variable rate protocol, also known as a dynamic restitution protocol in the literature , is a pacing protocol in which a train of stimuli were delivered at consecutively increasing pacing rate by 5 bpm at each stimulus (i.e. inversely decreasing cycle length by an exponential factor) (Figure 2.5.A and B). The standard S1S2 protocol involved pacing the cells at a given S1 rate while delivering an S2 stimulus in progressively shorter intervals. This protocol was repeated until the cells failed to capture the stimulation rate (Figure 2.5.C. Effective refractory period (ERP) as defined by the following three criteria (Goldhaber et al., 2005): 1) the stimulus interval of the last captured cycle or the S1S2 stimulus interval; 2) when the stimulus fails to generate a normal AP or CaT profile; and 3) when the AP amplitude decreases by 50%. However, only the results from variable rate protocol were included in the final analysis as the S1S2 protocol involves multiple recordings and prone to photobleaching. The results of S1S2 protocol were presented in Appendix A.

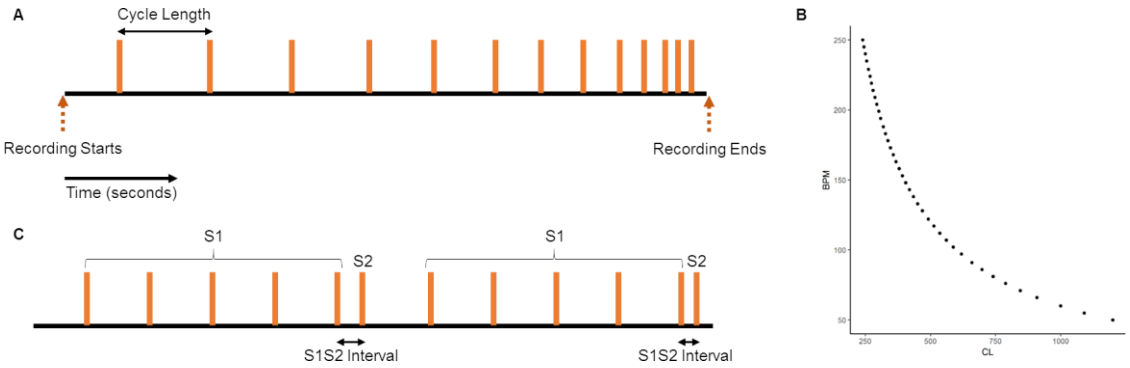

Figure 2.5. Stimulation protocols to investigate restitution properties.
A) Illustration of the dynamic pacing protocol in which consecutive stimuli were delivered by decreasing cycle length. B) Relationship between beats per minute and cycle length. C) Illustration of S1S2 pacing protocol in which 5 cycles of S1 were delivered for every S2 stimulus delivered at shorter and shorter cycle length. Vertical orange lines represent stimulation pulses.

2.7. Pharmacological analyses

The following drugs were purchased: vernakalant (Toronto Research Chemical, Cat: V128620), dofetilide (Tocris, Cat:3757), nifedipine (Sigma-Aldrich, Cat: N7634), 4-aminopyridine (Sigma-Aldrich, Cat: 275875), UCL 1684 (Tocris, Cat: 1310), AVE 0018 (Axon Medchem, Cat: 2243), and carbachol (Tocris, Cat: 28105). All drug stocks except for 4-aminopyridine were made by dissolving in DMSO (Sigma Aldrich, Cat: 472301) to final concentration of 10 mM. 4-aminopyridine was diluted in Ca^{2+} Tyrode's solution to a final concentration of 10 mM. Drug stocks were further diluted in Ca^{2+} Tyrode's solution prior to pharmacological testing with the final DMSO concentration in the experimental solution not exceeding 0.03% (v/v). The details of the drugs and concentrations used in this study are listed in Table 2.2.

Table 2.2. List of drugs and doses used in this study.

Compound	Primary Target(s)	Dose Range
Dofetilide	I_{Kr}	3, 10, 30, 100 nM
Vernakalant	I_{Na}, I_{Kur}, I_{KACh}	1, 3, 10, 30 µM
AVE0118	I_{Kur}, I_{KACh}, I_{to}	0.3, 1, 3, 10 µM
UCL1848	I_{SK}	0.3, 1, 3, 10 µM
4-aminopyridine	I_{Kur}	10, 30, 50, 100 µM
Nifedipine	$I_{Ca,L}$	10, 30, 100, 300 nM
Carbachol	M2 receptor; activates I_{KACh}	10 µM

2.8. Data Analysis

2.8.1. Waveform and Duration Analysis

Preliminary waveform analysis was performed by the custom-written IDL software. Signal photobleaching was corrected using a polynomial fit. All data were obtained from twelve regions of interest from each well covering the whole surface area in between the stimulation electrode (1 cm^2). Averaged traces were obtained from 18 consecutive cycles of AP and CaT. Duration measurement starts at 50% of upstroke and ends with the indicated percentage of repolarization (APD) or Ca^{2+} decay (CaTD) (Figure 2.6). All data visualizations were created using the ggplot2 library in R programming environment (version 3.6.0).

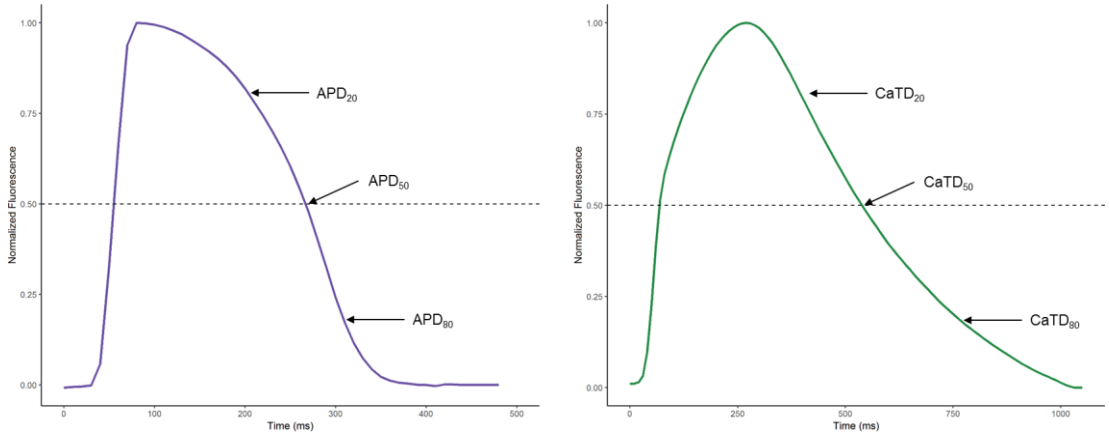

Figure 2.6. Measuring the durations of AP and CaT.
Action potential (left panel – purple) and Ca^{2+} transient (right panel – green) of hiPSC-vCMs. Dashed line indicates the level of normalized fluorescence at 50% where duration measurement starts at 50% of upstroke in both AP and CaT. Examples show the duration at 20%, 50%, and 80% of repolarization (APD_{20}, APD_{50}, and APD_{80}) and Ca^{2+} decay ($CaTD_{20}$, $CaTD_{50}$, and $CaTD_{80}$).

2.8.2. Statistical Analysis

Data were presented as mean ± SEM unless noted otherwise. Baseline conditions assessing the effect of RA compared to control differentiation protocol were analyzed using an unpaired t-test. Initial analysis of drug effects within each cell type was conducted using one-way ANOVA and Tukey-HD post-hoc test (results are presented in the supplementary section). For the drug response trend analysis, a linear regression was conducted with dose values transformed to log scale (duration ~ log(dose)). To analyze drug interactions between hiPSC-aCMs and -vCMs, durations measured at drug condition were normalized to percent change to baseline condition which were then analyzed using an unpaired t-test to compare the percentage change in duration of hiPSC-aCMs vs. -vCMs at each dose. Significance level for all statistical analysis was set at $p < 0.05$. *$p < 0.05$, **$p < 0.01$, ***$p < 0.001$.

2.8.3. Analysis of the Restitution Curve

To analyze the electrical restitution curve, the duration of repolarization and diastolic interval were measured as described in Figure 2.7. Data points from variable rate or S1S2 protocol were fitted to a mono-phasic exponential association function and the data were best fit to a non-linear least squares according to the asymptotic

regression model. The parameters measured from the line fit is described in Figure 2.8. The maximum slope of the restitution curve was obtained by Equation 1.

Equation 1: $$Slope = \left(APD80max - \frac{Y0}{\tau}\right) * e^{-\frac{DI}{\tau}}$$

Where APD_{80} is the duration at 80% of repolarization; Y_0 is the y-intercept; τ is the time constant at 36.7% of the minimum APD_{80}; DI is the diastolic interval.

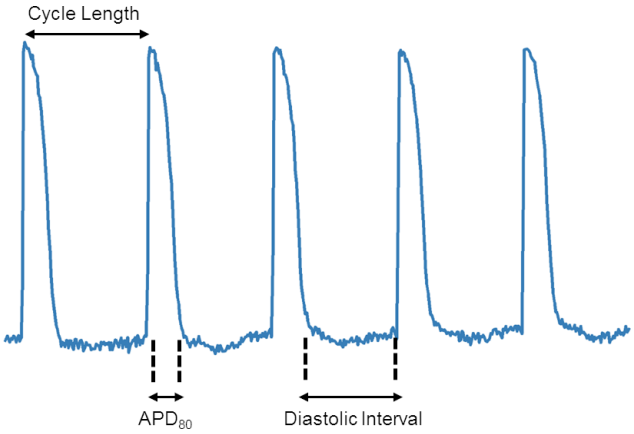

Figure 2.7. Measurement of APD_{80} and diastolic interval for analysis of restitution properties.

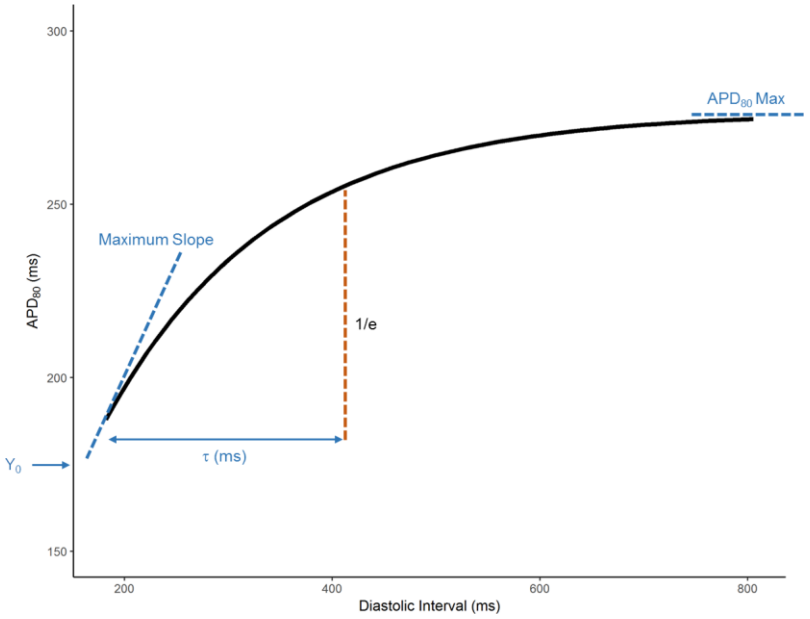

Figure 2.8. The components of the electrical restitution curve.
An example of an electrical restitution curve obtained through the variable rate protocol in hiPSC-vCMs. Thesolid black line represents the best fit mono-exponential curve. Dashed lines and arrows in blue represent the parameters measured by the exponential fit. Orange dashed line indicates the time constant (τ) of decay to e^{-1} of the peak value (36.7%) from the minimum APD_{80}.

Chapter 3.

Results

3.1. Cell Enrichment

3.1.1. Magnetic-Activated Cell Sorting Enriched Cardiac Population

To produce a more homogenous cardiac population, magnetic-activated cell sorting (MACS) was introduced as an enrichment method. As described briefly in the Methods section, the negative selection approach tags non-cardiomyocytes with antibodies conjugated to magnetic nano-beads. The non-cardiomyocytes are bound to the magnetic column leaving enriched cardiomyocytes in the flow-through. This section compares the performance of the negative selection portion of a commercial kit by Miltenyi Inc. and CD90 protocol. The CD90 protocol was adapted from the Keller Lab by my colleague Sarabjit in discussion with Dr. Stephanie Protze and I tested the efficacy of this method compared to a commercially available product. The initial testing used hiPC-vCMs stained with cTnT to ascertain the percentage of hiPSC-CMs in the total cell population.

Flow cytometry analyses showed that the Miltenyi Kit increased the final cardiac purity giving rise to a more homogenous hiPSC-CM population as quantified by increased cTnT expression (Figure 3.1.A & B). The pre-enrichment population of hiPSC-CMs displayed a mixed population with cells expressing $cTnT^+$ at a mean of 73.1 ± 5.8 %. After enrichment, the $cTnT^+$ population increased to a mean of 94.4 ± 4.0 %. The depleted non-cardiomyocytes displayed some expression of $cTnT^+$ at a mean of 22.8 ± 6.7% indicating some loss of hiPSC-CMs during the enrichment process. Additionally, the Miltenyi Kit did not affect subtype population distribution as measured by MLC-$2v^+$/$cTnT^+$ proportion (59 ± 2 % vs. 59 ± 3 %, in pre-enriched and post-enriched, respectively) (Figure 3.1.D). The test was carried out on three independent differentiation batches.

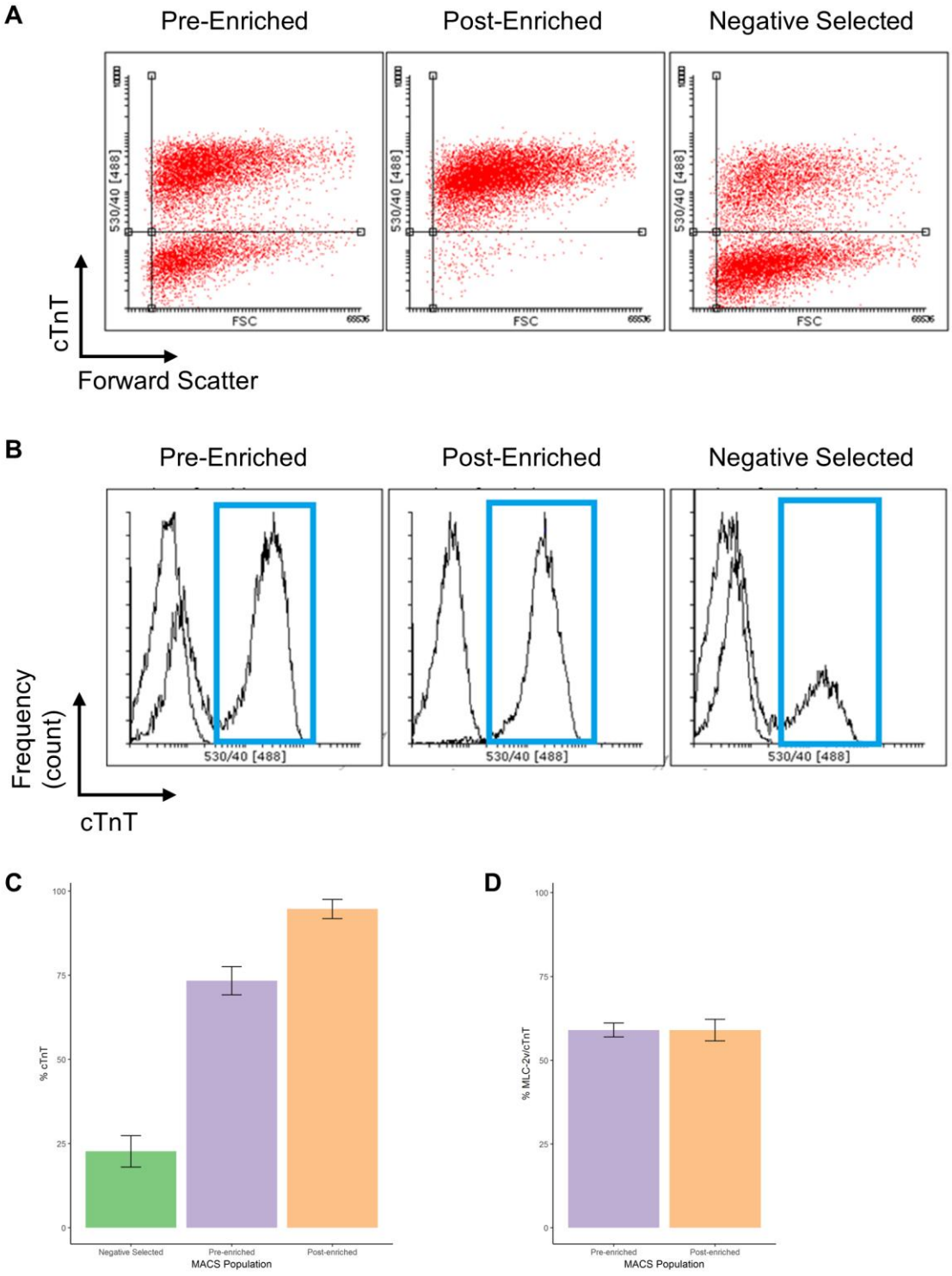

Figure 3.1. Effects of Magnetic-Activated Cell Sorting (MACS) using commerially available kit from Miltenyi Inc.

A) Flow cytometry analyses of pre-enriched, post-enriched, and negative-selected populations. B) Distribution of cells expressing cardiac troponin T (cTnT). The bue box indicates the fraction of cTnT positive cells. C) Quantification of cTnT expressing population. D) Quantification of relative MLC-2v expression.

The CD90 protocol was tested with the APC-tagged CD90 antibody titrated at three concentrations (1:1000, 1:500, 1:100). This protocol was tested on three independent differentiation batches. The success rate of cardiac enrichment at three antibody concentrations was highly variable with 1 in 3 of the test runs achieved cTnT enrichment (Figure 3.2.B). A direct comparison of the Miltenyi Kit and CD90 protocol was conducted on a single differentiation batch and this experiment showed success of the CD90 protocol with increased final $cTnT^+$ purity from 64.1% to 82.0% (Figure 3.2.A). However, the Miltenyi Kit outperformed the CD90 protocol with higher cTnT+ purity at 93.6%. Furthermore, the negative-selected population of the Miltenyi Kit contained a lower proportion of cTnT (37.7%) compared to the CD90 protocol (83.3%). Furthermore, a larger proportion of cardiomyocytes were present in the negative selected population indicating non-specificity of the CD90 antibody (Figure 3.2.C).

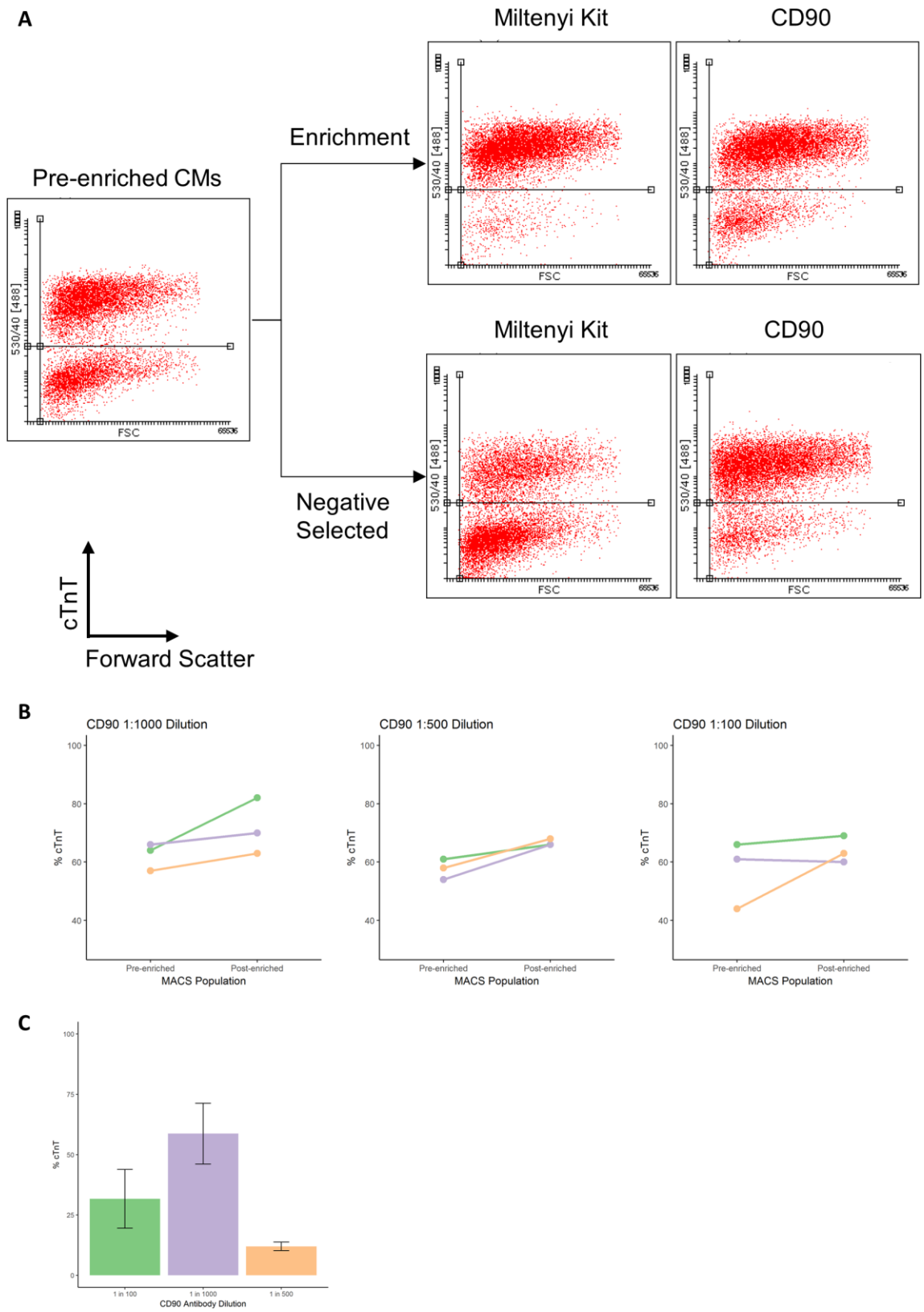

Figure 3.2. Magnetic-activated cell sorting (MACS) using negative selection of CD90 antibody.

A) Comparison between Miltenyi kit and CD90 protocol. B) Quantification of cTnT population with CD90 antibody dilution. Each data point represents an independent differentiation batch. C) The expression of cTnT in negative selected population in CD90 antibody dilution.

3.2. Directed Differentiation of hiPSC-derived Atrial Cardiomyocytes

My colleague, Sarabjit Sangha, and I worked together to develop a protocol for directed differentiation of atrial-like cardiomyocytes. Sarabjit Sangha developed and conducted the molecular assays; at the protein level using flow cytometry and at the transcriptome level using qRT-PCR. I conducted the functional assay using optical mapping. During protocol development, we conducted differentiation in parallel to demonstrate the reproducibility and robustness of the differentiation protocol under different users. To develop the atrial differentiation protocol, we systematically examined the effects of retinoic acid (RA) concentration and timing on cardiomyocyte differentiation. We finalized the atrial differentiation protocol to the daily addition of 0.75 μM RA from D4-D6 of the cardiac differentiation process.

3.2.1. RA Treatment Decreases Ventricular Population

Levels of cTnT and MLC-2v protein expression were measured using dual staining flow cytometry assay. cTnT expression demonstrates the quality of a given cardiac differentiation protocol while the presence of MLC-2v, the ventricular isoform of myosin light chain, was used as a positive marker for ventricular phenotype. Thus, a low relative MLC2v expression ($MLC\text{-}2v^{+}/cTnT^{+}$) indicates a low proportion of ventricular-like cells. Flow cytometric analyses showed that compared to the control protocol, treatment of RA at 0.75 μM during D4-D6 of cardiac differentiation significantly decreased relative MLC2v expression ($p < 0.05$) from 57 ± 1 % to 8 ± 1 % (Figure 3.3C), while maintaining cTnT expression 70 ± 4 % and 74 ± 4 %, for control and RA treatment, respectively (Figure 3.3B).

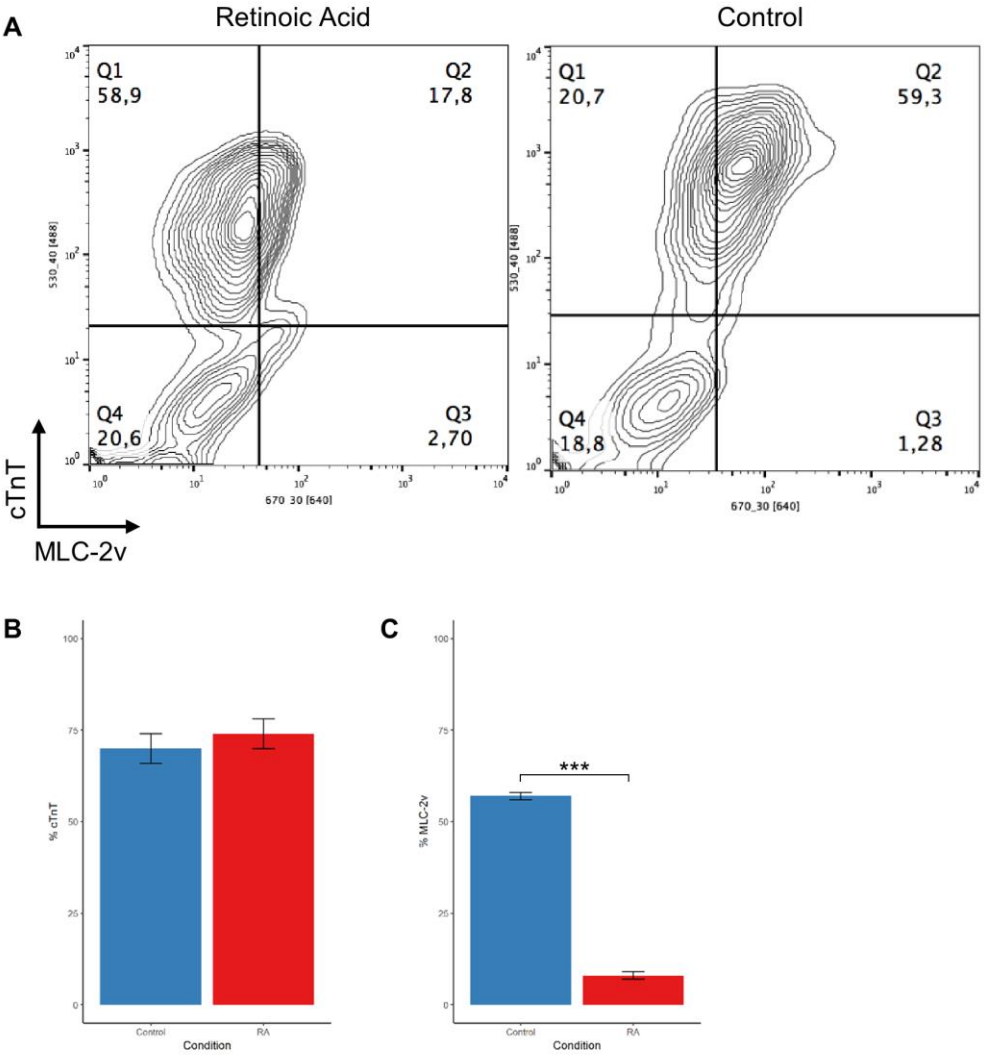

Figure 3.3. Flow cytometric analysis of RA treatment in hiPSC-CM differentiation.

A) Representative flow cytometric analysis of cTnT and MLC-2v. The proportion of B) $cTnT^+$ and C) $MLC\text{-}2v^+$ population in RA and control differentiation batches. Dual-stain flow cytometry experiments were conducted by Sarabjit Sangha. Data are presented as mean ± SEM with means compared using unpaired t-test. n = 4 (four independent differentiation batches). *** $p < 0.001$.

3.2.2. RA Treatment Upregulates Atrial-Specific Genetic Markers

As flow cytometry assay of MLC-2v is considered a negative stain for hiPSC-aCMs (Franco et al., 1999), qRT-PCR was used to measure a panel of genes to assess the trend in gene expression changes in response to RA treatment. At the transcriptome level, RA-treated CMs expressed significantly higher levels of atrial-specific ion-channels (*KCNA5, KCNJ3, CACNA1D*), transcription factor (*TBX5*), and markers (*NPPA* and

SLN), while showing significantly lower levels of ventricular markers *IRX4* (Figure 3.4) Additionally, there were no statistical in differences in expression of pan-cardiac markers *TNNT2* and *NKX2.5,* the SK channels variants *KCNN2* and *KCNN3,* and MYL2 (p-value 0.0752) (Figure 3.4). However, RA treatment significantly increased expression of nodal markers *SHOX2* and *HCN4* (Figure 3.4). For full gene names, please refer to Table 2.1 in Methods 2.4.

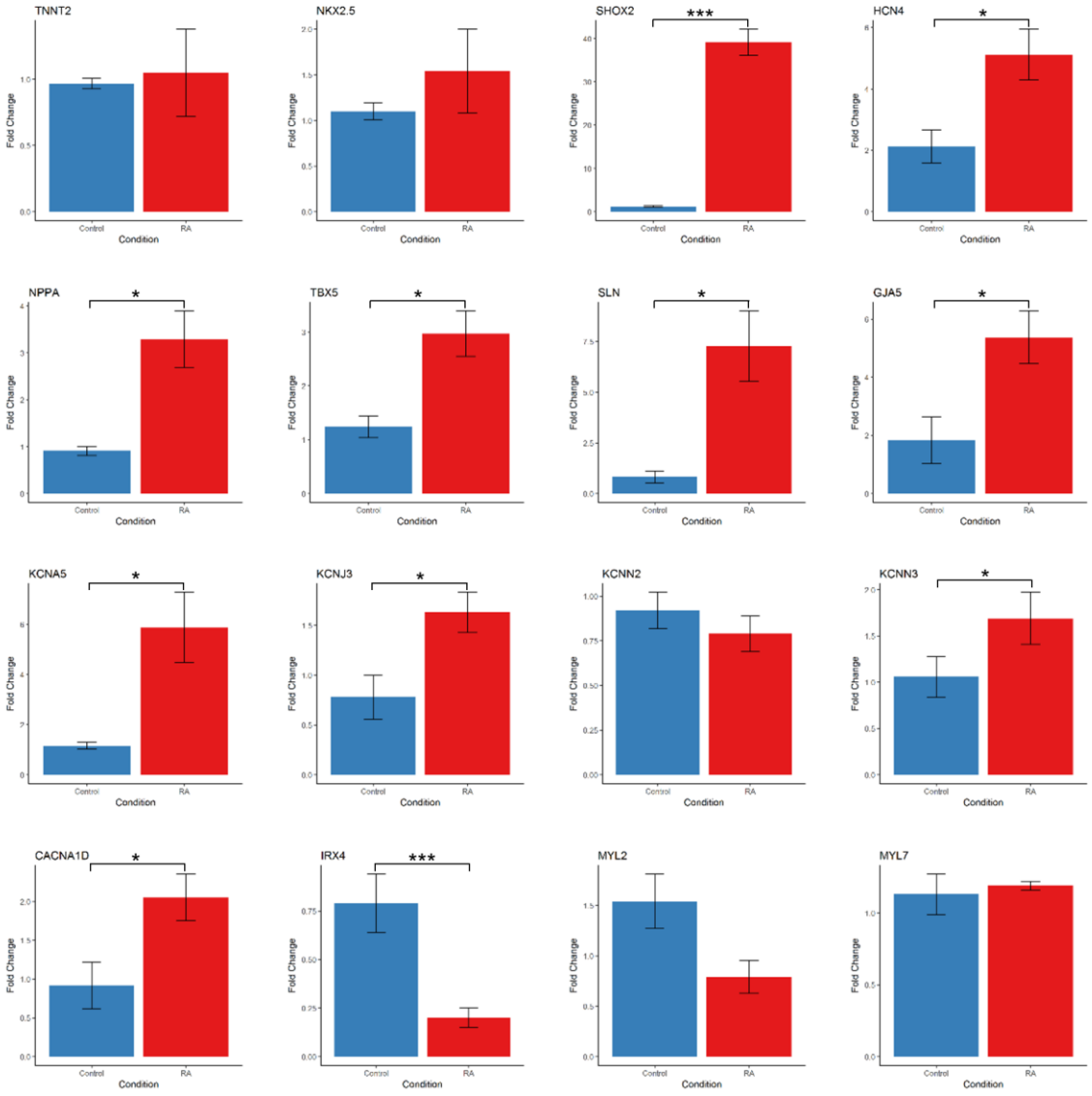

Figure 3.4. Gene expression analysis of RA treatment in hiPSC-CM differentiation.

qRT-PCR experiments were conducted by Sarabjit Sangha. For full gene names, please refer to Table 2.1 in Methods section. Data are presented as mean ± SEM with means compared using Student's t-test. n = 3 (three independent differentiation batches). * $p < 0.05$, *** $p < 0.001$

Overall, 3 doses of 0.75 μM RA at 24-hour intervals over the period of Days 4-7 of cardiac differentiation produced CMs with atrial-like genetic patterns and decreased ventricular markers. Therefore, for the remainder of this thesis, the cells generated from the RA-treated differentiation protocol are referred to as hiPSC-aCMs (hiPSC-derived atrial-like cardiomyocytes) while the CMs from the control protocol are referred to as hiPSC-vCMs (hiPSC-derived ventricular-like cardiomyocytes).

3.3. Functional Assessment of hiPSC-derived Atrial and Ventricular Cardiomyocytes

3.3.1. Atrial-CMs Have Shorter APD and Faster Calcium Cycling

The functional properties of hiPSC-aCMs and –vCMs were assessed using optical mapping with simultaneous measurement of AP and CaT by co-labelling with RH-237 and Rhod-2AM as described in the Methods section 2.6.2. Membrane voltage measurements revealed that AP of hiPSC-vCMs displayed ventricular-like AP morphology while hiPSC-aCMs displayed atrial-like morphology (Figure 3.5. A & B – upper panel; Figure C & D in purple). Paced at 1 Hz, the repolarization at 20% (APD_{20}: 84 ± 8 ms vs. 127 ± 6 ms), 50% (APD_{50}: 131 ± 12 ms vs. 191 ± 8 ms), 80% (APD_{80}: 179 ± 16 ms vs. 251 ± 12 ms) were significantly shorter in hiPSC-aCMs compared to hiPSC-vCMs (Figure 3.5.E). hiPSC-vCMs displayed ventricular-like AP morphology with a longer plateau phase as seen in the AP trace (Figure 3.5.D). However, the quantification of the plateau phase did not show statistical significance (APD_{20}/APD_{80}: 0.61 vs. 0.06 ± 0.57 ± 0.08) (Figure 3.5.F). On the other hand, both hiPSC-aCMs and –vCMs exhibited similar late repolarization kinetics as measured by the fractional repolarization ((APD_{50}-APD_{80}/APD_{80}): 0.26 ± 0.05 vs. 0.23 ± 0.05 in hiPSC-aCMs and -vCMs, respectively) (Figure 3.5.G).

The overall Ca^{2+} transient duration (CaTD) of hiPSC-aCMs was shorter than the CaTD of hiPSC-vCMs (Figure 3.5. A & B – bottom panel; Figure C & D in green). $CaTD_{20}$ (180 ± 12 ms vs. 266 ± 12 ms), $CaTD_{50}$ (282 ± 18 ms vs. 397 ± 16 ms), and $CaTD_{80}$ (474 ± 27 ms vs. 615 ± 18 ms) were significantly shorter in hiPSC-aCMs than in hiPSC-aCMs (Figure 3.5.H). Additionally, hiPSC-aCMs displayed significantly faster CaT time to peak (116 ± 7 ms vs. 246 ± 10 ms) and faster decay kinetics (τ: 350 ± 39 ms vs.

671 ± 118 ms) indicating that Ca^{2+} handling mechanics are accelerated in hiPSC-aCMs (Figure 3.5.I & J).

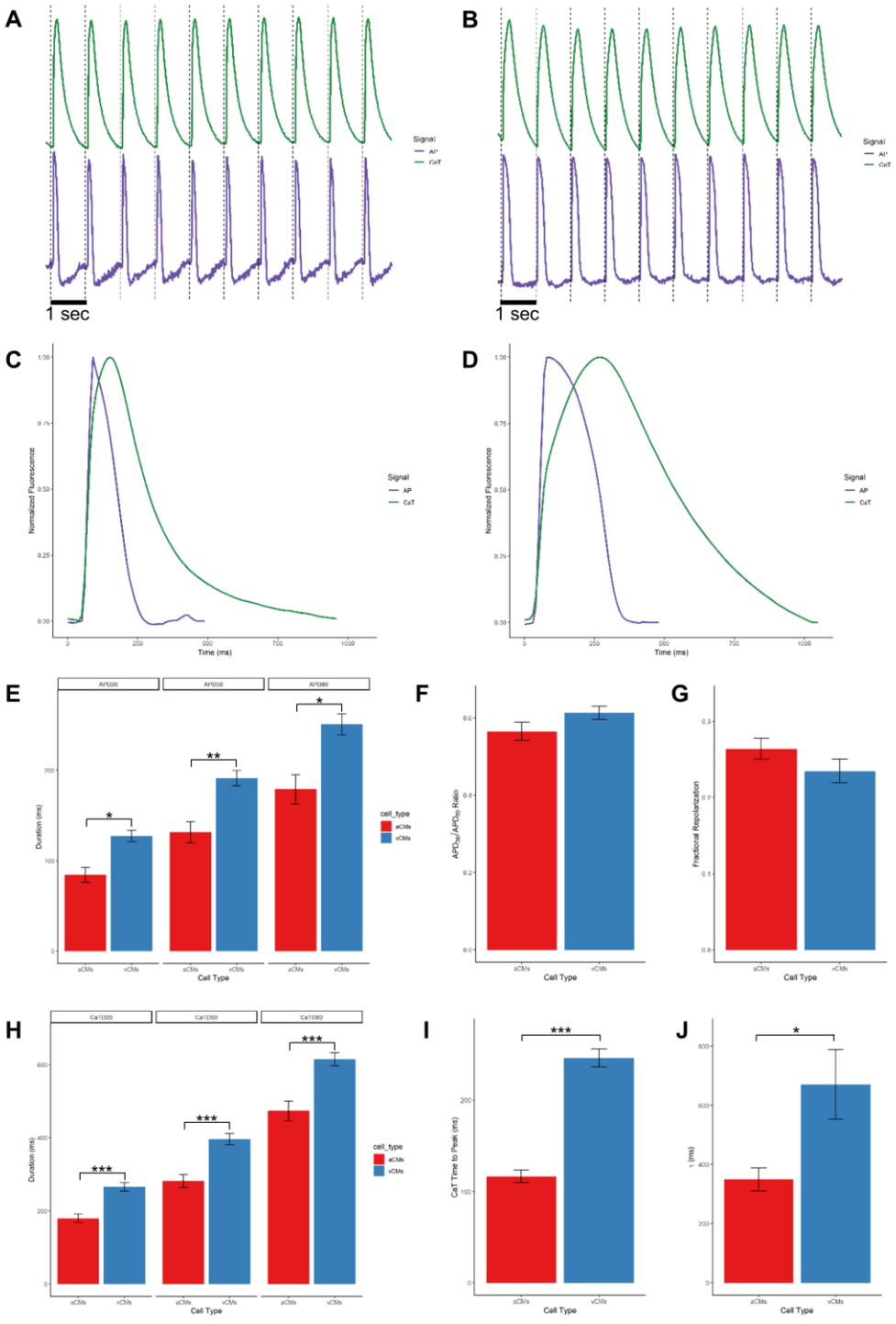

Figure 3.5. Functional analysis of hiPSC-derived atrial- and ventricular-like cardiomyocytes

Representative traces of action potential (top panel – purple) and Ca^{2+} transients (bottom panel – green) of A) hiPSC-aCMs and B) hiPSC-vCMs paced at 1 Hz. Representative averaged and

normalized traces of AP and CaT of C) hiPSC-aCMs and D) hiPSC-vCMs. E) Quantification of early- (APD_{20}), mid- (APD_{50}), and late- (APD_{80}) repolarization. F) APD_{20}/APD_{80} ratio. G) Fractional repolarization ((APD_{50} - APD_{80})/APD_{80}). H) Quantification of early- ($CaTD_{20}$), mid- ($CaTD_{50}$), and late- ($CaTD_{80}$) Ca^{2+} transient decay. I) Time-to-peak (TTP) of CaT. J) Time constant (τ) of Ca^{2+} decay. Cells were electrically paced at 1 Hz. n = 12 from 6 independent differentiation batches. Data are presented as mean ± SEM. * $p < 0.05$, ** $p < 0.01$, *** $p < 0.001$.

3.3.2. Subtype Differences in Restitution Dynamics

Electrical restitution is one of the hallmarks of cardiomyocyte function (Goldhaber et al., 2005). APD shortens with increasing heart rate due to the dynamics of ion channel activation and inactivation kinetics (Franz, 2003). A variable rate protocol was used to investigate electrical restitution dynamics in which the monolayer hiPSC-CMs were electrically paced with increasing frequency at every cycle (Methods 2.6.3).

The restitution measured at APD_{50} showed a shallow portion in hiPSC-vCMs at longer diastolic interval (Figure 3.6.A). However, the reverse is true for the electrical restitution curve measured at APD_{80} – hiPSC-aCMs displayed a flatter portion at longer diastolic interval (Figure 3.6.B). hiPSC-vCMs displayed a steadier decrease in APD_{80} at longer diastolic interval. The extensive shortening in APD_{80} starts at shorter shorter diastolic intervals for hiPSC-aCMs (< 175 ms) compared to hiPSC-vCMs (< 235 ms). The maximum slope of the restitution curve measured at APD_{80} is larger in hiPSC-vCMs compared to hiPSC-aCMs (1.26 ± 0.08 vs. 0.91 ± 0.04; Figure 3.6.E) indicating a faster kinetic in APD adaptation to higher pacing rate.

In addition to evaluating electrical restitution, I also analyzed the property of Ca^{2+} restitution (shortening of CaTD in response to increased rate. The dynamic range of CaT decreased with increasing pacing rate (Figure 3.6.). The Ca^{2+} restitution showed no difference in kinetics between hiPSC-aCMs and –vCMs when measured at $CaTD_{50}$ and $CaTD_{80}$ (Figure 3.6.C and D). In response to higher stimulation rate, shortening in $CaTD_{80}$ displayed more linear kinetics than shortening in $CaTD_{50}$ in both cell types.

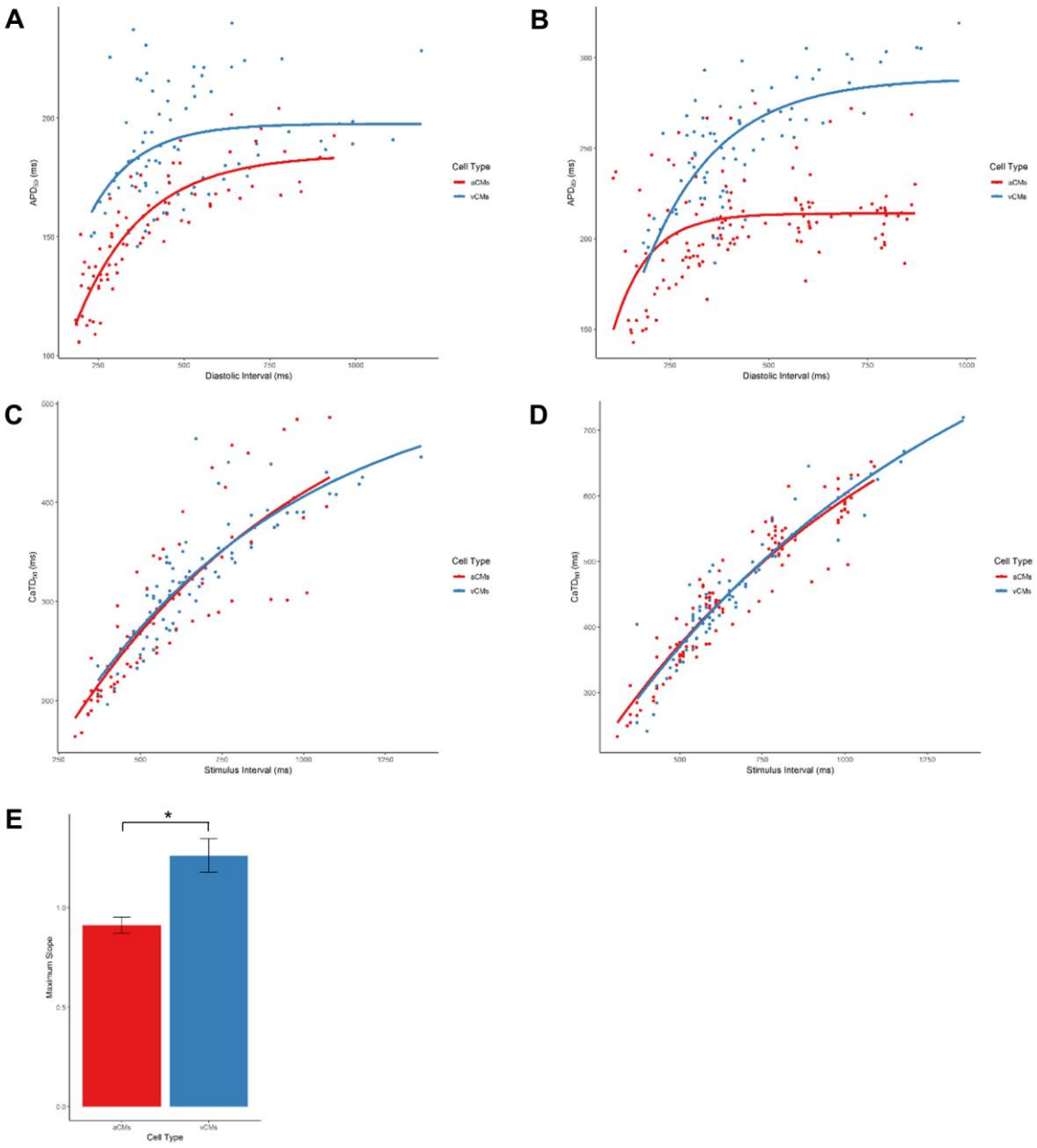

Figure 3.6. Evaluating the restitution dynamics of hiPSC-aCMs and -vCMs.
Electrical restitution dynamics measured at A) APD_{50} and B) APD_{80}. Calcium handling restitution measured at C) $CaTD_{50}$ and D) $CaTD_{80}$. E) Maximum slope of the electrical restitution measured at APD_{80}. n = 4 (four independent differentiation batches). Data are presented as mean ± SEM with means statistically compared using unpaired t-test. * $p < 0.05$, *** $p < 0.001$.

3.4. Cardiac-Subtype Specific Pharmacology

3.4.1. The Atrial-selective Response to the Clinically Relevant Compounds Vernakalant and Dofetilide

As dofetilide blocks I_{Kr} (Roden & Willerson, 2012), it served as the non-subtype selective blocker for optical mapping to detect presence of I_{Kr} in both hiPSC-aCMs and -vCMs. Dofetilide displayed main effect on both hiPSC-aCMs and -vCMs, elongating mid- (APD_{50}) and late- (APD_{80}) repolarization (Figure 3.7.A and B). Compared to baseline, dofetilide at 100 nM elongated APD_{80} from 182 ± 16 ms to 355 ± 24 ms and ventricular APD_{80} from 238 ± 20 ms to 319 ± 45 ms (Figure B.1.A and B). Interestingly, dofetilide elongated early-repolarization (APD_{20}) of hiPSC-vCMs at 10 and 30 nM while having no effect on atrial APD_{20} (Figure B.1.A and B). However, hiPSC-aCMs appeared to be more sensitive to dofetilide as APD_{80} was significantly elongated starting at 3 nM (Figure B.1.A). This is confirmed by the steeper trend in the atrial prolongation of APD_{80} (Figure 3.7.A). hiPSC-aCMs also displayed larger proportional increase in APD_{80} at all doses (Figure 3.8.A). Dofetilide linearly prolonged atrial CaTD at all levels while the effect on ventricular CaTD seemed to be attenuated at 3 nM (Figure 3.7.B). Additionally, dofetilide appeared to have only affected early- to mid- Ca^{2+} decay of hiPSC-vCMs (30 nM dofetilide elongated $CaTD_{20}$ and $CaTD_{50}$ by 33 ± 8.5 % and 30 ± 6 %, respectively) (Figure 3.8.B)

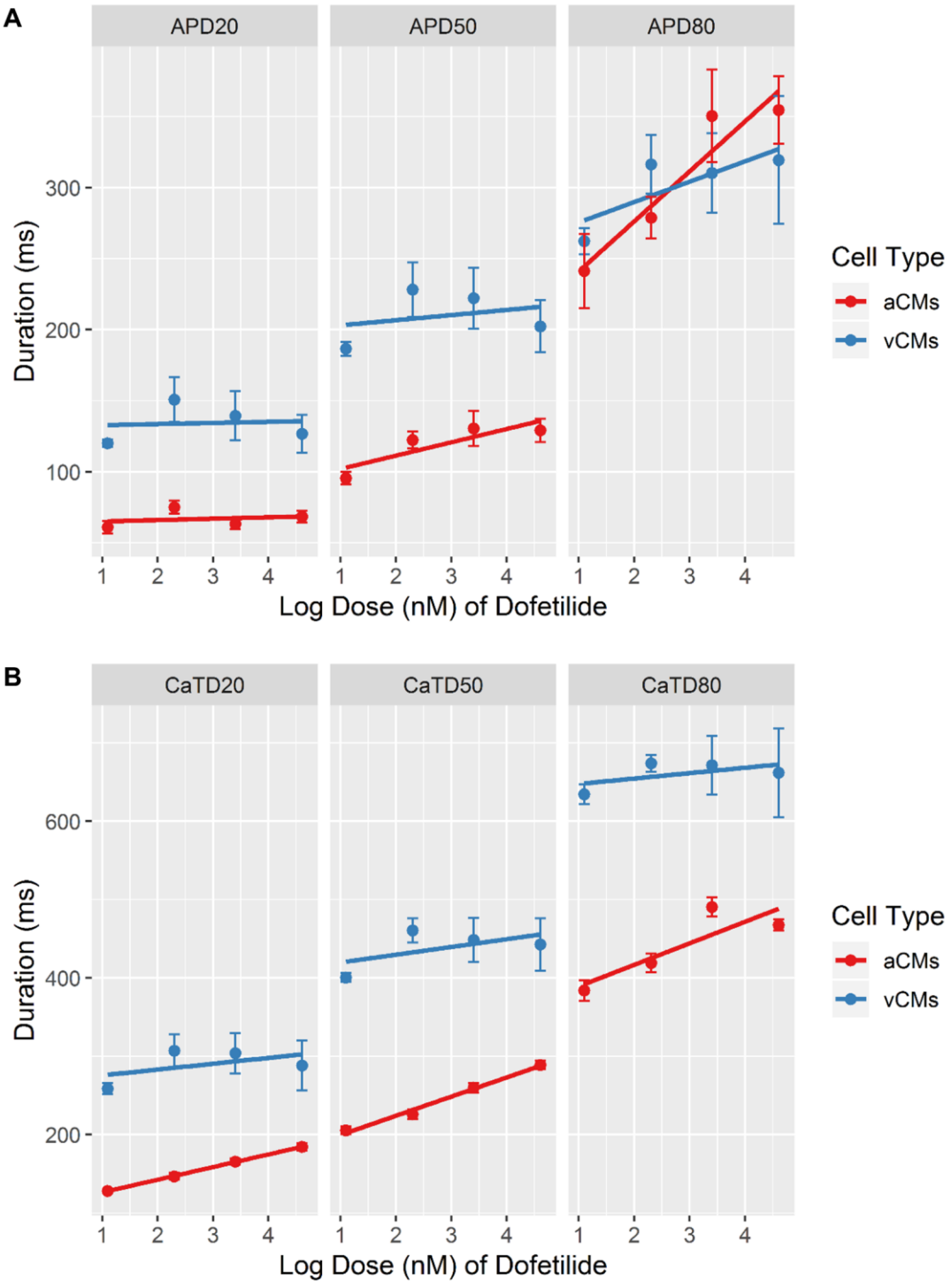

Figure 3.7. Dose-response relationship between dofetilide, duration and, cardiac cell type.

The dose response of dofetilide on A) action potential duration (APD), and B) Ca^{2+} transient duration (CaTD); both parameters measured at 20, 50, and 80%. hiPSC-derived atrial cardiomyocytes (aCMs) are shown in red while hiPSC-derived ventricular cardiomyocytes (vCMs) are presented in blue. n = 6 from six independent differentiation batches. Data are presented as mean ± SEM. Linear regression is shown as a solid line.

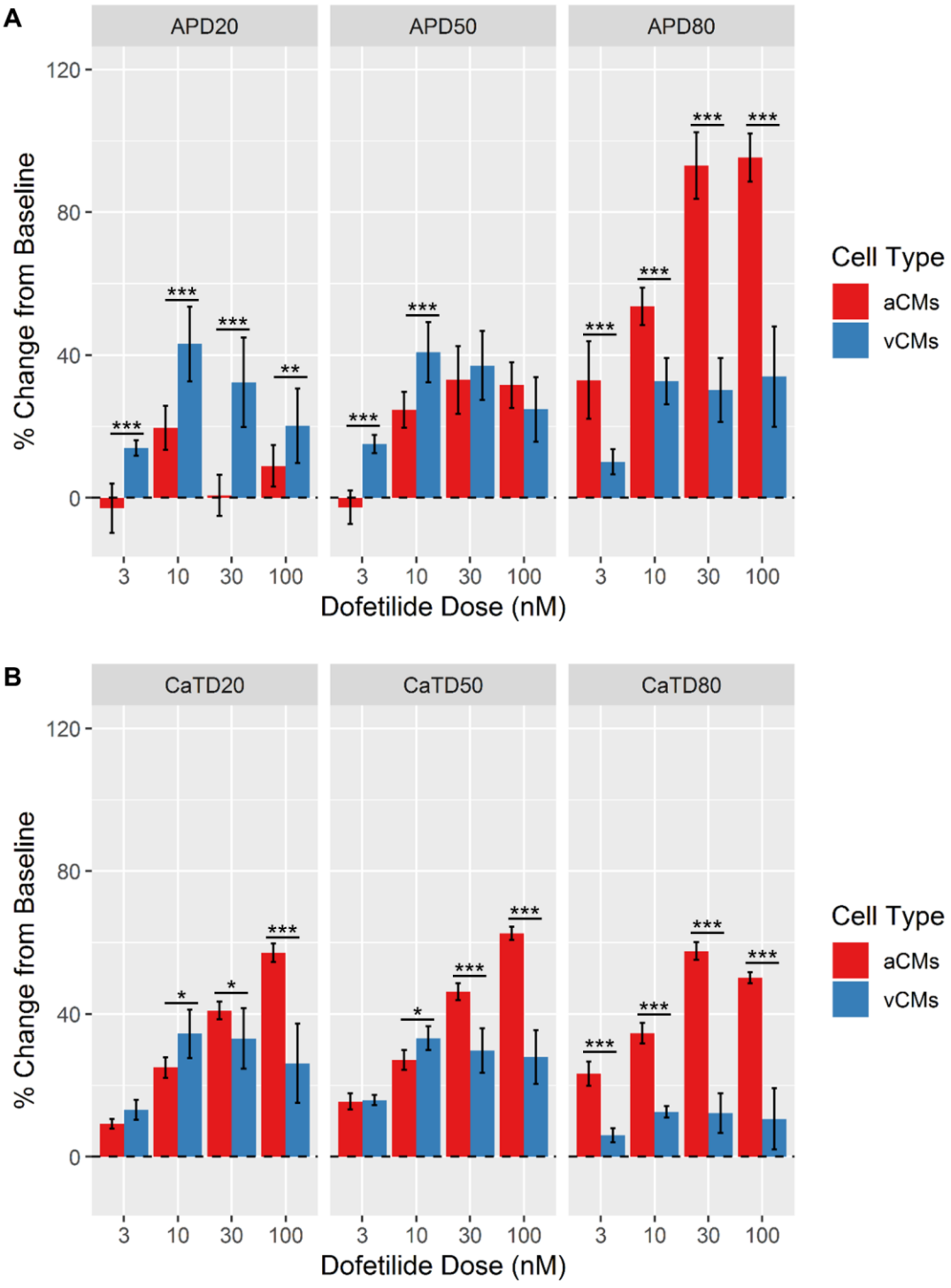

Figure 3.8. The effects of dofetilide on hiPSC-aCMs and –vCMs.
The effects of dofetilide on normalized (percent change from pre-drug baseline) A) action potential duration (APD), and B) Ca^{2+} transient duration (CaTD); both parameters being measured at 20, 50, and 80%. Dashed line is the normalized pre-drug control. n = 6 from six independent differentiation batches. hiPSC-derived atrial cardiomyocytes (aCMs) are shown in red while hiPSC-derived ventricular cardiomyocytes (vCMs) are presented in blue. Data are presented as mean ± SEM. * $p < 0.05$, **$p < 0.001$, *** $p < 0.001$

Vernakalant is a multi-ion channel blocker that blocks I_{Na} $I_{Kur,}$ I_{KAch} that is used clinically for intravenous cardioversion of patients in paroxysmal atrial fibrillation (Roy, Pratt, et al., 2008). Vernakalant elicited a positive dose response in both APD and CaTD of hiPSC-aCMs with no measureable effects on hiPSC-vCMs (Figure 3.9.A and B; Figure 3.10.A and B). Vernakalant demonstrated atrial-selectivity with statistically significant differences between APD and CaTD of hiPSC-aCMs and –vCMs at doses of 3, 10, and 30 µM (Appendix B2.A-D). Compared to APD at baseline, vernakalant at 10 µM significantly elongated atrial APD_{20}, APD_{50}, and APD_{80} by 84 ± 6 %, 70 ± 5 %, and 77 ± 4 %, respectively (Figure 3.11.A). Additionally, vernakalant at 10 µM elongated atrial $CaTD_{20}$, $CaTD_{50}$, $CaTD_{80}$ by 58 ± 4 %, 50 ± 3 %, 35 ± 5%, respectively (Figure 3.11.A). At clinically relevant concentrations (30 µM), vernakalant greatly affected early repolarization of hiPSC-aCMs (APD_{20} elongated by 124 ± 8 %) while the drug effects on atrial CaTD seem to attenuate at the same dose ($CaTD_{50}$ elongated by 57 ± 3 %) (Figure 3.11.A and B). At 30 µM, vernakalant elongated APD_{80} of hiPSC-vCM by 20 ± 7 % (APD_{80}: 238 ± 22 ms at baseline vs. 289 ± 30 ms at 30 µM), although no statistical significance was found (Figure 3.12.A; Appendix B2.D). At all doses tested, vernakalant had no statistically significant effect APD and CaTD of hiPSC-vCMs' (Appendix B2.B and D). It is important to note that vernakalant showed a tendency towards a slight shortening of early repolarization (APD_{20}) of hiPSC-vCMs (Figure 3.10.A; Figure 3.11.A). However, the sensitivity of hiPSC-aCMs was demonstrated by the steep slope of the dose-response relationship at all measured APD and CaTD parameters (Figure 3.10.A and B).

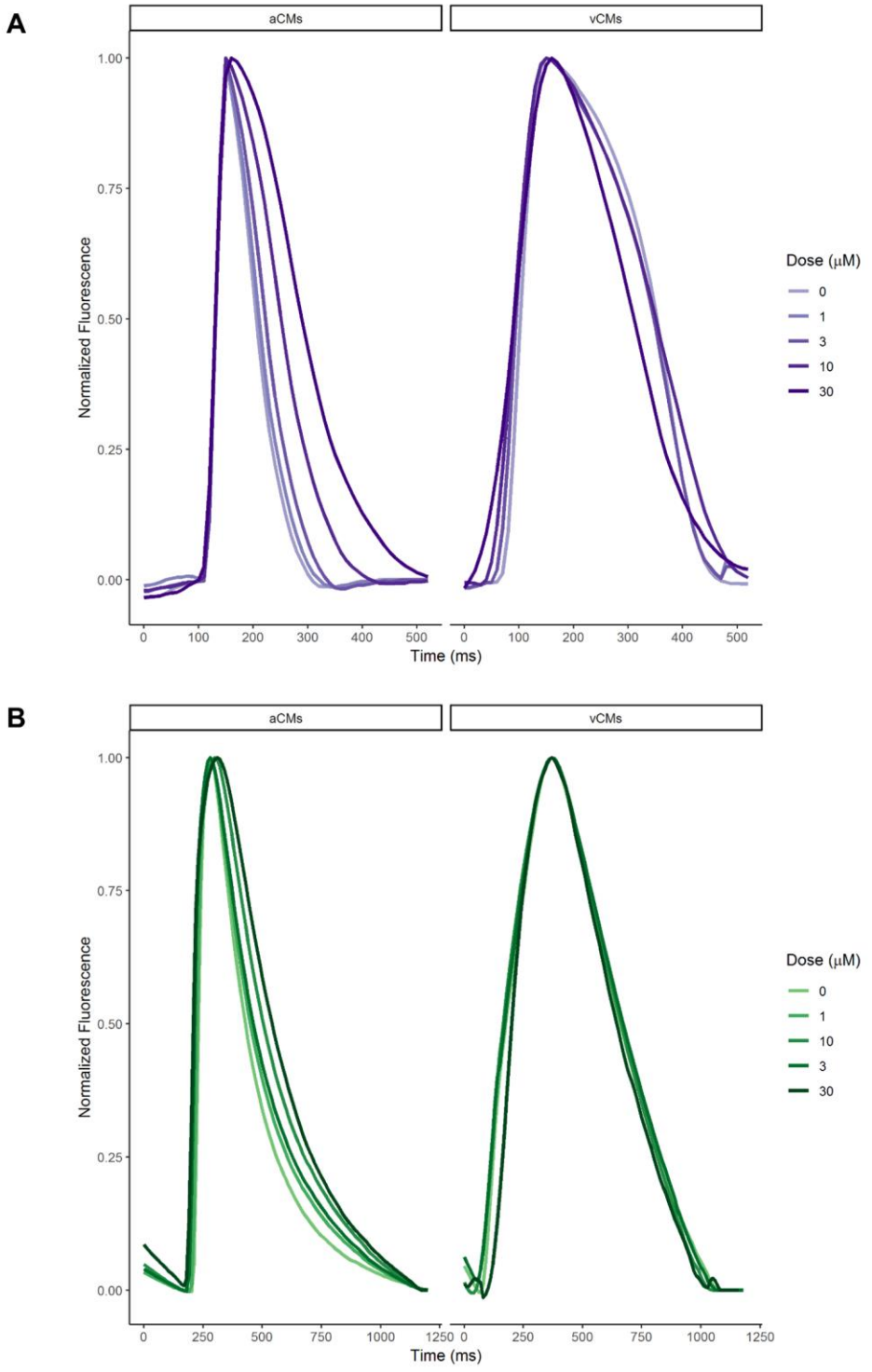

Figure 3.9. Representative traces of vernakalant effects.
Representative A) action potential and B) calcium transient traces of hiPSC-aCMs and –vCMs. Increasing drug dose is presented by the darker shade. The cells were paced at 1 Hz.

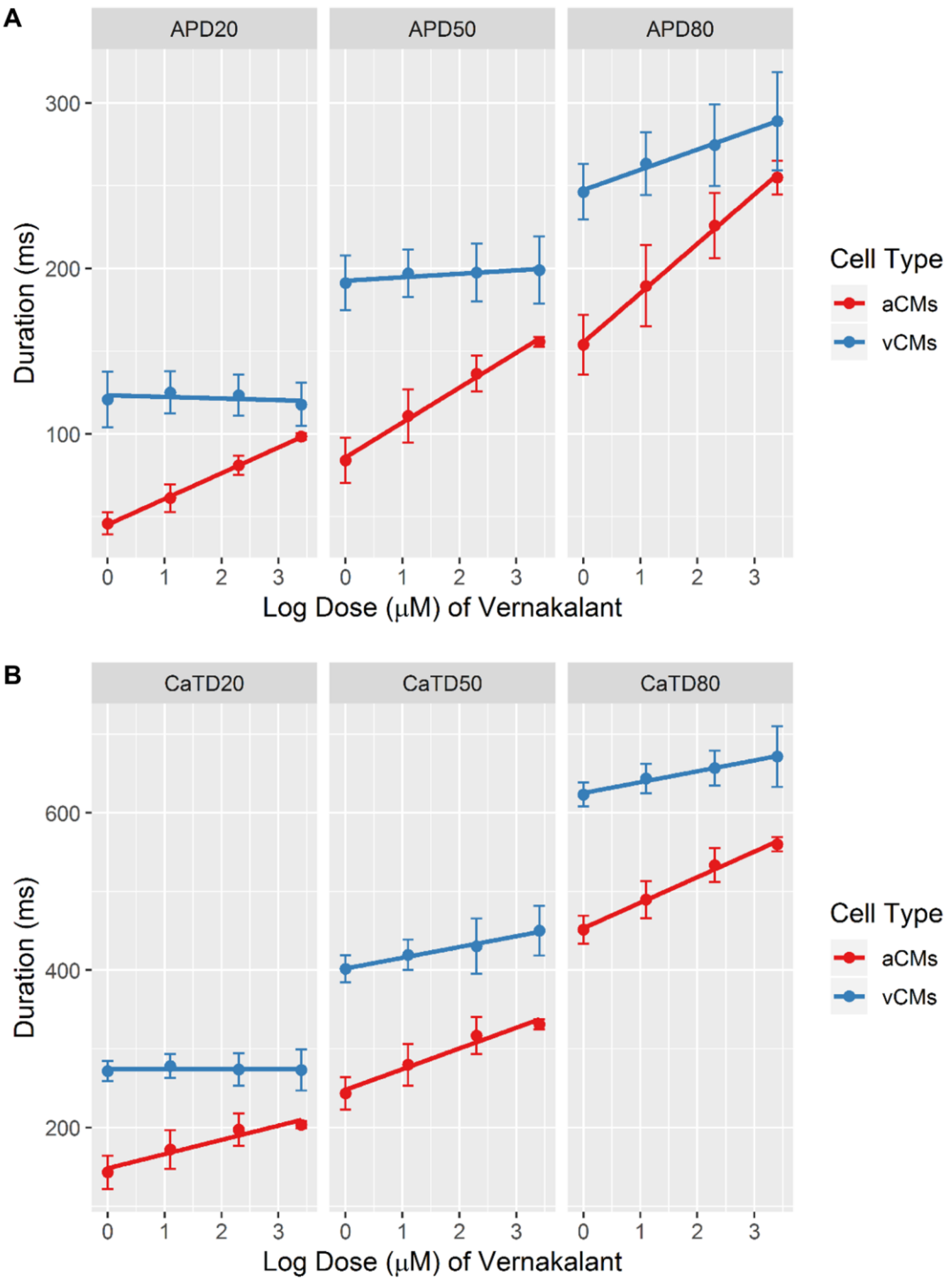

Figure 3.10. Dose-response relationship between vernakalant, duration and, cardiac cell type.

The dose response of vernakalant on A) action potential duration (APD), and B) Ca^{2+} transient duration (CaTD); both parameters were measured at 20, 50, and 80%. hiPSC-derived atrial cardiomyocytes (aCMs) are shown in red while hiPSC-derived ventricular cardiomyocytes (vCMs) are presented in blue. n = 6 from six independent differentiation batches. Data are presented as mean ± SEM. Linear regression is shown as solid line.

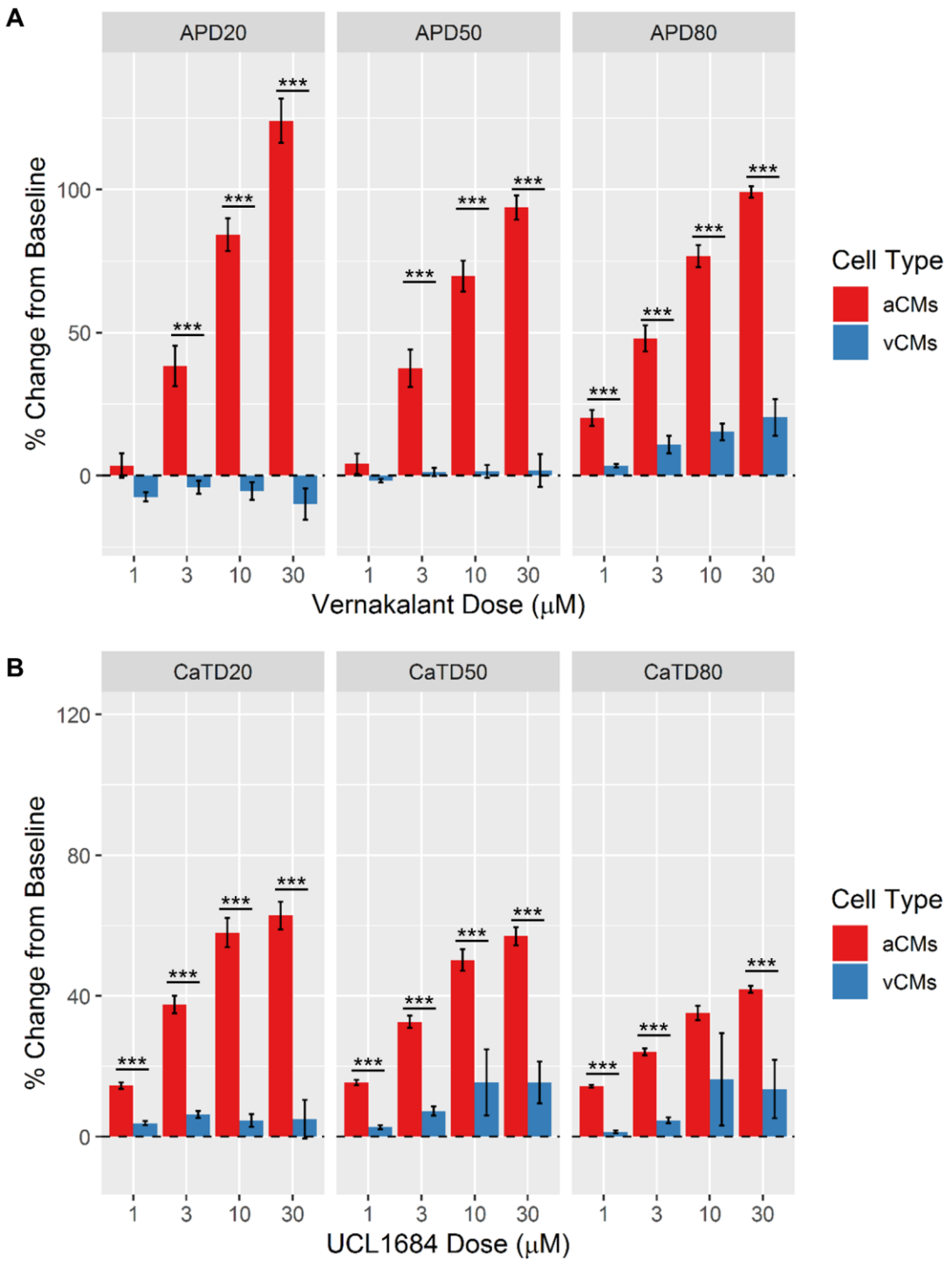

Figure 3.11. The effects of vernakalant on hiPSC-aCMs and –vCMs.
The effects of vernakalant on normalized (percent change from pre-drug baseline) A) action potential duration (APD), and B) Ca^{2+} transient duration (CaTD); both parameters were measured at 20, 50, and 80%. Dashed line is the normalized pre-drug control. n = 6 from six independent differentiation batches. hiPSC-derived atrial cardiomyocytes (aCMs) are shown in red while hiPSC-derived ventricular cardiomyocytes (vCMs) are presented in blue. Data are presented as mean ± SEM. * $p < 0.05$, **$p < 0.001$, *** $p < 0.001$

3.4.2. K_v1.5 is Specific to hiPSC-aCMs

4-aminopyridine (4AP) was used to dissect the presence of functional K_v1.5 in hiPSC-aCMs (Marczenke et al., 2017). In hiPSC-aCMs, 4AP prolonged APD and CaTD in dose-dependent manner inducing statistically significant change starting at 30 µM (Figure 3.12.A and B; Figure B.3.A and B). 4AP prolonged early-repolarization (APD_{20}) of hiPSC-aCMs by 46 ± 2 % and 66 at ± 2 % at 50 and 100 µM, respectively (APD_{20} at baseline: 82 ± 8 ms, at 50 µM: 120 ± 9 ms, at 100 µM: 131 ± 9 ms) (Figure 3.14.A; Figure B.3.A). In contrast, 4AP prolonged ventricular APD_{20} by 23 ± 4 % (APD_{20} at baseline: 138 ± 8 ms, at 100 µM: 170 ± 9 ms) at the highest tested dose of 100 µM (Figure 3.14.B; Figure B.3.B). However, 4AP significantly prolonged ventricular APD_{50} and APD_{80} starting at 50 µM (Figure B.3.B) with a linear trend (Figure 3.13.A). The atrial APD showed greater relative change to baseline at all concentrations compared to hiPSC-vCMs (Figure 3.14.A), suggesting selective sensitivity of hiPSC-aCMs to 4AP due to a greater expression of K_v1.5. This is confirmed by the steeper trend of the dose response relationship in hiPSC-aCMs (Figure 3.13.A). Additionally, overall atrial CaTD was elongated after exposure to 4AP while the drug had no effect on overall ventricular CaTD ($CaTD_{50}$ elongation from baseline: 68 ± 2 % vs. 12 ± 2 %) (Figure 3.13.B; Figure 3.14.B).

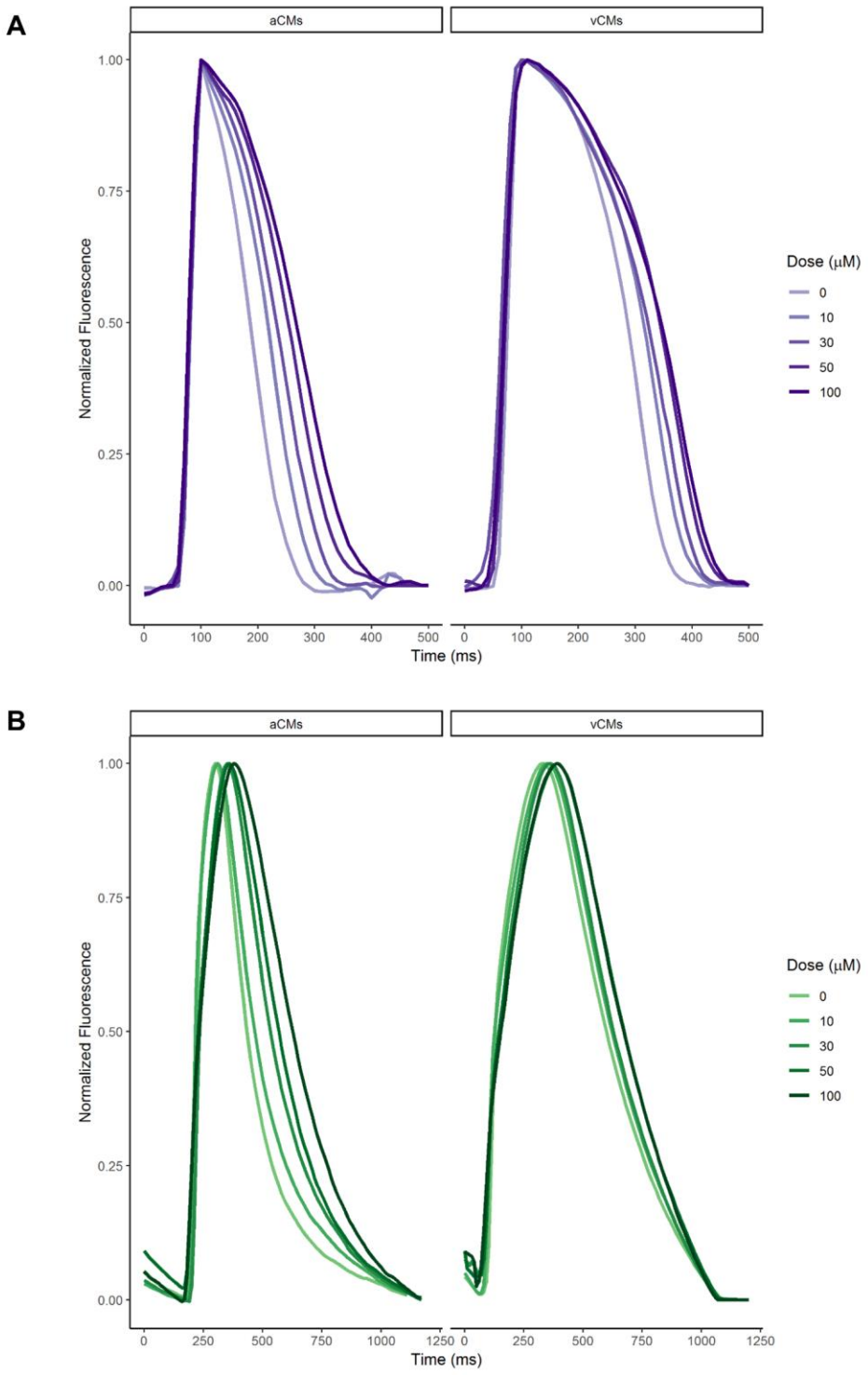

Figure 3.12. Representative traces of 4-aminopyridine effects.
Representative A) action potential and B) Calcium transient traces of hiPSC-aCMs and –vCMs. Increasing drug dose is presented by the darker shade. The cells were paced at 1 Hz.

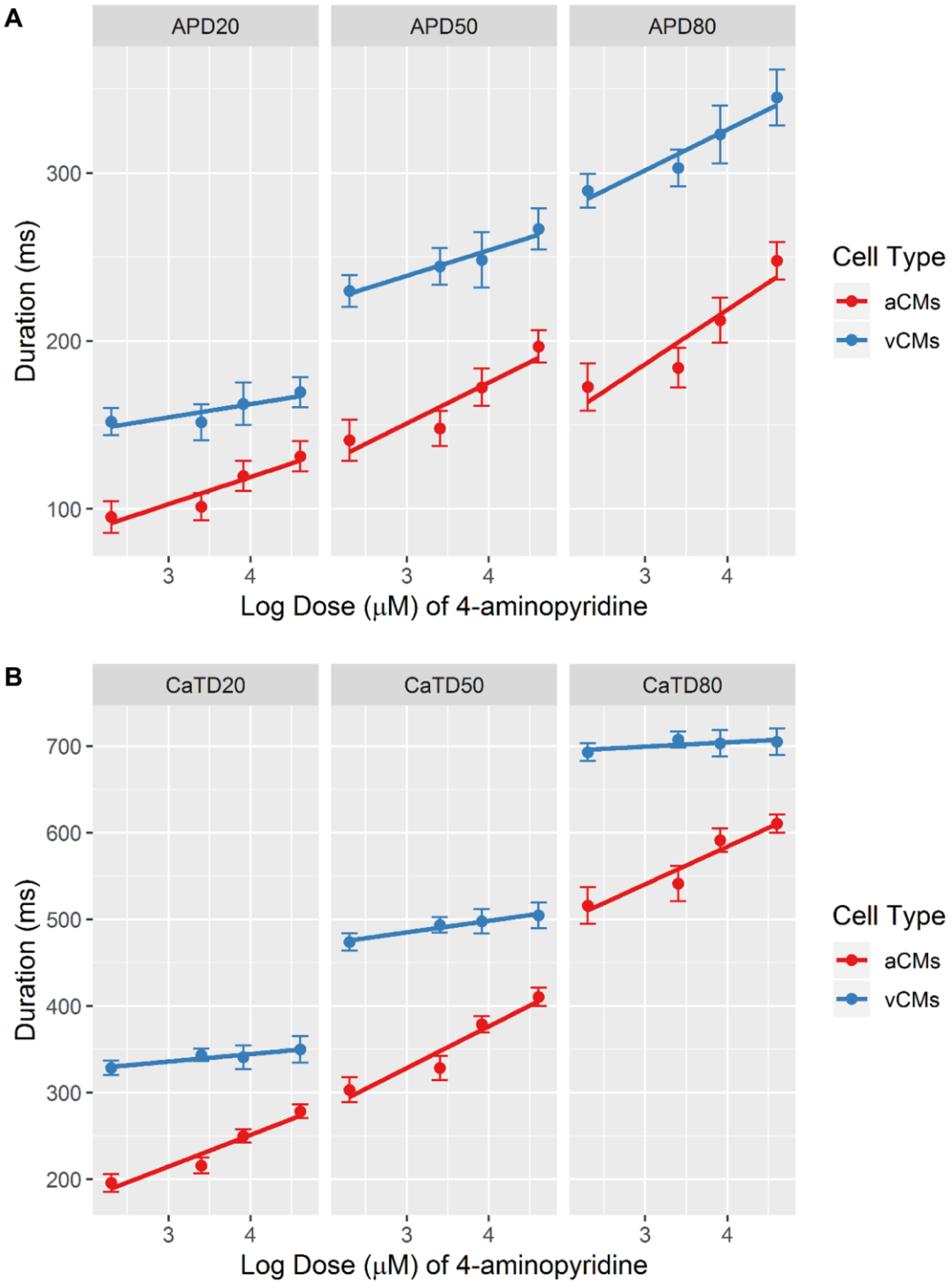

Figure 3.13. Dose-response relationship between 4-aminopyridine, duration and, cardiac cell type.

The dose response of 4-aminopyridine on A) action potential duration (APD), and B) Ca^{2+} transient duration (CaTD); both parameters measured at 20, 50, and 80%. hiPSC-derived atrial cardiomyocytes (aCMs) are shown in red while hiPSC-derived ventricular cardiomyocytes (vCMs) are presented in blue. n = 6 from six independent differentiation batches. Data are presented as mean ± SEM. Linear regression is shown as solid line.

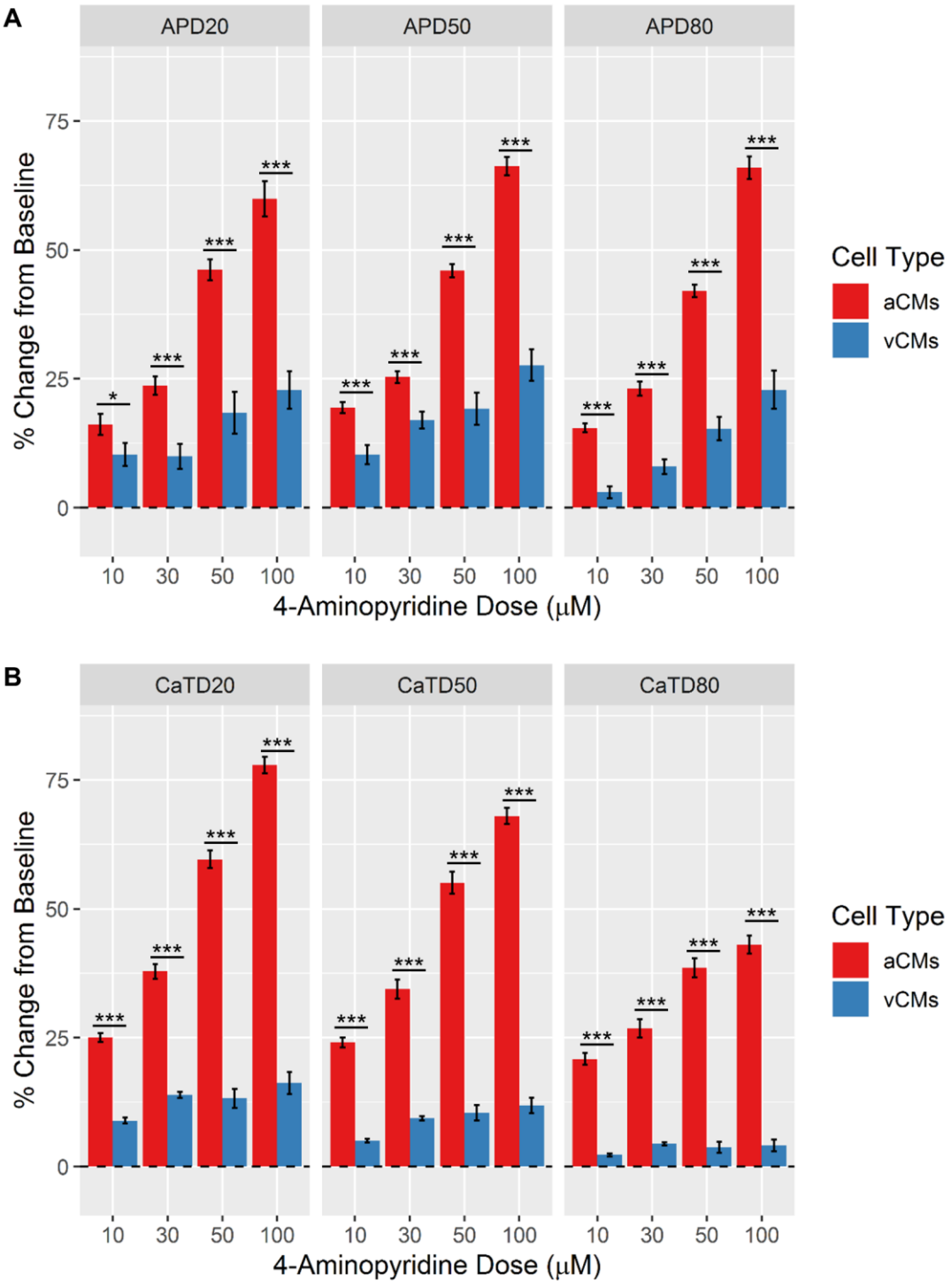

Figure 3.14. The effects of 4-aminopyridine on hiPSC-aCMs and –vCMs.
The effects of 4-aminopyridine on normalized (percent change from pre-drug baseline) A) action potential duration (APD), and B) Ca^{2+} transient duration (CaTD); both parameters were measured at 20, 50, and 80%. Dashed line is the normalized pre-drug control. n = 6 from six independent differentiation batches. hiPSC-derived atrial cardiomyocytes (aCMs) are shown in red while hiPSC-derived ventricular cardiomyocytes (vCMs) are presented in blue. Data are presented as mean ± SEM. * $p < 0.05$, **$p < 0.001$, *** $p < 0.001$

AVE 0118 is an experimental drug that blocks I_{Kur} $I_{KAch,}$ and I_{to} (Wettwer et al., 2004). The selective effects of AVE 0118 were more nuanced as the drug prolonged APD of both hiPSC-aCMs and -vCMs in a similar manner (Figure 3.16.A; Figure B.4.A and B). AVE 0118 significantly prolonged mid- and late- repolarization of hiPSC-aCMs (APD_{50} at baseline: 138 ± 9 ms, at 3 μM: ± ms, at 10 μM: 220 ± 11 ms; APD_{80} at baseline: 200 ± 14 ms, at 3 μM: ± ms, at 10 μM: 302 ± 15 ms) (Figure B.4.A). Likewise, the drug significantly prolonged APD_{50} (baseline: 174 ± 15 ms, 3 μM: 218 ± 13 ms, 10 μM: 237 ± 13 ms) and APD_{80} (baseline: 251 ± 16 ms, 3 μM: 301 ± 15 ms, 10 μM: 325 ± 14 ms) of hiPSC-vCMs at the same doses (Figure B.4.A). AVE 0118 had large effects on atrial CaTD at all tested doses ($CaTD_{50}$ at baseline: 277 ± 13 ms, at 0.3 μM: 346 ± 15 ms, at 1 μM: 382 ± 12 ms, at 3 μM: 417 ± 10 ms, at 10 μM: 427 ± 7 ms) (Figure B.4.C). In contrast, the drug significantly affected ventricular CaTD only at the highest (10 μM) tested dose ($CaTD_{50}$ at baseline: 382 ± 21 vs. 499 ± 19 ms) (Figure B.4.D).

Even though the drug effects on duration were similar between the two cell types, at 1 - 10 μM, AVE 0118 elicited a larger percentage elongation in mid- and late-repolarization (APD_{50} and APD_{80}) in hiPSC-aCMs than in hiPSC-vCMs (Figure 3.17.A). Furthermore, AVE 0118 induced a larger percent prolongation in CaTD in hiPSC-aCMs at all doses (Figure 3.17.B). Interestingly, early repolarization (APD_{20}) of hiPSC-aCMs displayed a large dose-dependent response (Figure 3.16.A) with a larger proportional prolongation at 10 μM (63 ± 2% vs. 43 ± 5%; Figure 3.17A), indicating that AVE0118 displayed small sensitivity which can likely be attributed to its $K_v1.5$ blocking component.

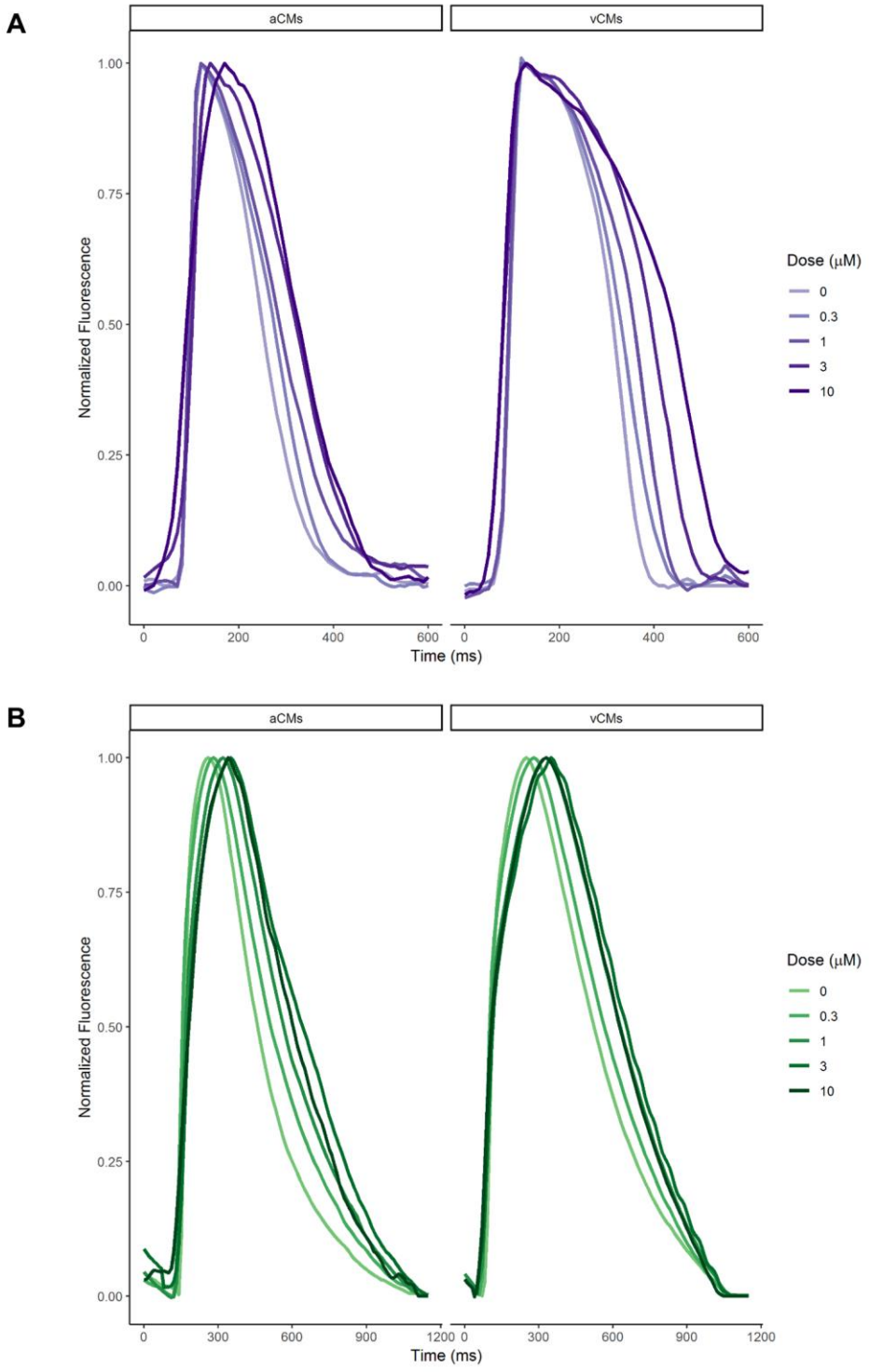

Figure 3.15. Representative traces of AVE 0118 effects.
Representative A) action potential and B) Ca^{2+} transient traces of hiPSC-aCMs and –vCMs. Increasing drug dose is presented by the darker shade. The cells were paced at 1 Hz.

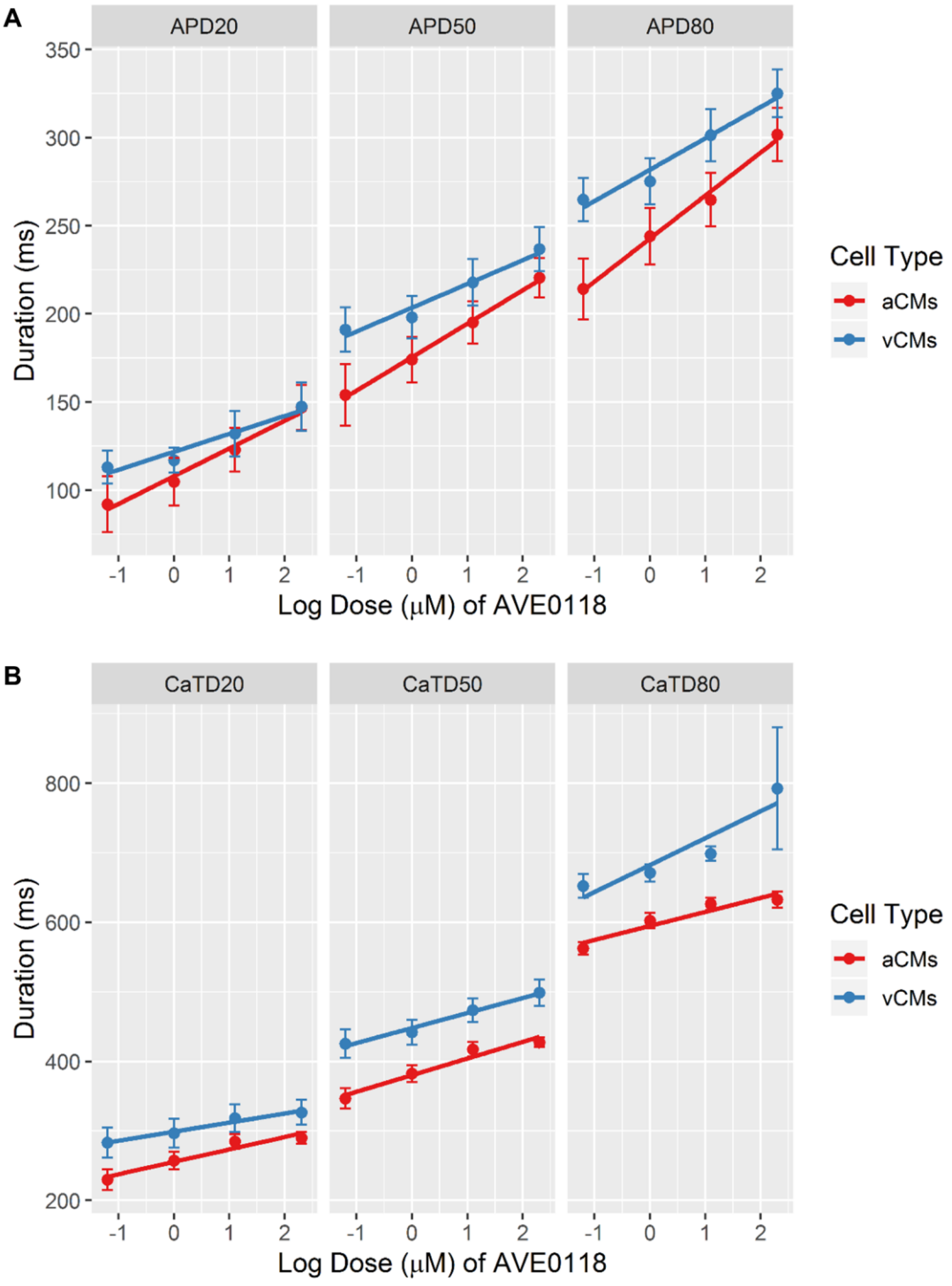

Figure 3.16. Dose-response relationship between AVE0118, duration and, cardiac cell type.

The dose response of 4-aminopyridine on A) action potential duration (APD), and B) Ca^{2+} transient duration (CaTD); both parameters were measured at 20, 50, and 80%. hiPSC-derived atrial cardiomyocytes (aCMs) are shown in red while hiPSC-derived ventricular cardiomyocytes (vCMs) are presented in blue. n = 6 from six independent differentiation batches. Data are presented as mean ± SEM. Linear regression is shown as solid line.

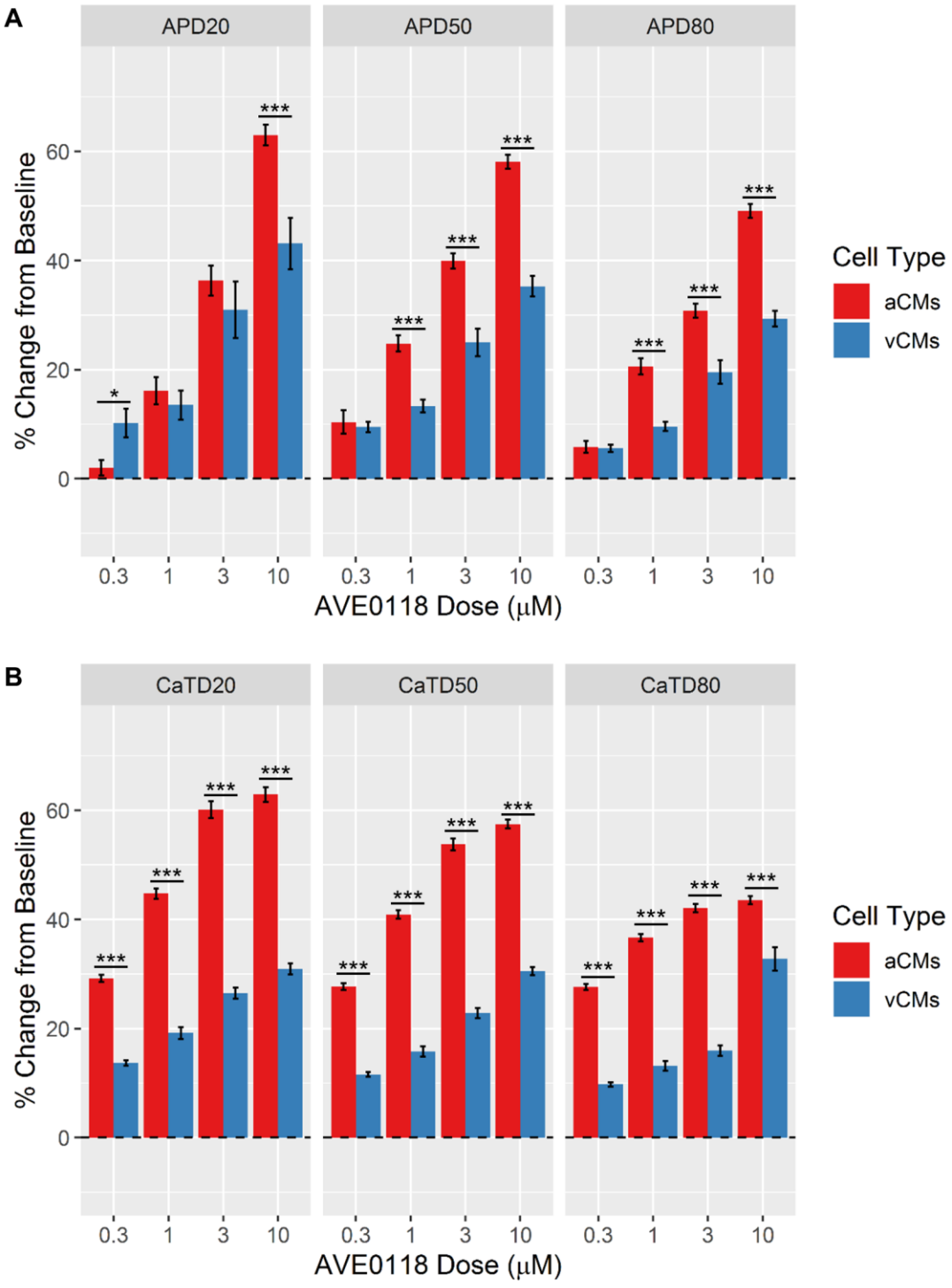

Figure 3.17. The effects of vernakalant on hiPSC-aCMs and –vCMs.
The effects of vernakalant on normalized (percent change from pre-drug baseline) A) action potential duration (APD), and B) Ca^{2+} transient duration (CaTD); both parameters were measured at 20, 50, and 80%. Dashed line is the normalized pre-drug control. n = 6 from six independent differentiation batches. hiPSC-derived atrial cardiomyocytes (aCMs) are shown in red while hiPSC-derived ventricular cardiomyocytes (vCMs) are presented in blue. Data are presented as mean ± SEM. * $p < 0.05$, **$p < 0.001$, *** $p < 0.001$

3.4.3. hiPSC-aCMs Showed No Response to Carbachol-induced I_{KAch} Activation

The acetylcholine activated K^+ current (I_{KAch}) is one of the major determinants of the electrophysiogical behavior of human atrial myocytes (Machida et al., 2011). To characterize I_{KAch} in hiPSC-aCMs, carbachol (CCh) was used to activate the Kir3.1/3.4 channel complex through the M2 receptors and elicit I_{KAch}. In my study, CCh did not affect APD and CaTD of either hiPSC-aCMs or hiPSC-vCMs (Figure 3.18.A-F).

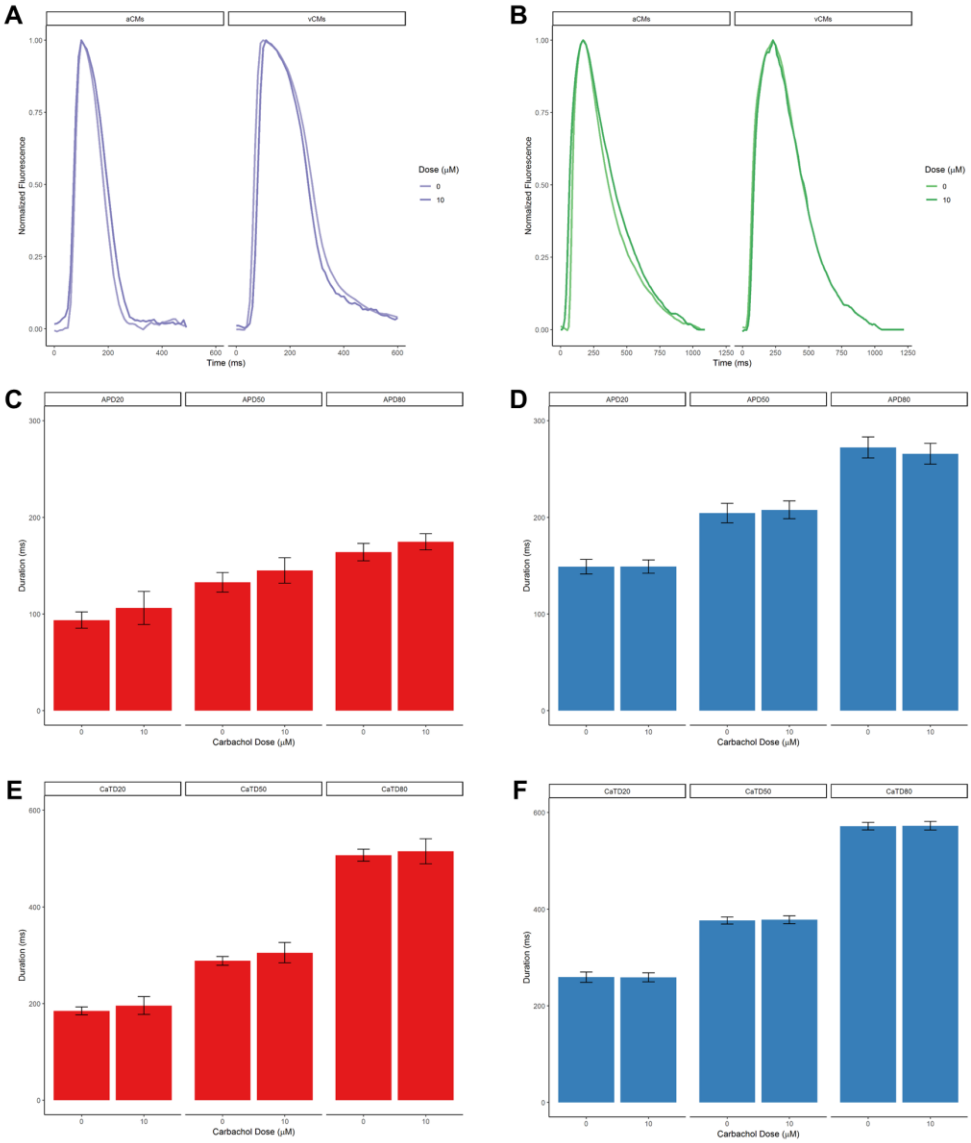

Figure 3.18. The effects of carbachol on hiPSC-aCMs and –vCMs.
Representative traces of A) action potential and B) Ca^{2+} transient. The effects of carbachol on hiPSC-aCMs (C: APD; D: CaTD) and hiPSC-vCMs (E: APD; F: CaTD). Data are presented as mean ± SEM for durations. n = 3 (three independent differentiation batches).

3.4.4. hiPSC-aCMs Possess Functional SK3 Channels

UCL 1684 is a potent direct pore blocker of the SK1-3 channels and was used to test functional SK3 channels in hiPSC-aCMs (D Strøbaek et al., 2000). UCL 1684 induced a visible dose-dependent response of atrial AP and CaT (Figure 3.19.A and B). The sensitivity of hiPSC-aCMs to UCL 1684 was reflected in the positive linear trend of the dose-response relationship (Figure 3.20.A). In contrast, UCL 1684 induced a minimal prolongation in APD_{80} of hiPSC-vCMs (Figure 3.20.A) which strongly demonstrated the drug specificity. In hiPSC-aCMs, UCL 1684 significantly elongated atrial APD_{80} from 136 ± 11 ms to 205 ± 32 ms at 10 μM (Figure B.5.A). At 3 and 10 μM, the drug induced significantly larger percentage change in APD_{50} and APD_{80} of hiPSC-aCMs than in hiPSC-vCMs (Figure 3.21.A). At 10 μM, UCL 1684 elongated overall atrial CaTD compared to baseline ($CaTD_{50}$: 254 ± 24 ms vs. 188 ± 8 ms; Figure B.5.A and B). UCL 1684 induced statistically significant elongation in late-repolarization (APD_{80}) of hiPSC-vCMs at 3 μM (Figure B.5.A). There were no measurable differences in proportional elongation of APD between hiPSC-aCMs and hiPSC-vCMs at lower doses of UCL 1684 (0.3 and 1 μM) but the drug had statistically significant effects at 3 and 10 μM on late-repolarization (APD_{80}) of hiPSC-aCMs (Figure 3.21.A). However, hiPSC-aCMs exhibited a high degree of variability in the drug response with percent change of APD_{80} from baseline to 10 μM showing 49 ± 11 % elongation and 95% CI [20, 78].

UCL 1684 prolonged overall CaTD of hiPSC-aCMs at all tested doses (Figure 3.20.B). This effect was observed in $CaTD_{80}$ (baseline: 300 ± 15 ms, at 0.3 μM: 372 ± 23 ms, at 1 μM: 387 ± 33 ms, at 3 μM: 413 ± 24 ms, at 10 μM: 416 ± 39 ms; Figure B.5.C). The effect on ventricular $CaTD_{80}$ was only observed at 3 and 10 μM (Figure B.5.D). The drug response of early- to mid-Ca^{2+} decay ($CaTD_{20}$ and $CaTD_{50}$) as measured by percent change from baseline appeared to be linear in hiPSC-aCMs while the CaTD of hiPSC-vCMs elongated then shortened (Figure 3.21.B)

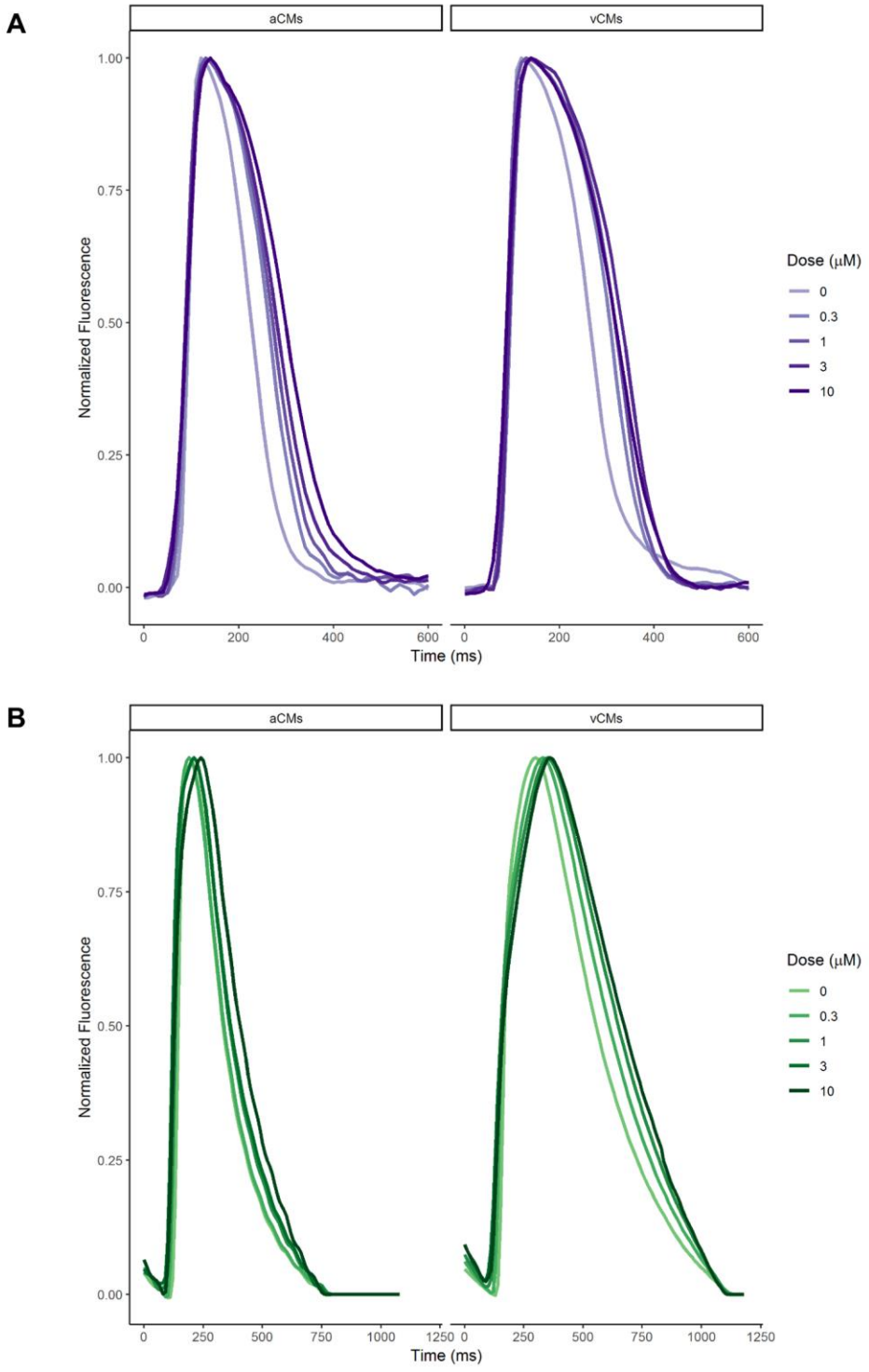

Figure 3.19. Representative traces of UCL 1684 effects.
Representative A) action potential and B) Ca^{2+} transient traces of hiPSC-aCMs and –vCMs. Increasing drug dose is presented by the darker shade. The cells were paced at 1 Hz.

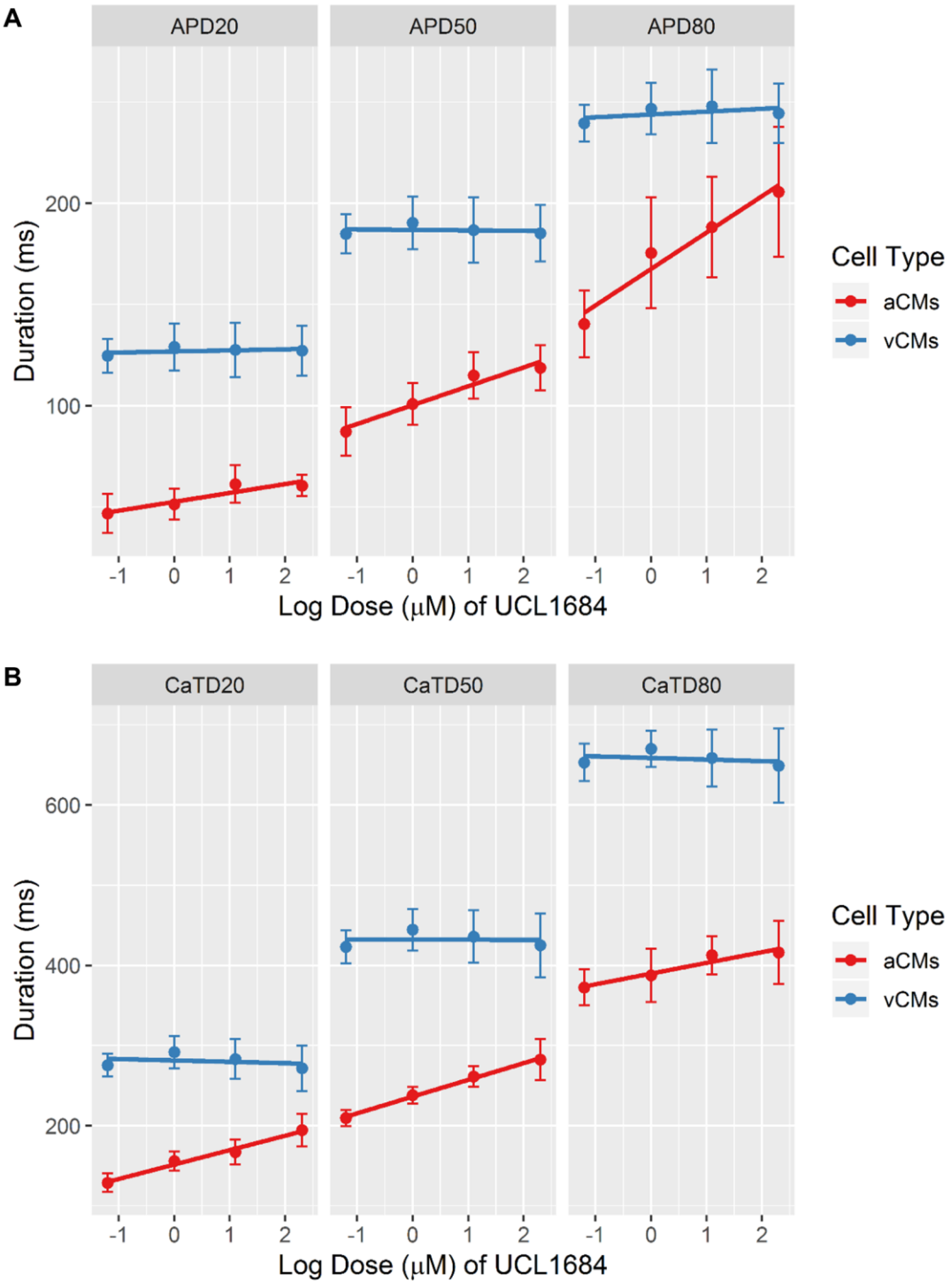

Figure 3.20. Dose-response relationship between UCL 1684, duration and, cardiac cell type.

The dose response of 4-aminopyridine on A) action potential duration (APD), and B) Ca^{2+} transient duration (CaTD); both parameters were measured at 20, 50, and 80%. hiPSC-derived atrial cardiomyocytes (aCMs) are shown in red while hiPSC-derived ventricular cardiomyocytes (vCMs) are presented in blue. n = 6 from six independent differentiation batches. Data are presented as mean ± SEM. The linear regression fit is shown as solid line.

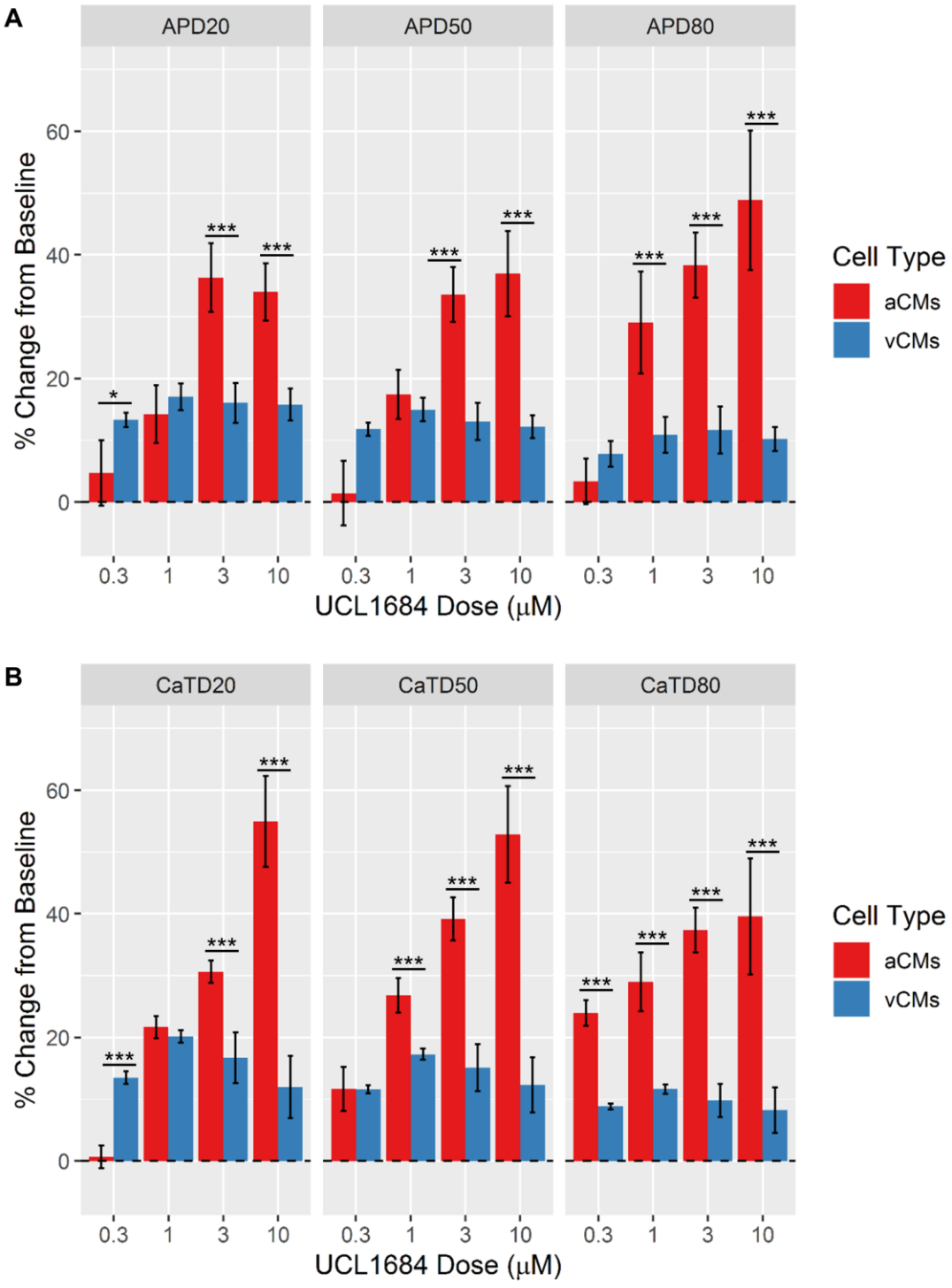

Figure 3.21. The effects of vernakalant on hiPSC-aCMs and –vCMs.
The effects of vernakalant on normalized (percent change from pre-drug baseline) A) action potential duration (APD), and B) Ca^{2+} transient duration (CaTD); both parameters were measured at 20, 50, and 80%. Dashed line is the normalized pre-drug control. n = 6 from six independent differentiation batches. hiPSC-derived atrial cardiomyocytes (aCMs) are shown in red while hiPSC-derived ventricular cardiomyocytes (vCMs) are presented in blue. Data are presented as mean ± SEM. * $p < 0.05$, **$p < 0.001$, *** $p < 0.001$

3.4.5. Ca^{2+} Handling of hiPSC-aCMs Does Not Depend on L-type Voltage-gated Ca^{2+} Channels

In native atrial myocytes, $Ca_V1.3$ is the predominant voltage-gated L-type Ca^{2+} channel (LTCC) (Gaborit et al., 2007). Nifedipine, an effective LTCC blocker with preferential blocking of $Ca_V1.2$, was used to test the functional differentiator of the main voltage-gated Ca^{2+} channel phenotypes in the two cardiac subtypes.

Although, nifedipine had no statistically significant effect on atrial APD and CaTD at all tested doses (Figure B.6.A and C), the drug slightly shortened early- and mid-repolarization as reflected in the negative trend of APD_{20} and APD_{50} (Figure 3.23.A). However, this negative trend is steeper in hiPSC-vCMs (Figure 3.23.A). Nifedipine showed effects on APD of hiPSC-vCMs at 100 and 300 nM (Figure B.6.B). At 300 nM, nifedipine decreased ventricular APD_{50} from 170 ± 14 ms to 121 ± 16 ms (28 ± 4 % shortening) and decreased $CaTD_{20}$ from 240 ± 9 ms to 169 ± 18 ms (30 ± 3 % shortening) (Figure 3.24.B; Figure B.6.B and D). At this high dose, nifedipine also collapsed the plateau phase of ventricular AP (Figure 3.22.A). Observing the percent change from baseline, nifedipine induced differential response in overall APD and CaTD between hiPSC-aCMs and –vCMs at 10, 100, and 300 nM (Figure 3.24.A and B).

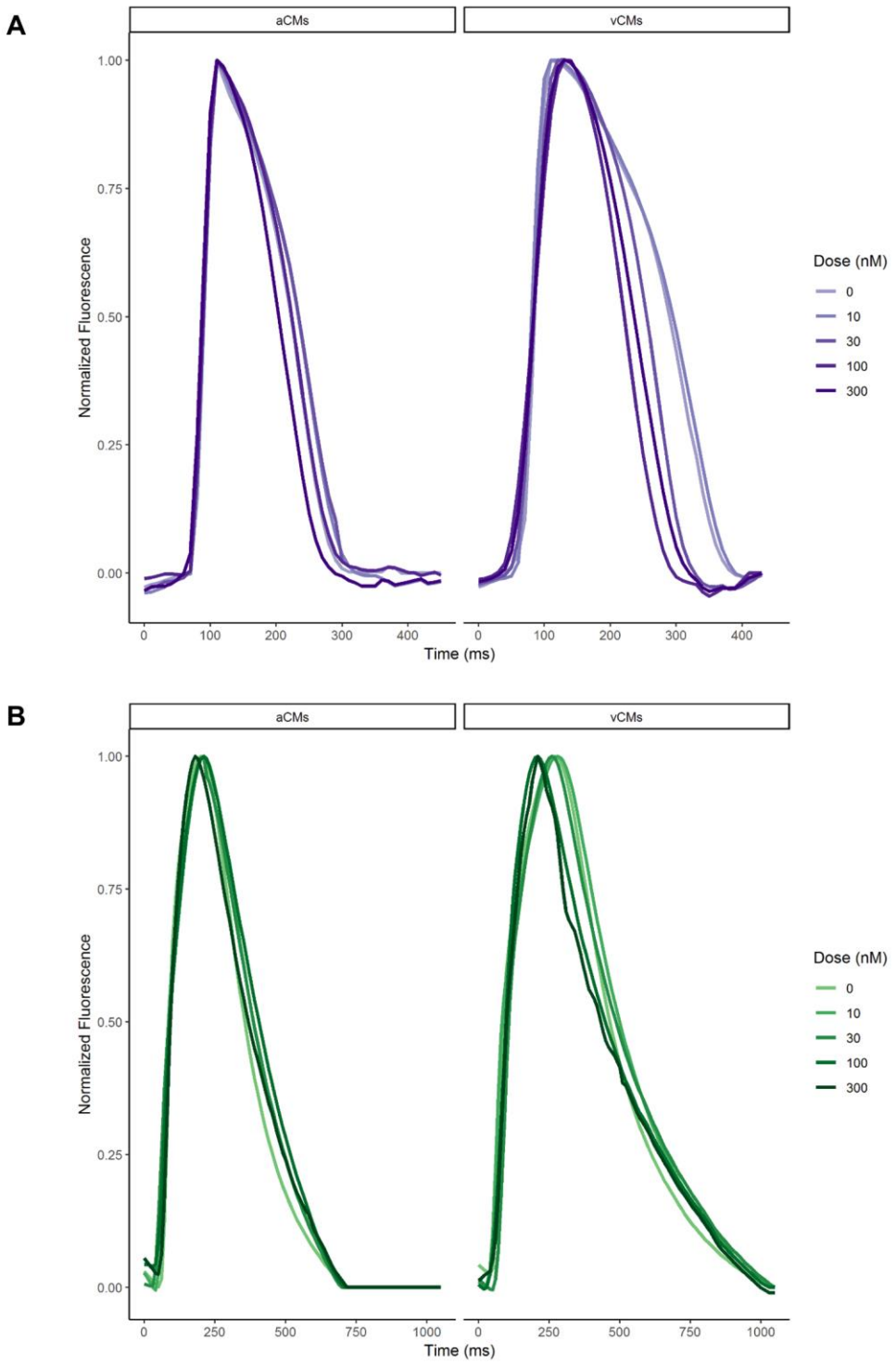

Figure 3.22. Representative traces of nifedipine effects.
Representative A) action potential and B) Ca^{2+} transient traces of hiPSC-aCMs and –vCMs. Increasing drug dose is presented by the darker shade. The cells were paced at 1 Hz.

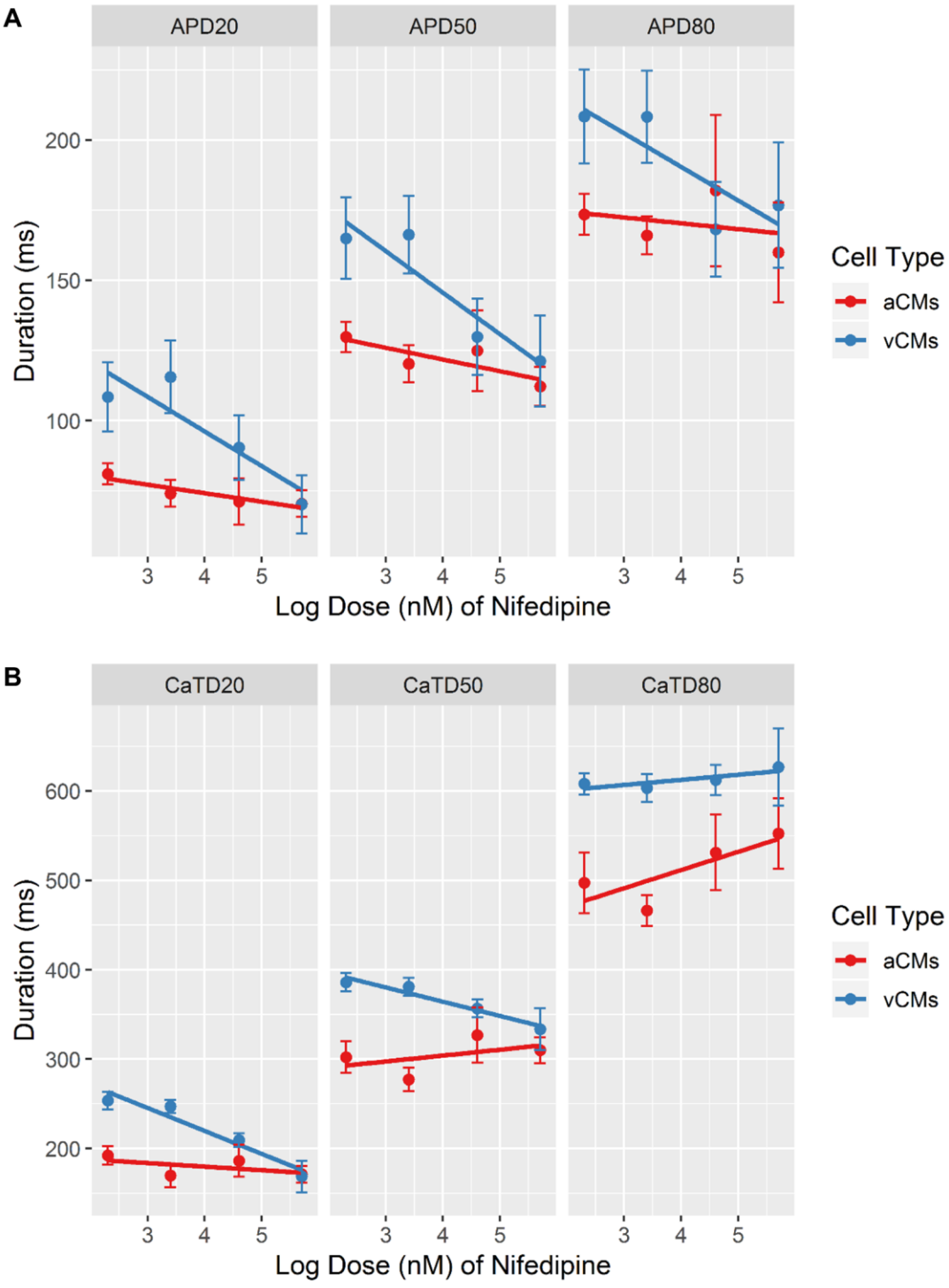

Figure 3.23. Dose-response relationship between nifedipine, duration and, cardiac cell type.

The dose response of nifedipine on A) action potential duration (APD), and B) Ca^{2+} transient duration (CaTD); both parameters were measured at 20, 50, and 80%. hiPSC-derived atrial cardiomyocytes (aCMs) are shown in red while hiPSC-derived ventricular cardiomyocytes (vCMs) are presented in blue. n = 6 from six independent differentiation batches. Data are presented as mean ± SEM. Linear regression is shown as solid line.

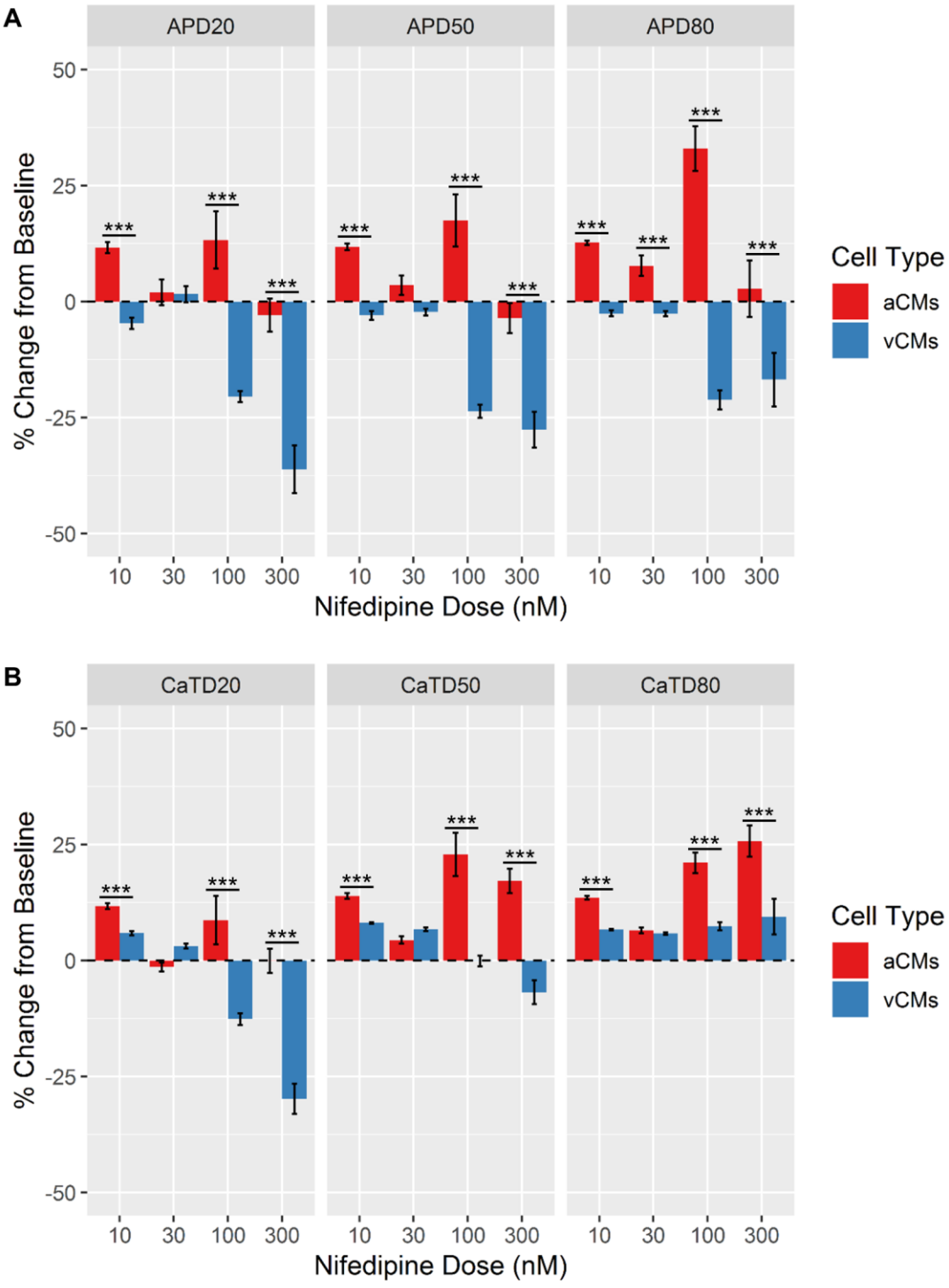

Figure 3.24. The effects of nifedipine on hiPSC-aCMs and –vCMs.
The effects of nifedipine on normalized (percent change from pre-drug baseline) A) action potential duration (APD), and B) Ca^{2+} transient duration (CaTD); both parameters were measured at 20, 50, and 80%. Dashed line is the normalized pre-drug control. n = 6 from six independent differentiation batches. hiPSC-derived atrial cardiomyocytes (aCMs) are shown in red while hiPSC-derived ventricular cardiomyocytes (vCMs) are presented in blue. Data are presented as mean ± SEM. * $p < 0.05$, **$p < 0.001$, *** $p < 0.001$

Chapter 4.

Discussion

4.1. Protocol for Atrial Differentiation

The differentiation protocol of hiPSC-CMs to a ventricular phenotype are well established (Burridge et al., 2014; Lian et al., 2013; Q. Zhang et al., 2011). However, current protocols for the generation of hiPSC-aCMs in a simplified monolayer format are limited and less characterized. Here, we applied RA during the mesoderm formation stage of the cardiac differentiation process to alter the subtype lineage and created a defined protocol for the generation of hiPSC-aCMs. We found that RA treatment in a specified time window produced a cardiomyocyte population with decreased MLC-2v^{+} proportion as well as upregulated gene expression of multiple atrial markers and downregulated ventricular marker with no observed differences in pan-cardiac markers. This suggests constant exposure to RA during mesoderm formation drives the cardiac differentiation process into the atrial lineage while not impacting cardiogenesis efficiency. Additionally, the gene expression data were comparable with a published study using a similar protocol (Cyganek et al., 2018). Our hiPSC-aCMs protocol is a simplified monolayer format based on the GiWi protocol (Lian et al., 2013), the most common hiPSC-CM differentiation protocol in literature, making it widely adaptable. The protocol we have developed is also less laborious and easier to use than embryoid body formation-based protocols (Devalla et al., 2015; J. H. Lee et al., 2017).

4.2. Functional Differences in Chamber-specific Phenotype

Electrophysiological differences are major determinants of functional differences between atrial and ventricular phenotypes. hiPSC-aCMs show atrial-like AP and Ca^{2+} handling properties. Overall, APD and CaTD of hiPSC-aCMs are significantly shorter than hiPSC-vCMs. In hiPSC-aCMs, the APs have a less pronounced plateau phase while the CaTs exhibited a more rapid rise to peak and extrusion. Even though hiPSC-aCMs displayed atrial-like AP morphology, the APD_{20}/APD_{80} ratio that is often used in literature to quantify the plateau phase, was not statistically different from hiPSC-vCMs.

The significantly shorter CaTD and faster Ca^{2+} decay kinetics suggests that hiPSC-aCMs faster Ca^{2+} extrusion mechanics.

The presence of specific ion channel currents (I_{Kur}, I_{KAch}, and I_{CaL}) underlie the functional differences between the two cardiac chamber sub-types. Here, I used a series compounds (4-aminopyridine (4AP), carbachol (CCh), and nifedipine) to dissect presence and absence of functional currents in hiPSC-aCMs and demonstrate the functional differences to hiPSC-vCMs.

The compound 4AP blocks $K_v1.4$ (I_{to}) and $K_v1.5$ (I_{Kur}) (Wang, Fermini, & Nattel, 1995). Thus, I expected 4AP to illicit a selective response in hiPSC-aCMs at a lower dose than in hiPSC-vCMs. Confirmation of the atrial expression of I_{Kur} channels was demonstrated by the stronger response of hiPSC-aCMs to 4AP at three of the tested doses (30, 50 and ,100 μM) and the increasing trend in the dose-response relationship. The effects of 4AP were observed at higher doses (50 and 100 μM) in hiPSC-vCM which is inconsistent with the findings of a recent study that showed 4AP having no effects on hiPSC-vCMs at 100 μM (Cyganek et al., 2018). The effect of the compound on hiPSC-vCMs may be due to our differentiation protocol giving predominantly a ventricular phenotype yet remains a heterogeneous population containing a small proportion of non-ventricular phenotype (i.e. atrial myocytes and nodal cells). The study that tested the effects of 4AP on hiPSC-aCMs used a protocol that claimed over 80% MLC-2v+ expression while our protocol produced MLC-2v+ population of 56% (Lemme et al., 2018). The study also employed a 3-dimensional culture technique that increased the maturation of hiPSC-aCMs thus increasing the expression density of $K_v1.5$ (Lemme et al., 2018).

Using nifedipine, I investigated the functional differences in Ca^{2+} handling dynamics between hiPSC-aCMs and -vCMs. Although we did not measure the gene expression of *CACNA1C* ($Ca_v1.2$), we can infer from the literature that the GiWi protocol produces CMs with high expression of $Ca_v1.2$ as confirmed at the transcript (Cyganek et al., 2018; Q. Liu et al., 2018) and functional levels (Argenziano et al., 2018). In this study, I demonstrated that hiPSC-vCMs are sensitive to nifedipine, with shortening of APD_{50} at 300 nM, confirming the functional presence of $Ca_v1.2$. In contrast, hiPSC-aCMs were relatively insensitive to nifedipine showing small negative linear association to dose which demonstrates that Ca^{2+} handling in hiPSC-aCMs may be reliant on other voltage-

gated Ca^{2+} channels such as $Ca_v1.3$. $Ca_v1.3$ channel is blocked less potently by nifedipine with IC_{50} of 289 nM compared to $Ca_v1.2$ IC_{50} of 2.2 nM as determined in heterologous expression of HEK cells (Y. Wang et al., 2018). Moreover, our qRT-PCR assay confirmed that hiPSC-aCMs had higher expression of *CACNA1D* ($Ca_v1.3$). This result is in line with the shorter TTP and faster decay time constant of the CaT as the kinetics of $Ca_v1.3$ are much faster than $Ca_v1.2$ (Bock et al., 2011). Additionally, we can infer that hiPSC-aCMs possess the voltage-gated T-type channel ($Ca_v3.1$), encoded by *CACNA1G*, as the expression of this channel was confirmed in the RNA-sequencing and patch-clamp study of hiPSC-aCMs (Argenziano et al., 2018). However, it is important to note that T-type Ca^{2+} channels appear in fetal/neonatal native cardiomyocytes (Robertson, Tran, & George, 2013) and may well be present in hiPSC-vCMs. Thus, it is necessary to have further pharmacological testing of T-type Ca^{2+} channels.

The results of CCh were inconsistent with the current literature. I expected late repolarization (APD_{80}) of hiPSC-aCMs to shorten upon exposure of CCh with no to minimal effects on hiPSC-vCMs. In this study, however, hiPSC-aCMs did not show a response to CCh. There are two potential reasons for the no effect observed: 1) hiPSC-aCMs may lack the appropriate muscarinic receptors (M2), and/or 2) the OM assay could not capture the effects of CCh due to the limitations of camera frame rate (100 fps). The M2 receptor gene (*CHRM2*) is not significantly expressed in hiPSC-aCMs compared to hiPSC-vCMs as described previously by RNA-sequencing data of pooled subtype-specific hiPSC-CMs (Cyganek et al., 2018). It is possible that the M2 receptor is expressed at a later more mature stage. Others have shown the sensitivity of hiPSC-aCMs to CCh, however, these studies are typically conducted using patch clamp technique to directly measure the I_{KAch} current (Argenziano et al., 2018; Laksman et al., 2017; J. H. Lee et al., 2017) or employed maturation process in their protocol. One example is Lemme et al. (2018) who used an engineered tissue approach to create 3D CM structure and measured APD using a microelectrode technique in which they found CCh at 10 µM shortened APD_{90} by a mean of 12.4% across three cell lines (data: 7.9% ± 1.6%, 20% ± 2.6%, 9.4% ± 1.7%). Taking all these data into account, it is highly probable that the OM system cannot detect a change as small as 12.4% in hiPSC-aCMs where the average APD_{80} is 179 ± 16 ms. The Orca Flash4 camera with maximum frame rate of 100 fps is likely to be insufficient in capturing a 22 ms (equivalent to 2 frames) difference in duration in our cell preparation in a statistically significant manner.

Next, I evaluated the rate-dependent properties of hiPSC-aCMs and -vCMs. The electrical restitution curve reflects the ability of the cardiac system to accommodate and is described as APD in relation to the diastolic interval (DI). The measured parameter of maximum slope of the electrical restitution curve infers the link between electrical alternans and the propensity of arrhythmogenesis in both atrial and ventricular fibrillation (Franz et al., 2012; Miyauchi et al., 2003; Narayan, Kazi, Krummen, & Rappel, 2008; Qu et al., 1999; Watanabe & Koller, 2002). A slope > 1 means that at the highest rate, small changes in DI induce a large change in APD which deposes the system to stay in alternans when alternans do occur (Franz, 2003). The electrical restitution dynamic was measured with a variable rate pacing protocol in which cycle duration decreased at each stimulus cycle. The variable rate is most suitable in optical mapping due to the limitations of the fluorescence system. Interestingly, hiPSC-vCMs displayed a maximum slope > 1 which suggests that APD_{80} shortens at a faster in relation to the diastolic interval. The maximum slope of the restitution curve of hiPSC-aCMs was < 1 which resembles the slope of restitution kinetics of clinical normal patients (Narayan et al., 2008). On the other hand, Ca^{2+} restitution does not follow the same shape as the electrical restitution displaying a more linear change at $CaTD_{80}$ suggesting that Ca^{2+} recycling kinetics in response to rate change is similar between hiPSC-aCMs and –vCMs.

4.3. Efficacy of Optical Mapping and hiPSC-CMs in Assessing Atrial-Selective Compounds

With 4AP and nifedipine demonstrating the functional differences between hiPSC-aCMs and -vCMs, I next investigated the capability of the OM assay in determining atrial-selective effects. Here, I tested a series of drugs used clinically (dofetilide and vernakalant) for AF treatment and experimental compounds (AVE 0118 and UCL 1684) that have been proposed for AF treatment due to their targeted atrial effects.

Dofetilide served as the positive control in confirming the presence of I_{Kr} in both hiPSC-aCMs and -vCMs. As expected, dofetilide affected the repolarization of both cell types. At two of the highest tested doses (300 and 100 nM), dofetilide induced a larger proportional prolongation in the late-repolarization of hiPSC-aCMs. At clinically relevant doses (3 and 10 nM), hiPSC-aCMs displayed greater sensitivity to the drug indicating the effectiveness of the drug in AF treatment. Clinically, dofetilide is used in AF

treatment, however, its clinical use is limited due to QTc prolongation and an increased risk of TdP (Jaiswal & Goldbarg, 2014). The elongation of APD_{80} which is a marker of QTc demonstrated the capability of OM in possible prediction of ventricular proarrhythmic risk *in vitro*.

Vernakalant is a touted atrial-selective compound clinically approved for intravenous cardioversion of AF (Canada, 2018). I expected vernakalant to have greater dose-dependent effect on hiPSC-aCMs than hiPSC-vCMs due to the atrial-specific K^+ current blocking component. Remarkably, vernakalant showed the most pronounced atrial-selective effects even though it is a blocker of multiple ion channels. No statistically significant change was observed in hiPSC-vCMs at early- and mid- repolarization while the slight change at APD_{80} at the clinically relevant dose (30 μM) can be attributed to I_{Na} blocking component of vernakalant. Vernakalant prolonged APD and CaTD of hiPSC-aCMs showing the sensitivity of the assay in establishing atrial selective drug effects.

hiPSC-aCMs showed slight sensitivity to AVE 0118 as demonstrated by the greater dose effect in early repolarization. Although the effects were larger in hiPSC-aCMs, AVE 0118 prolonged mid- and late-repolarization of both hiPSC-aCMs and -vCMs in a similar fashion. The drug only showed proportionally larger atrial effects on early-repolarization at the highest tested dose (10 μM). Interestingly, AVE 0118 greatly affected Ca^{2+} handling in hiPSC-aCMs compared to hiPSC-vCMs with larger proportional elongation of $CaTD_{50}$ at all doses. These results disproved my initial hypothesis that AVE 0118 would be highly specific to hiPSC-aCMs due to its I_{Kur} blocking component. Perhaps this observed effect is due to the drug binding to I_{to} (IC_{50} of 3.4 μM), producing mixed-effects at the tested doses of 3 μM. Additionally, AVE 0118 blocks I_{Kr} with IC_{50} of 9.6 μM which may explain the main effect of elongation in late-repolarization of both sub-types. The drug was also shown to be effective in terminating certain ventricular arrhythmias (Billman & Kukielka, 2008) which may be predicted based on the non-specificity observed in the optical mapping results.

The SK channel pore blocker UCL 1684 displayed high specificity and sensitivity towards hiPSC-aCMs. The drug confirmed the presence of functional SK3 channels in hiPSC-aCMs at 10 μM. However, the drug appeared to have a background effect on hiPSC-vCMs due to dose-independent prolongation of APD and CaTD at all tested doses. This can be attributed to the function of SK2 channel as UCL 1684 at this dose

also blocks the SK2 variant. Our qRT-PCR confirmed the expression of *KCNN2* in both hiPSC-aCMs and -vCMs. In native human heart, *KCNN2* is upregulated after heart failure and the expression observed in hiPSC-vCMs may likely due to immaturity. The qRT-PCR assay also confirmed that *KCNN3* was upregulated in hiPSC-aCMs. In the literature, UCL 1684 at 1 μM was sufficient in terminating rapid-burst induced AF in guinea pigs and rat models (Jonas G. Diness et al., 2011; Diness et al., 2010). Perhaps SK channel function are upregulated at high intracellular Ca^{2+} levels as seen in high beat rates of AF and a low dose of UCL 1684 can terminate AF (Jonas Goldin Diness et al., 2010). With that said, UCL 1684 has only been evaluated in animal models and has not been tested in any clinical trials.

Overall, these results demonstrated the sensitivity and specificity of the OM assay in characterizing compounds that have preferential effects on hiPSC-aCMs. By capturing the atrial-selective response of hiPSC-aCMs, we can further characterize and screen for other atrial-selective drugs for AF treatment.

4.4. MACS as an Enrichment process

The cardiac purity of any given differentiation protocol is variable. Here, we demonstrated the efficacy of MACS as a process to enrich hiPSC-CMs. Enrichment is important in the scalability and reproducibility of a higher-throughput assay and regenerative medicine. More traditional cell sorting and purification methods include fluorescence activated cell sorting (FACS) and antibiotic selection. The advantages of using MACS as the enrichment approach compared to the more traditional methods are three-fold: 1) Compared to selection through knocked-in antibiotic resistance, MACS avoids the potential issue of antibiotic “scarring” of hiPSC-CMs (Miyaoka et al., 2014) and provides the ability to enrich hiPSC-CMs generated from various lines of iPSCs as the process relies on the expression of cell surface markers native to non-cardiomyocytes; 2) FACS rely on high pressured tubes and electrical charge to sort cells making it not suitable for downstream live imaging as cell viability is greatly decreased (Ban, Bae, & Yoon, 2017); 3) The ease of use of MACS allows for minimal training and the speed of the protocol isolates millions, and up to billions, of highly-pure hiPSC-CMs in a short amount of time.

In our hands, the commercial kit performed better than negative selection of CD90 alone suggesting that CD90 alone as the negative marker may not be adequate for MACS. Overall, the CD90 protocol produced inconsistent enrichment results and thus cannot be used as the enrichment protocol of choice. CD90 is expressed in fibroblasts, however, this differentiation protocol gives rise to other non-CMs such as endothelial, smooth muscle cells and non-differentiated hiPSCs (Kisselbach, Merges, Bossie, & Boyd, 2009). In addition to the higher yield, the Miltenyi kit had minimal cardiac proportion in the negative-selected population suggesting a more efficient process. The Miltenyi kit also did not change the subtype distribution as measured by MLC-2v expression in both hiPSC-aCMs and -vCMs. Unfortunately, the components of Miltenyi kit remain proprietary. However, by purveying the available literature, it is highly likely that the non-CMs selection of the commercial kit uses more than one cell surface marker. We did not test the positive selection of the kit for fear of changing the functional properties of the magnets bound to cell-surface. The manufacturer's literature suggests that the magnetic beads wash out after a few media changes, however, for subsequent culture, it is best to not introduce an external variable as it may affect cardiac function. Aside from using the commercial kit which follows the same principles, we could also use positive selection using SIRPA and VCAM1 as cell-surface markers (Dubois et al., 2011; Uosaki et al., 2011). Overall, MACS produced a higher cardiac purity, offering a viable approach for cardiac enrichment in future applications.

4.5. Limitations and Future Directions

4.5.1. Further Pharmacological Tests

The two-pore-domain K^+ channels, also known as TASK channels, are another atrial-specific K^+ channel that presents another potential target in AF treatment. The $K_{2p}3.1$ (TASK-1) and $K_{2p}9.1$ (TASK-3), encoded by *KCNK3* and *KCNK9* genes respectively, are highly expressed in atrial myocytes (Gaborit et al., 2007; Limberg et al., 2011). There are several experimental TASK channel blockers) that have demonstrated to have selective binding such as ML 365 (TASK-1) and PK-THPP (TASK-3 blocker) (Veldkamp et al., 2018b). The TASK channel blockers were not tested in this study due to time constraints. The evaluation of functional TASK channels in hiPSC-aCMs by studying the effects of the blockers remains a future goal.

The voltage-gated T-type Ca^{2+} channel (encoded by *CACNA1G*) is distinct from their paralog LTCC. T-type Ca^{2+} channels have small single channel conductance and are less sensitive to several Ca^{2+} blockers in the market including the dihydropyridines (e.g. nifedipine) (T.-S. Lee et al., 2006; Shcheglovitov et al., 2005). In this study, I confirmed the insensitivity of hiPSC-aCMs to nifedipine, however, the confirmation of functional T-type channel using selective pharmacology remains a future goal. Candidate blockers that have demonstrated some selectivity in blocking T-type Ca^{2+} channel in human model and other systems include mebafridil (Richard;, Mangoni, Nargeot, & Richard, 2001; Rossier et al., 1998), Z944 (Casillas-Espinosa et al., 2015), and NNC 55-0396 (K. H. Kim et al., 2015).

4.5.2. Transcriptome Profiling of hiPSC-aCMs

Although it is important to characterize the whole transcriptomic profile to better understand global gene expression changes and possible gene-gene interactions in atrial differentiation, qRT-PCR assays are typically limited to a panel of selected genes. Next generation sequencing (NGS) techniques such as RNA-sequencing and chromatin immunoprecipitation sequencing (ChIP-Seq) are useful in measuring the full transcriptome profiles and assessing the gene regulations of hiPSC-aCMs (Argenziano et al., 2018; Cyganek et al., 2018; Devalla et al., 2015). However, running RNA-sequencing or ChIP-Seq can be financially (~$500 per reaction) and computationally expensive. Thus, new emerging technologies without the immense cost burden are providing viable alternative to traditional NGS techniques. One such technology is NanoString which enables the assessment up to 800 genes in a single run (Geiss et al., 2008) with current cost at ~$400 per reaction. We are currently pursuing the NanoString assay for the analysis of 250 genes including, pluripotency markers, structural markers, transcription factors, cell surface receptors, and cardiac-specific markers assessing atrial, ventricular, and nodal specificity. Using NanoString, we will be tracking the effect of RA on changes in gene expression.

4.5.3. Studying Atrial Fibrillation

In this study, I examined the components of AF (ie. AP and CaT) and their response to drugs but not AF itself in the form of triggered response or re-entry. Moving forward, it is best to induce “AF in a dish” and study the mechanisms of the disease in

that environment. One instance is to use burst pacing model to produce rotor formation and study pharmacological rescue *in vitro* (Laksman et al., 2017). Additionally, we can use genome editing to study the impact of genetic variants thought to be associated with lone AF. One example is the SNP rs13376333 in the intronic region of *KCNN3* that was discovered in a genome wide association study (GWAS) study (Ellinor et al., 2010; Gudbjartsson et al., 2007). The *KCNN3* SNP increases the odds ratio of AF by 1.56 (Ellinor et al., 2010), however, the understanding of the mechanisms in the current literature is limited. A SNP rs13376333 hiPSC line was generated in-lab using CRISPR and we will pursue the characterization of this mutation. We will assess the impact of this mutation on downstream gene expression using NanoString as well as assessing the function using OM and pacing protocols to challenge the mutated cells and potentially observe AF-like events and markers.

4.5.4. Chemically-Defined Differentiation of hiPSC-aCMs

The application of RA is a broad approach to atrial differentiation as RA is one of the master regulators of cell fate. Another potential method is to use specific retinoic acid receptor (RAR) agonists to increase the specificity of promoting the cells down the atrial lineage. Work done by Lee et al. (2017) have shown that addition of small molecule agonists AM580 (α receptor), AC55649 (β receptor), and CD437 (γ receptor) increased atrial phenotype in ESC-derived CMs. However, manually titrating each of the RAR agonists to optimize of each cell line may prove to be difficult. As such, scaling up to large culture systems (ie. 96-well plate formats) and assay throughput may be necessary. Additionally, one can introduce further chemically-defined differentiation methods to minimize batch-to-batch variability due to less reliance on animal sourced materials such as albumin and growth factors (Burridge et al., 2014).

4.5.5. Increasing Purity of hiPSC-CMs

There are a few approaches to increase cardiac population in hiPSC-CMs: 1) metabolic selection; 2) cell sorting through FACS or MACS; and 3) genetically tagged reporters. Increasing the cardiac purity is important in applications such as regenerative medicine. However, with the ability to differentiate hiPSC-aCMs, we are also interested in increasing the chamber specific population in the future.

Out of all the options presented here, metabolic selection using lactate remains the simplest, easiest, and cheapest to technique to increase purity of hiPSC-CMs. Switching the energy source from glucose to lactate during the early phase of differentiated hiPSC-CMs has demonstrated increased cTnT purity up to 99% (Tohyama et al., 2013). However, no studies have assessed the functional impact of switching energy sources on parameters such as AP characteristics, Ca^{2+} handling, metabolic pathways. Thus, more studies to be conducted if one is interested in using lactate as the purification method.

For cell sorting for terminal experiments such as qPCR, flow cytometry, and immunocytochemistry, the experimenter can use several strong chamber specific intracellular markers such as SLN (Josowitz et al., 2014) and MLC-2v (Bizy et al., 2013). However, sorting live cells is necessary for functional studies, thus live cell sorting is dependent on the presence of specific cell surface markers. Both commonly used sorting techniques, MACS and FACS, are limited in the numeric availability of cell surface markers – higher expression increases the probability of labelling success. Also, antibody specificity plays a large role in picking up the cell surface markers thus limiting the options for live-cell sorting. Recent work has identified a new combination of surface markers $CD77^{+}/CD200^{-}$ to enrich for hiPSC-vCMs using FACS (Veevers et al., 2018). These cell surface markers may potentially be adopted into MACS.

For increasing the subtype-specific purity in hiPSC-aCMs and hiPSC-vCMs, one can use genetically-tagged reporters via approaches such as expression of exogenous markers attained through gene editing or viral-based gene delivery. Expression of fluorescent proteins driven by a subtype-specific promoter (SLN, MLC2V, HCN4) has been shown to capture subtype-specific phenotypes (Z. Chen et al., 2016). However, this approach may be limited by expression, and some cells will not have uniform gene expression patterns. A potential method is to combine both genetically-tagged reporters and cell sorting approaches. To enrich atrial population in hiPSC-CMs, one can use the expression of SLN promoter-driven fluorescent protein tagged on the plasma membrane such as ASAP1, a voltage sensing domain (VSD)-tagged extracellular cGFP (please see Chapter 5: Genetically Encoded Fluorescent Indicators for more details on the construct), or by expressing an “artificial” cell-surface marker which can then be used in positive or negative selection in MACS, respectively.

4.5.6. Maturation and 3D Structure of hiPSC-CMs

Current hiPSC-CM differentiation protocols produce CMs with relative immaturity close to that of fetal phenotype at the transcriptome (van den Berg et al., 2015; Xu, Soo, Sun, & Zweigerdt, 2009), structural morphology (McCain & Parker, 2011; Pasqualini, Sheehy, Agarwal, Aratyn-Schaus, & Parker, 2015; X. Yang, Pabon, & Murry, 2014), and functional levels (Blazeski et al., 2012; Ribeiro et al., 2015; Robertson et al., 2013). Thus, maturation is necessary to closer mimic adult human physiology. Maturation is also the crux in regenerative medicine applications as well as understanding disease etiology (Tu, Chao, & Wu, 2018). While a more detailed understanding of hiPSC-CMs maturity has come to fruition in the last few years, techniques to improve maturity of hiPSC-CMs are still being developed (Tu et al., 2018). In general, engineering approaches in cardiac maturation must incorporate the following: 1) environmental manipulation through cell culture formats and conditions such as surface chemistry (Corda, Samuel, & Rappaport, 2000), topography (Besser et al., 2018), and 3-dimensional scaffolds for cell growth (Gao et al., 2017); 2) electrical stimulation ; 3) stretch or force induction ; and 4) co-culture with helper cells such as cardiac fibroblast (Liau, Jackman, Li, & Bursac, 2017). Culturing hiPSC-CMs in 3D has garnered much attention in the field of bioengineering resulting in new devices such as Biowire (Nunes et al., 2013) and engineered heart tissues (EHT) (Tiburcy et al., 2017). In the Biowire device, CMs grown around a flexible wire are matured through a combination of mechanical stretch and electrical pacing with increasing rate in step-wise fashion (Nunes et al., 2013). The biowire platform has also recently been used to generate hESC-derived aCMs and -vCMs (Aschar-Sobbi et al., 2019). The EHT platform grown in PDMS medium that is cast around two micro-posts that produce stretch and contraction (Tiburcy et al., 2017). The EHT are also stimulated electrically over the course of maturation (Tiburcy et al., 2017). Employing these maturation techniques give a more physiologically relevant tissue preparation to that of a human heart tissue.

4.5.7. Advancements in Cell Culture Technology and High-Throughput Imaging Systems

This study focused on medium throughput 24-well plate with semi-automation operation capabilities. The 24-well plate system is a precursor to high-throughput screening (HTS) to screen for exponentially more drug compounds at a time. Current

HTS systems use 96, 384, 1536, or 3456 wells. However, 96- or 384- well plate formats will likely be the most suitable in getting the read-out of hiPSC-CMs. An experimenter could potentially screen 384 compounds in a single plate or increase experimental replicates for each compound in the screening campaign. This high-throughput ability is incredibly crucial in identifying new drug targets and discovering potential drug candidates including libraries of small molecules and siRNA. Furthermore, the experimenter can screen libraries of lentivirus and CRISPR sgRNAs for targeted gene regulation studies. In hiPSC-CMs, HTS has been utilized to assess tyrosine kinase inhibitor (TKI) induced cardiotoxicity (Sharma et al., 2017) and the CiPA screen.

HTS requires high-capacity technologies in cell culture and imaging systems. However, higher throughput cell culture will also require higher throughput enrichment. One can use the commercially available MACS with the advantage being its ability to process multiple samples at once. The major disadvantage of MACS is the cost of scaling up. For scalability and ease of use, it may be cheaper to use metabolic selection by switching glucose to lactate as the source of energy. However, the automated cell culture systems can be used to optimize RAR agonists in differentiation protocol.

Chapter 5.

Future Direction: Genetically Encoded Fluorescent Indicators

5.1. Background

The current optical mapping technology using organic fluorescent dyes enables the simultaneous measurement of AP and CaT of hiPSC-CMs in applications such as acute drug response. However, dyes are not suitable for longitudinal studies such as evaluating chronic drug effects as dyes are subject to rapid photobleaching and decomposition (T.-W. Chen et al., 2013a; Hochbaum et al., 2014). Furthermore, the labelling nature of fluorescent dyes leads to inaccurate spatial targeting which produces undesired signals and/or contribution to background signal. For instance, the Rhod-2AM dye will pass through any plasma membrane and will not only measure cytosolic Ca^{2+} levels but may also measure Ca^{2+} levels in organelles such as mitochondria (Carrasco-Pozo et al., 2012). Thus, for experiments that require longitudinal recording and spatial targeting, an alternative approach is needed. One such alternative is genetically encoded fluorescent indicators (GEFI) which are chimeric fluorescent proteins that can be used to monitor certain signals of interest such as membrane voltage and cytosolic Ca^{2+} levels.

There are several advantages of using GEFI over traditional chemical-fluorescence: 1) precise control of expression on the genetic level; 2) compartmentalized spatial targeting of probes using target-specific aminoacid sequences; 3) decreased signal noise to the more precise tagging; 4) ability to conduct longitudinal studies as the GEFIs are continually replenished via constitutive endogenous expression.

With that said, GEFI are also have limitations: 1) the potential deleterious impact of GEFIs on cell function must be fully assessed; 2) large fluorescent proteins have spatial limitations thus decreasing the density of the probe in a given area and lowering overall fluorescence intensity; 3) the response kinetics of the genetic probe may be slower than dyes due to inherent quantum mechanics. However, depending on the imaging modality, the non-optimal response kinetic may not be an issue.

In the context of this thesis, the approach described in this section includes the methodology behind GEFIs that monitor AP and CaT in living hiPSC-CMs including the design and selection, optimization of gene delivery methods and protein expression, and validation of fluorescent probes.

5.1.1. Considerations in Indicator Design

The basic principle of GEFI is to engineer a chimeric protein by tagging a synthetic fluorescent protein (the reporter) to a naturally occurring or modified protein (the sensor). The reporter can be a monomeric fluorescent protein such as eGFP or Förster resonance energy transfer (FRET)-based sensor such as Mermaid (Tsutsui, Karasawa, Okamura, & Miyawaki, 2008). The details of indicator design have been reviewed elsewhere (Sanford & Palmer, 2017). In brief, for simultaneous imaging of two signals (i.e. AP and CaT), the main considerations in selecting and/or designing fluorescence probes are 1) brightness of the fluorescent proteins; 2) dynamic range of the probes (i.e. $\Delta F/F$ – the fold change in response to the change in signal compared to the baseline fluorescence); 3) the response kinetics – how quickly the probe responds to the measured parameter; 4) spectral crosstalk between the two or more fluorescence reporters.

5.1.2. Calcium Indicators

In addition to the basic requirements of good probes, the most important factor for GECI is the Ca^{2+} sensitivity normally expressed as the K_d (Pérez Koldenkova & Nagai, 2013). Depending on the application, the K_d must be in similar range as the physiological conditions to reliably report Ca^{2+} levels. For instance, in the context of this setup the K_d of the probe must be close to quiescent cytosolic Ca^{2+} levels for measuring global CaT. However, the K_d must be much higher in reporting on Ca^{2+} levels of SR or mitochondria (J. Wu, Prole, et al., 2014).

The most commonly used GECI for determining $[Ca^{2+}]$ is GCaMP, circularly permutated GFP fused to calmodulin (CaM) and M13 domain from myosin light chain kinase (Nakai, Ohkura, & Imoto, 2001). In the presence of Ca^{2+}, CaM undergoes a conformational change and tether to the M13 domain thereby opening the solvent pathway to de-protonate the chromophore of GFP to produce fluorescence (Akerboom

et al., 2009). GCaMP has undergone a variety of permutations to be tailored in different applications from GCaMP3 through GCaMP8. GCaMP6f is the most updated permutation with the fastest kinetics that reliably reports on cytosolic Ca^{2+} handling dynamics with K_d of 0.4 µM (T.-W. Chen et al., 2013b).

The Genetically Encoded Calcium indicators for Optical imaging (GECO) series are improved variants of the GCaMP (pre-GCaMP6 permutation). Using a directed evolution technique, the Campbell lab at the University of Alberta has generated a series of indicators with varying properties including the K_d and dynamic range as well as expanding the options of fluorescence reporters in GECI (Hochbaum et al., 2014; Qian et al., 2019; Shen, Lai, & Campbell, 2015; J. Wu, Abdelfattah, et al., 2014). One member of this GECI family to be highlighted is R-GECO1.2 which possess a K_d of 1.2 µM (Shen et al., 2015). In addition to measuring cytosolic Ca^{2+} levels, the GECO family was further optimized to detect Ca^{2+} levels in the ER (J. Wu, Prole, et al., 2014).

5.1.3. Voltage Indicators

The design of genetically encoded voltage-sensing indicators (GEVIs) are technically challenging in that they must satisfy several criteria to reliably report on transmembrane voltage changes. In addition to the basic parameters of making good fluorescent indicators (low toxicity, bright, and highly photostable), the probes must localize to the plasma membrane, display high sensitivity to changes in voltage, ideally have a linear response to voltage, and fast response kinetics (H. H. Yang & St-Pierre, 2016). The most commonly used evolution of voltage indicators include a four-pass transmembrane voltage-sensing domains (VSD) of voltage sensitive phosphatase (H. H. Yang & St-Pierre, 2016). The VSD acts as the electro-mechanical transducer, undergoing conformational change in response to change in V_m which then induces a conformational change in its tagged fluorescent reporter (H. H. Yang & St-Pierre, 2016).

One such reporter is ArcLight, a construct of GFP-tagged VSD of the voltage sensitive phosphatase found in the sea-squirt *Ciona intestinalis* (Jin et al., 2012). ArcLight was the first GEVI reported for use in hiPSC-CMs (Leyton-Mange et al., 2014) for the application of drug response (Shinnawi et al., 2015) and optical mapping in studying rotor formation *in vitro* (Shaheen et al., 2018). However, ArcLight displayed slow upstroke kinetics and has a limited frequency response (Jin et al., 2012). A more

recent evolution of VSD-based reporters is the Accelerated Sensor of Action Potentials 1 (ASAP1) which used the VSD from the common chicken (*Gallus gallus)* with a circularly permuted GFP tagged to the S3-S4 linker loop in the extracellular space (St-Pierre et al., 2014). ASAP1 boasts fast kinetics with reported significantly faster time constant (τ) of activation and inactivation compared to ArcLight. Another construct is FliCR1, a membrane voltage indicator based on the red fluorescent protein variant mApple. Unlike ASAP1, the fluorescent reporter of FliCR1 is situated on the N-terminus of the VSD (Abdelfattah et al., 2016). FliCR1 has fast kinetics with τ of activation of 0.74 ms and reported AP trains in hippocampal neurons with high degree of accuracy (Abdelfattah et al., 2016). While the application of both ASAP1 and FliCR1 have been reported in primary hippocampal neurons (Abdelfattah et al., 2016; St-Pierre et al., 2014), they have not been reported for use in hiPSC-CMs.

Other constructs such as the Voltage Sensing Fluorescent Protein (VSFP) family, a FRET-based VSD GEVI, was reported to reliably measure AP of hiPSC-CMs (Z. Chen et al., 2016). However, a FRET-based reporter is not suitable for simultaneous imaging of AP and CaT as it increases the spectral crosstalk when gathering multiple fluorescent signals in a single recording.

5.1.4. Considerations in Imaging Modality

The simultaneous imaging of two fluorescent signals presents additional challenges to imaging modality. Spectral crosstalk is perhaps the most important factor as it presents a bottleneck in the imaging workflow and influences overall experimental design. In standard imaging protocols, separation of two fluorescence spectra can be addressed by separation through dual excitation and dual emission wavelength channels or through dual emission channels but a shared single excitation wavelength.

Single excitation is perhaps the best approach as it minimizes spectral crosstalk in excitation and emission channels during simultaneous imaging. One of the probes must have a long Stokes shift to accommodate single wavelength excitation. However, spectral separation in both excitation and emissions is the most straight forward approach as most microscopes are equipped with common filters for collecting GFP and RFP. Therefore, for simplicity and validation purposes, the configurations in the final design used in this study are dual-excitation and dual-emission for multiplex imaging of

GFP and RFP signals. For this purpose, the following two combinations were selected: 1) ASAP1 and R-GECO1.2; 2) FliCR1 and GCaMP6f.

5.1.5. Methods of Gene Expression

Genome Editing Using CRISPR

Genome editing using techniques such as CRISPR allows for endogenous expression with the main advantage of precise control of gene locus integration and copy number expression driven by selected promoters. The control of expression can also be achieved through homozygous or heterozygous knock-in in a given allele (Koch et al., 2018). However, multiple rounds of CRISPR to integrate multiple GEFI constructs into the genome decreases cell health and decreases the number of potential targeting sites. Additionally, multiplex CRISPR experiments for multiple knock-ins must be carefully designed to avoid potential off-target cleaving (Minkenberg, Wheatley, & Yang, 2017). Also, the cost and time investment of CRISPR can hardly justify its use in the validation step of GEFIs. That being said, genome editing may come to be useful in generating permanent cell lines for long-term studies such as tracking the development of CaT in cardiac maturation after each individual probe is validated.

Transient Gene Delivery

Transient gene delivery systems for exogenous gene expression such as liposomal transfection and electroporation are the most cost effective and simple options in gene delivery. Liposomal transfection, also known as lipofection in which DNA is packaged in lipid vesicle complexes, is effective in transfecting primary cell lines such as HEK293 but it is ill-suited in cardiomyocyte application as transfection rates are low (<15%) (Djurovic, Iversen, Jeansson, Hoover, & Christensen, 2004). Electroporation is not the best choice in delivering plasmids into cardiomyocytes due to its low rates of survival (Djurovic et al., 2004) and cardiac cultures cannot recover from high death rate as cardiomyocytes are non-dividing cells. However, improvements in micromachining approaches have been developed in recent years. One such technique is the nanostraw-electroporation platform that perhaps present a viable approach in large-scale gene delivery to hiPSC-CMs (Cao et al., 2018). The bed of nanostraw ensures even distribution of contact and deliver gene constructs by applying low field potential current to create local tiny ruptures of the plasma membrane (Cao et al., 2018). Compared to

traditional electroporation this technique has been shown to increase the recovery and viability of the cells (Cao et al., 2018).

Viral-Based Gene Delivery

Viral-based gene delivery systems present a practical approach for stable gene expression while offering the flexibility in multiplexing gene constructs delivery into multiple cell lines. The commonly used viral-based gene delivery systems are retrovirus, adenovirus, adeno-associated virus (AAV), and lentivirus.

Retroviruses have a high transducing efficiency and are a popular tool in clinical applications but they are limited to transducing dividing cells (Lentz, Gray, & Samulski, 2011), thus cannot be utilized in hiPSC-CMs. Adenoviruses are highly efficient in transducing dividing and non-dividing cells for transient gene expression and do not integrate into the host genome (Wold & Toth, 2013). However, the transient nature of the adenovirus is not suitable for stable expression of GEFIs. Adeno-associated virus (AAV) is a small virus that is commonly used *in vivo* applications due to low immunogenicity and having a variety of serotypes that can target specific tissues (Burger et al., 2004). Some limitations of AAV include the capability of only packaging relatively small genes (i.e. ~4.8 kb), low efficiency *in vitro* (Ellis et al., 2013), and the potential optimization step of finding serotypes to best transduce hiPSC-CMs adds another layer of complexity to overall experimental design (Ellis et al., 2013).

Lentiviruses are commonly used for both *in vivo* and *in vitro* transduction of non-dividing cells with genes delivered by the virus randomly integrating into the host genome (Milone & O'Doherty, 2018; Sakuma, Barry, & Ikeda, 2012). The approach offers a few advantages including stable long-term expression, high *in vitro* transduction efficacy, and capacity to package large genes with limits around 8 kb (Park & Kay, 2001). This technique has been used in generating a stable ArcLight expressing iPSC line (Shaheen et al., 2018). Lentivirus also has evolved in terms of biosafety. Second and third generation lentiviral systems have increased safety to the user as the viruses are self-inactivating and the viral envelope plasmids are delivered in a separate vector thereby minimizing the probably of infecting the user (Dull et al., 1998; Zufferey et al., 1998). However, the random integration into the genome is a major limitation in this technique. Ultimately, a lentiviral system was selected as the gene delivery tool for this

study due to its greater ability for gene integration and flexibility in delivering multiple constructs in one application.

5.2. Materials and Methods

5.2.1. Molecular Cloning

pcDNA3.1/Puro-CAG-ASAP1 was a gift from Michael Lin (Addgene plasmid #52519) and CMV-FliCR1 was a gift from Robert Campbell (Addgene plasmid #74142). The functional inserts of these two probes were cloned into the lentiviral transfer vector pWPXL (a gift from Didier Trono; Addgene plasmid #12257) using PCR cloning. BamHI (GGATCC) and EcoRI (GAATTC) restriction sites were added by PCR amplification of cDNA with primers as listed in Table 5.1. The resulting cDNA products were purified using PCR Purification Kit (QIAGEN, Cat: 28104) and digested with the high-fidelity restriction enzymes BamHI and EcoRI (New England Biolabs, Cat: R3136S and R3101S, respectively). Furthermore, the EGFP insert of pWPXL was excised with BamHI and EcoRI. The backbone of pWPXL and the coding region insert of ASAP1 or FliCR1 were isolated using the Gel Extraction Kit (QIAGEN, Cat: 28115) and then ligated with T4 DNA ligase (New England Biolabs, Cat: M0202S). The final products were termed the lentiviral vector constructs pLenti-ASAP1 and pLenti-FliCR1.

CMV-R-GECO1.2 was a gift from Robert Campbell (Addgene plasmid #45494) and pGP-CMV-GCaMP6f was a gift from Douglas Kim (Addgene plasmid #40755). The functional inserts of these two probes were subcloned into pWPXL using double digestion with the restriction enzymes BamHI and EcoRI. Similar to PCR cloning, the R-GECO1.2, and GCaMP6f inserts, and the pWPXL backbone were isolated by gel purification and ligated using T4 ligase resulting in the final lentiviral vector construct pLenti-R-GECO1.2 and pLenti-GCaMP6f.

All plasmid constructs (pLenti-ASAP1, pLenti-FliCR1, pLenti-R-GECO1.2, and pLenti-GCaMP6f) were transformed into DH5-α competent cells (New England Biolabs, Cat: C2987H). Transformed DH5-α cells were plated on ampicillin plates for the selection of single colonies to be cultured overnight in 5 mL of liquid LB broth. After overnight culture, the lentiviral vectors were isolated and purified using Plasmid Minirep Kit (QIAGEN, Cat: 27104) which were then sequence verified.

Table 5.1. List of primer sequences for PCR cloning.

Name	Sequence (5`- 3`)
ASAP1-BamHI-Forward	TAAGCAGGATCCATGGAGACGACTGTGAGGTATGAACAG
ASAP1-EcoRI-Reverse	TGCTTAGAATTCTCATTAGGTTACCACTTCAAGTTGTTTCTTCTG
FliCR1-BamHI-Forward	CTGAGGATCCACCATGGAGGGATTCGACGGTTCAGATTTTAGTCC
FliCR1-EcoRI-Reverse	TTATTGAATTCCTAACGCGTAGCCTCCCAGCCCATGGTCTTC

5.2.2. Lentivirus Production

Before lentivirus production, lentiviral vectors (pLenti-ASAP1, pLenti-FliCR1, pLenti-R-GECO1.2, and pLenti-GCaMP6f) were grown in overnight large culture (50 mL) and isolated using a Maxiprep Kit (QIAGEN, Cat: 12163) for higher yield. The lentivirus transfer vectors were packaged in human embryonic kidney 293FT (HEK 293FT) cells by co-transfection of 13 µg pLenti vectors along with helper plasmids 6.5 µg psPAX2 (a gift from Didier Trono; Addgene plasmid #12260) and 6.5 µg pMD2.G (a gift from Didier Trono; Addgene plasmid #12259) or in 2:1:1 ratio. Large scale lentivirus production was conducted using 15 cm plates with HEK 293FT cells seeded at 60% confluency before transfection. Lentivirus-containing media was harvested at 48- and 72-hours post-transfection and filter sterilized using low protein binding syringe 0.22 µm filter (Merck Millipore, Cat: SLGP033RB). The lentiviral particles were further concentrated using a PEG-based gradient centrifugation at 5,000 g for 20 minutes (Applied Biological Materials, Cat: LV999) and suspended in RPMI 1640 medium. Lentiviral stocks were cryopreserved by flash-freezing using liquid nitrogen and stored at -80°C for long-term storage. Cryopreserved lentiviral stocks were rapidly thawed in warm water before downstream usage. Viral titer was determined using a qRT-PCR titration kit (Applied Biological Materials, Cat: LV900). Viral titer is quantified as Infectious Unit (IU) per 1 mL of suspension with 1 IU representing 1 viral particle. The lentivirus production workflow is summarized in Figure 5.1.

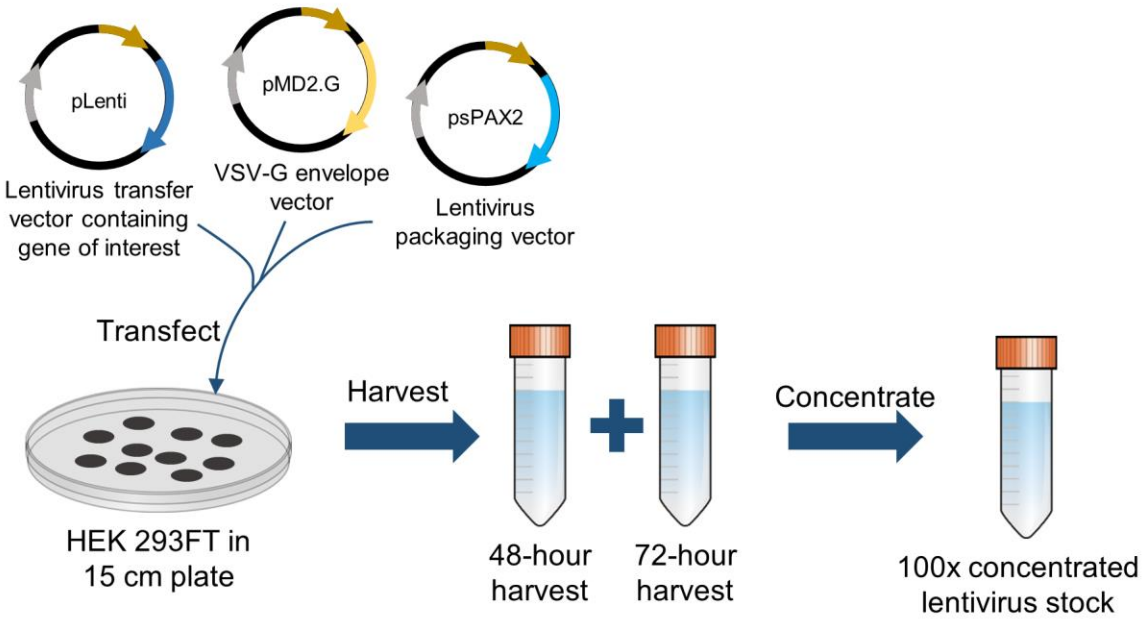

Figure 5.1. Lentivirus production workflow.

5.2.3. Lentivirus Transduction

hESC-aCMs were transiently transduced with pLenti-ASAP1 and pLenti-R-GECO1.2; while hiPSC-vCMs were transiently transduced with pLenti-FliCR1 and pLenti-GCaMP6f. Cells were transduced with the lentiviruses at a multiplicity of infection (MOI) of 10 twice at 24-hour intervals to increase transduction efficiency. Cells were then imaged 10-15 days after viral transduction.

5.2.4. Confocal and Epifluorescence Microscopy

To validate the constructs FliCR1 and GCaMP6f, fluorescence imaging was conducted on two microscope systems. First, a Nikon A1R Laser Scanning confocal system equipped with photomultiplier tube and 60x oil immersion objective. Samples were excited with 488 and 561 nm lasers and fluorescence signals were collected using 525±50 and 585±30 emission filters. For confocal imaging, hiPSC-vCMs were seeded at $5x10^4$ cells in a glass bottom 35 mm dish (MatTek; Cat: P35G-1.0-14-C). Second, a Nikon Ti Eclipse epifluorescence microscope equipped with 20x and 40x phase objectives and an Andor Zyla VSC-00876 CMOS camera. Samples were excited with a Sutter Lambda XL Xenon Arc Lamp filtered at 485±20 and 560±25 nm; fluorescence signals were collected using 525±30 and 607±36 nm emission filters. For

epifluorescence imaging, hiPSC-vCMs were seeded at $5x10^5$ cells in a 24-well plate. To validate R-GECO1.2, fluorescence imaging was conducted on a dual-channel optical mapping system equipped with Orca Flash 4 CMOS camera. A second optical mapping system equipped with EMCCD cameras and GFP detecting capability was used to evaluate ASAP1.

Waveform analysis from optical mapping was conducted using custom software written in IDL. Waveform analysis of confocal and epifluorescence microscopy images were conducted using ImageJ (Plugin: Time Series Analyzer V3). Figures were generated using Microsoft Excel and R (version 3.4.4, library: ggplot).

5.3. Preliminary Results

5.3.1. Developing Lentivirus Production Protocol and Optimizing Titer

Initial lentivirus production yielded titers of 5.21×10^6, 4.83×10^6, 9.56×10^6, and 8.76×10^6 IU/mL for ASAP1, FliCR1, R-GECO1.2, and GCaMP6f, respectively (Figure 5.2.A). As the original titer was low, I introduced a concentration protocol using a simple commercially-available PEG-based centrifugation protocol. The concentration produced higher viral titers: 6.55×10^8, 5.98×10^8, 1.08×10^9, and 9.70×10^8 IU/mL for ASAP1, FliCR1, R-GECO1.2, and GCaMP6f, respectively (Figure 5.2.B). To quantify the loss of active lentivirus after cryopreservation, lentiviral viral titer was determined after long-term storage at -80 ^oC. qRT-PCR quantification showed that cryopreservation decreased the original concentrated titer to 4.22×10^8, 3.46×10^8, 6.48×10^8, and 5.94×10^8 Infection Units (IU)/mL for ASAP1, FliCR1, R-GECO1.2, and GCaMP6f, respectively (Figure 5.2.B).

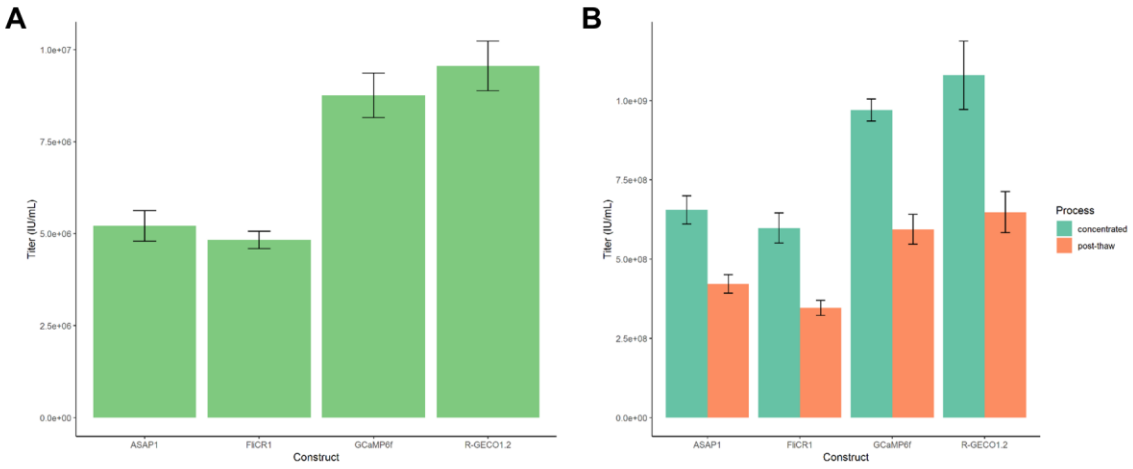

Figure 5.2. Quantification of lentivirus titer for all genetically-encoded fluorescent indicator constructs.

A) Pre-concentrated lentiviral titer of ASAP1, FliCR1, GCaMP6f, and R-GECO1.2. B) Lentiviral titer of each construct after concentration and the recovery rate post-thaw cryopreservation. n = 4 independent production batches.

5.3.2. Validation of Calcium Indicators

The construct R-GECO1.2 was validated in embryoid bodies (EBs) of hESC-derived atrial-like cardiomyocytes (hESC-aCMs). hESC-aCMs displayed robust expression of R-GECO1.2 signals (Figure 5.3.A, left panel) with high fidelity of CaT measurement (Figure5.3. A, right panel). R-GECO1.2 was able to measure the CaT of a single cluster of hESC-aCMs (Figure 5.3.B) and was able to detect CaT prolongation after exposure to 500 nM bepridil, a Ca^{2+} sensitizing agent (Figure 5.3.C).

The construct GCaMP6f was validated in hiPSC-vCMs. Expression of GCaMP6f was robust in the cytosol (Figure 5.4.A). GCaMP6f was able to record CaTs and had high dynamic range along with a high signal-to-noise ratio (Figure 5.4.B). Single cell time-lapse imaging showed a Ca^{2+} signal propagation across the cell (Figure 5.4.C).

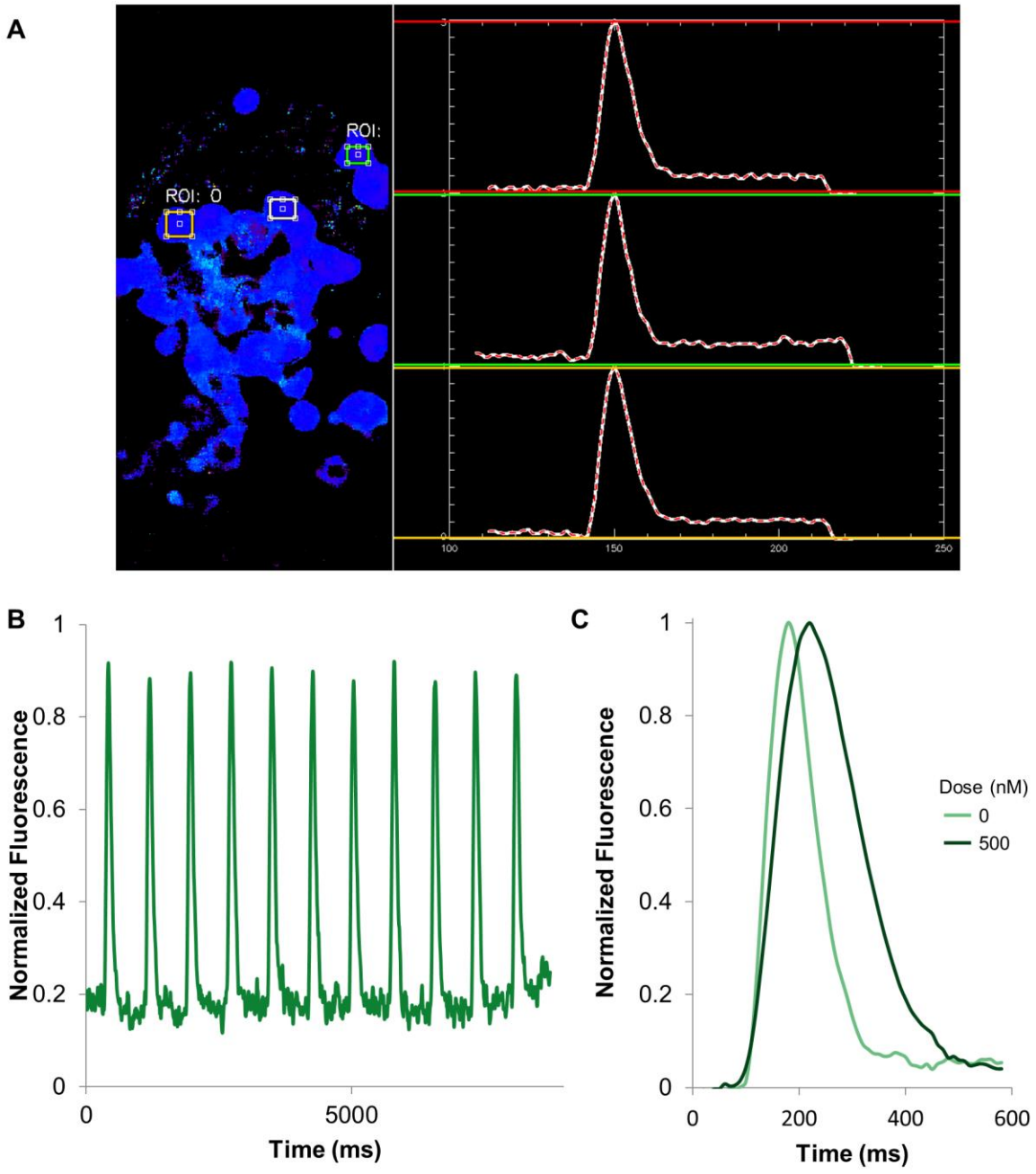

Figure 5.3. Validation of R-GECO1.2 in hESC-aCMs.
A) Left panel: clusters of hESC-derived atrial-like cardiomyocytes imaged on the optical mapping system. Three regions of interest (ROI) are labelled corresponding to the averaged traces on the right panel. B) Representative train of Ca^{2+} transients (CaT) measured by R-GECO1.2. C) Effects of 500 nM bepridil, a Ca2+ sensitizing agent, on prolongation of CaT measured by R-GECO1.2. Averaged trace was obtained from 10 cycles. Recordings were conducted in collaboration with Dr. Sanam Shafaattalab.

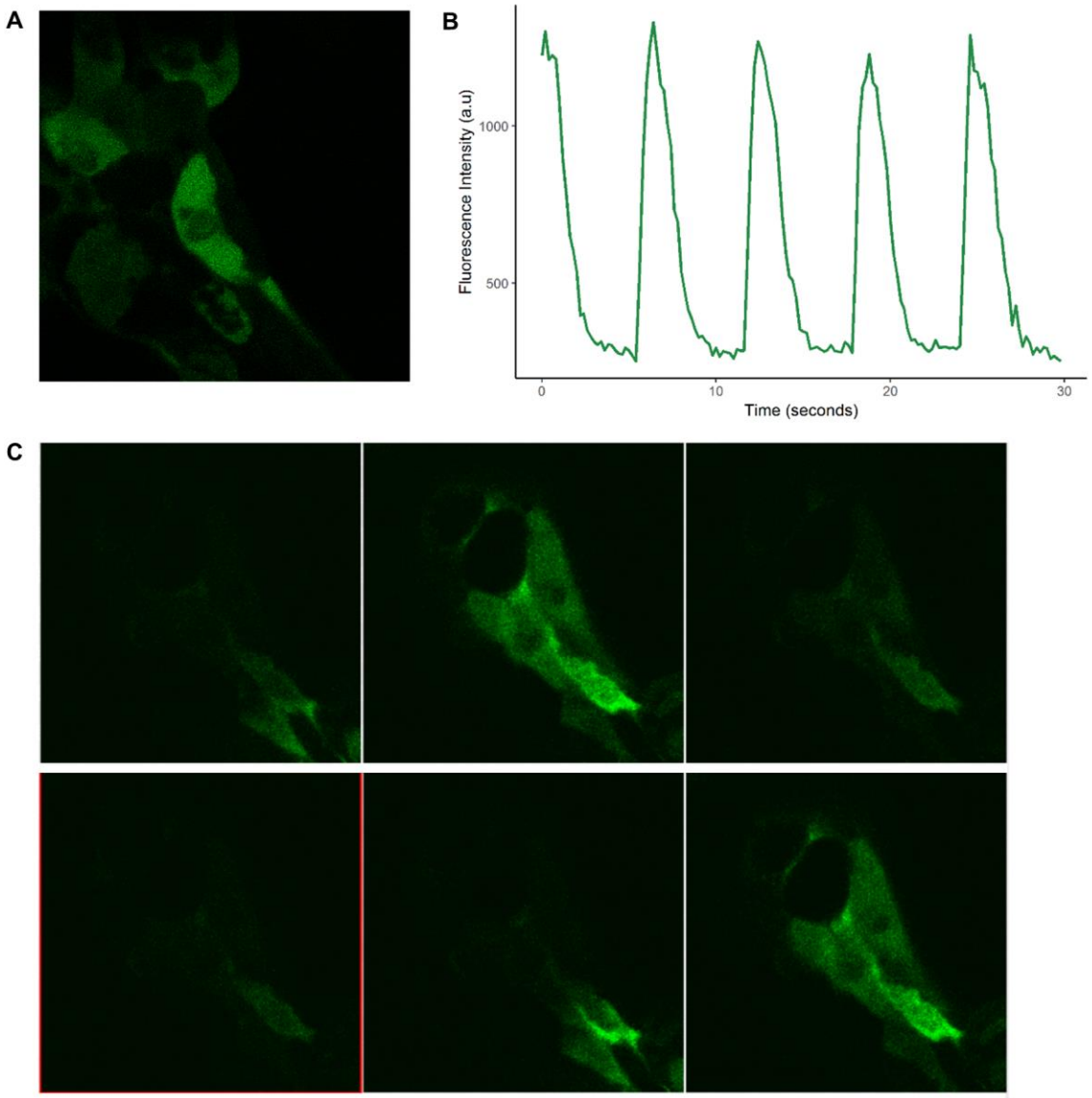

Figure 5.4. Robust expression of GCaMP6f in hiPSC-vCMs.
A) A cluster of hiPSC-vCMs expressing GCaMP6f. Image acquired at 60x magnification using confocal microscopy. B) Representative Ca^{2+} transient trace from GCaMP6f fluorescence measurement of a single hiPSC-vCM. C) Time series of a single hiPSC-vCM expressing GCaMP6f at 1 fps demonstrates the Ca^{2+} cycling dynamics propagate from one distal end to another. Images acquired at 60x magnification using confocal microscopy. Frame rate was 1 fps.

5.3.3. Evaluation of Voltage Indicators

The construct ASAP1 was evaluated in hESC-aCMs. Although, the fluorescence signal could be detected in hESC-aCMs infected with ASAP1 (Figure 5.5.A), no voltage transients were measured (Figure 5.5.B). FliCR1 was evaluated in hiPSC-vCMs.

Confocal and epifluorescence imaging revealed fluorescence to be concentrated in puncta-like structures (Figure 5.5.C and D). These fluorescence puncta did not respond in fluorescence intensity change (data not shown).

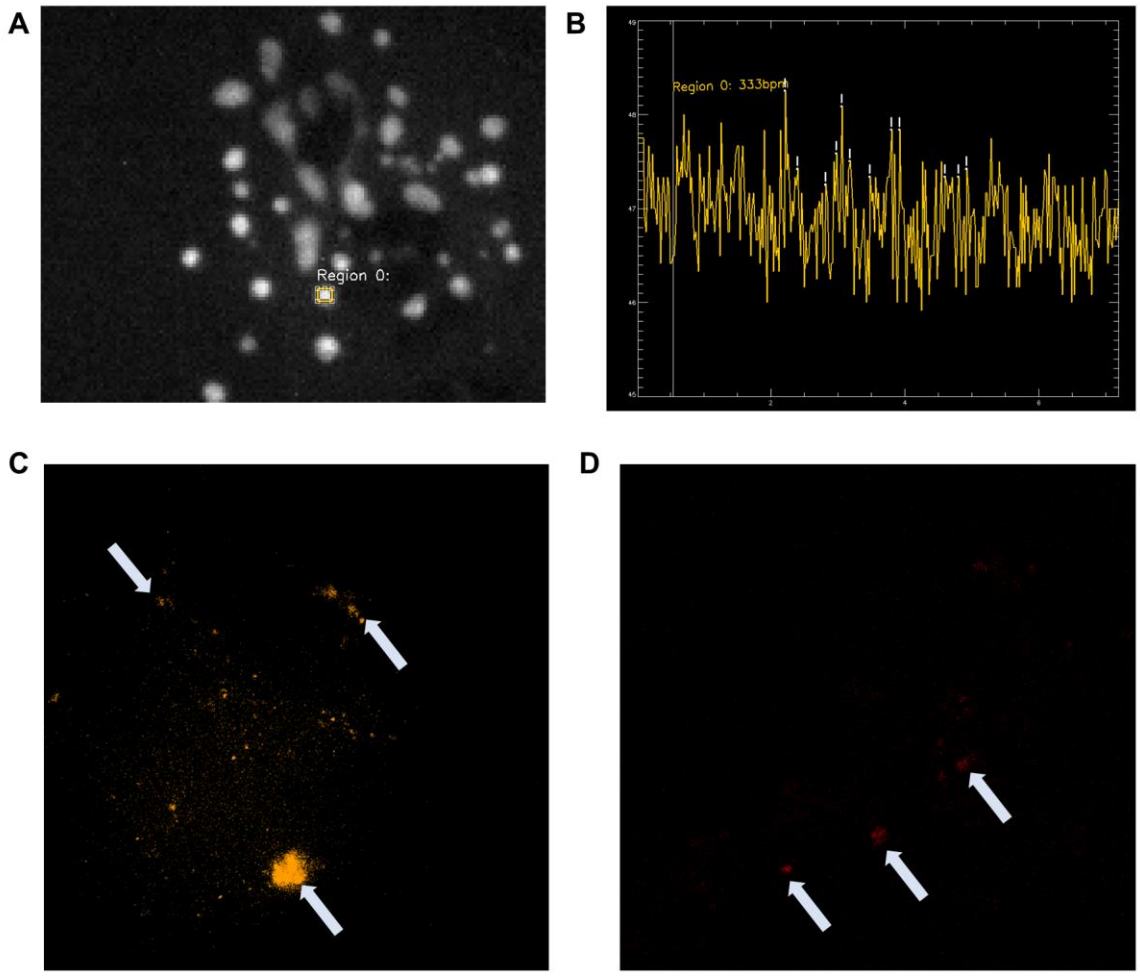

Figure 5.5. Evaluation of voltage indicators ASAP1 and FliCR1.
A) Representative image of ASAP1 expressed in hESC-aCMs. B) Representative trace of fluorescence signal from the indicated region of interest. No transients were observed. Representative images of FliCR1 expressed in hiPSC-vCMs taken at C) 40x magnification and D) 60x magnification. The arrows highlight red fluorescence clusters.

5.4. Discussion

Here, I developed a lentiviral production workflow and evaluated the utility of genetically-encoded fluorescent indicators. Producing high yield viral titer is important in delivering enough gene copies of GEFIs to hiPSC-CMs for large scale imaging purposes. The simplified second-generation lentivirus production workflow introduced in

this study takes advantage of scaling to large culture. Lentiviral titer appears to be construct dependent with a higher initial titer in the Ca^{2+} indicators compared to voltage indicators. Concentrating the lentivirus preparation dramatically increased the final density by 100-fold enabling infection of around 10 million hiPSC-CMs with a single viral production step. However, the recovery rate of lentivirus after cryopreservation is around 61% which suggests that best practice must include a qRT-PCR titer step after cryopreservation to confirm the recovery rate to determine accurate MOI.

GEFIs are attractive alternatives for fluorescence imaging as the highly photostable fluorescent proteins are suitable longitudinal and targeted measurements of AP and CaT characteristics of hiPSC-CMs. I aimed to design a multiplex imaging modality by taking advantage of the spectral wavelength separation between the two fluorescent proteins (GFP and RFP). In this study, however, each of the constructs was validated independently.

The two GECI constructs were validated in two different systems. As expected, GCaMP6f provided strong fluorescence signals with a high signal-to-noise ratio. Furthermore, the signal propagation of GCaMP6f demonstrated the high spatiotemporal resolution of the probe in measuring CaT in a single cell. Similarly, R-GECO1.2 reported CaT with both high fidelity and high signal-to-noise measurements. Additionally, R-GECO1.2 was able measure elongation in CaT in response to the Ca^{2+} sensitizing agent bepridil. It is important to note that in this study R-GECO1.2 was excited at 532 nm which is suboptimal from the peak excitation of mApple at 560 nm. These results strongly indicate that GECIs are readily applicable in long-term Ca^{2+} imaging studies of hiPSC-CMs such as pharmacological characterization or studying inherited cardiac arrhythmia in the context of Ca^{2+} mishandling due to genetic mutations.

The results for voltage indicators were not expected. I initially hypothesized that both FlicR1 and ASAP1 would provide strong fluorescence signals with high signal-to-noise ratio and reliably report AP. ASAP1 appeared to have some expression in hESC-aCMs although no APs were recorded. However, as the fluorescence signal is low and close to background noise, the detected fluorescence could be due to auto-fluorescence of the cell clusters and not from GFP expression. Perhaps the extracellular GFP of ASAP1 are not favoured in the EB condition due to a potential steric hindrance and spatial limitations in surface of cell clusters. Future evaluation of the probe must be

conducted in a monolayer format. FliCR1 displayed minimal expression in hiPSC-vCMs with fluorescence signals clustering in the intracellular space with the possibility of being stored compartments of the cells. The unresponsive puncta structures were also observed in neuronal cell bodies (Abdelfattah et al., 2016). It is highly likely that FliCR1 are packaged into lysosomes in autophagy as evidence has suggested that GFP-like proteins undergo similar process (Katayama, Yamamoto, Mizushima, Yoshimori, & Miyawaki, 2008). This protein dysfunction through misfolding or improper trafficking of the chimeric protein to the cell membrane.

Future work must investigate whether the absence of GEVI signals was due to lack of expression, improper folding of the proteins and/or membrane trafficking issues. To address gene expression, one could conduct a simple qRT-PCR assay to detect mRNA levels of cGFP and mApple. The promoter could also be changed to improve gene expression. To address protein misfolding, one could examine ER retention by staining ER and observe whether GEVIs are localized to ER. To address the fundamental membrane trafficking machinery, one could identify the trafficking determinant amino acid sequence motifs which often lie in the C-terminus. As the mApple reporter is on the C-terminus of FliCR1, this configuration may interfere with membrane trafficking and modifications to the C-terminus may be necessary.

Once expression and membrane trafficking issues are resolved, a new approach could be to tether the GEVI together to GECI so that signal readouts are spatially and temporally coupled. One such construct is CaViar which integrated GCaMP6f and QuasAr2, a far red GEVI (excitation/emission peak of 640/720 nm) (Dempsey et al., 2016; Hou, Kralj, Douglass, Engert, & Cohen, 2014). CaViar was demonstrated to reliably report V_m and CaT in hiPSC-vCMs and was used in a cardiotoxicity screening application (Dempsey et al., 2016). However, QuasAr2 needed high power laser activation at 50W/cm^2 (Dempsey et al., 2016). Another weakness of the tethered approach is that the GECIs are localized close to the plasma membrane and may lose fidelity in reporting global CaT.

Chapter 6.

Conclusions: Significance and Contributions

In the first study, the aim was to establish a platform that uses human chamber specific hiPSC-CMs for drug screening of atrial-selective compounds. We adapted and validated recently published RA-based protocols to generate hiPSC-aCMs in a simplified monolayer format. The results demonstrated that hiPSC-aCMs displayed consistent atrial-like phenotypes at both molecular and functional levels. The optical mapping assay of membrane voltage and Ca^{2+} handling measurements present a comprehensive functional characterization of hiPSC-aCMs. Additionally, we demonstrated that our atrial differentiation protocol and optical mapping have capability to detect atrial-selective pharmacology. The hiPSC-aCMs and optical mapping system can also be used to study the molecular and cellular mechanisms of AF. Overall, this model system serves as a platform technology to functionally assay hiPSC-aCMs and thus extending the current capabilities for preclinical *in vitro* drug screening and disease modelling of AF.

In the second study, I developed a standardized protocol for in-house lentivirus production. I introduced a simplified workflow of concentrating lentivirus with PEG centrifugation gradient and quick titer measurement using qRT-PCR. The in-house lentivirus production protocol can be applied to other genetic constructs to be delivered into hiPSC-CMs. Furthermore, I reported the validation of an alternative optical mapping approach using genetically encoded fluorescent indicators. Even though the results of GEVIs warrant further troubleshooting and investigation, the GECI constructs can be readily applied in longitudinal Ca^{2+} imaging studies.

In summary, this thesis contributed to the knowledge of chamber-specific cardiac differentiation, atrial-specific pharmacological characterization, and developed and expanded the toolkit for functional characterization of chamber-specific hiPSC-CMs.

References

Abdelfattah, A. S., Farhi, S. L., Zhao, Y., Brinks, D., Zou, P., Ruangkittisakul, A., … Campbell, R. E. (2016). A Bright and Fast Red Fluorescent Protein Voltage Indicator That Reports Neuronal Activity in Organotypic Brain Slices. *The Journal of Neuroscience : The Official Journal of the Society for Neuroscience*, *36*(8), 2458–72. https://doi.org/10.1523/JNEUROSCI.3484-15.2016

Agency, E. M. (2010). Brinavess vernakalant hydrochloride, *1*(June), 1–2.

Akerboom, J., Rivera, J. D. V., Rodríguez Guilbe, M. M., Malavé, E. C. A., Hernandez, H. H., Tian, L., … Schreiter, E. R. (2009). Crystal structures of the GCaMP calcium sensor reveal the mechanism of fluorescence signal change and aid rational design. *Journal of Biological Chemistry*, *284*(10), 6455–6464. https://doi.org/10.1074/jbc.M807657200

Andrade, J. G., Verma, A., Mitchell, L. B., Parkash, R., Leblanc, K., Atzema, C., … CCS Atrial Fibrillation Guidelines Committee. (2018). 2018 Focused Update of the Canadian Cardiovascular Society Guidelines for the Management of Atrial Fibrillation. *The Canadian Journal of Cardiology*, *34*(11), 1371–1392. https://doi.org/10.1016/j.cjca.2018.08.026

Argenziano, M., Lambers, E., Hong, L., Sridhar, A., Zhang, M., Chalazan, B., … Darbar, D. (2018). Electrophysiologic Characterization of Calcium Handling in Human Induced Pluripotent Stem Cell-Derived Atrial Cardiomyocytes. *Stem Cell Reports*, *10*(6), 1867–1878. https://doi.org/10.1016/j.stemcr.2018.04.005

Aschar-Sobbi, R., Radisic, M., Backx, P. H., Jekic, D., Zhang, B., Pahnke, A., … Davenport Huyer, L. (2019). A Platform for Generation of Chamber-Specific Cardiac Tissues and Disease Modeling. *Cell*, *176*(4), 913–927.e18. https://doi.org/10.1016/j.cell.2018.11.042

Bachmann, A., Gutcher, I., Kopp, K., Brendel, J., Bosch, R. F., Busch, A. E., & Gögelein, H. (2001). Characterization of a novel Kv1.5 channel blocker in Xenopus oocytes, CHO cells, human and rat cardiomyocytes. *Naunyn-Schmiedeberg's Archives of Pharmacology*, *364*(5), 472–478. https://doi.org/10.1007/s002100100474

Backx, P. H., & Marban, E. (2012). Background potassium current active during the plateau of the action potential in guinea pig ventricular myocytes. *Circulation Research*, *72*(4), 890–900. https://doi.org/10.1161/01.res.72.4.890

Baman, T., Latchamsetty, R., & Oral, H. (2011). Complications of Radiofrequency Catheter Ablation for Atrial Fibrillation. *Journal of Atrial Fibrillation*, *4*(3), 345. https://doi.org/10.4022/jafib.345

Ban, K., Bae, S., & Yoon, Y.-S. (2017). Current Strategies and Challenges for Purification of Cardiomyocytes Derived from Human Pluripotent Stem Cells. *Theranostics*, *7*(7), 2067–2077. https://doi.org/10.7150/thno.19427

Bedut, S., Seminatore Nole, C., Lamamy, V., Caignard, S., Boutin, J. A., Nosjean, O., … Coge, F. (2016). High-throughput drug profiling with voltage and calcium-sensitive fluorescent probes in human iPSC-derived cardiomyocytes. *American Journal of Physiology - Heart and Circulatory Physiology*, (May), ajpheart.00793.2015. https://doi.org/10.1152/ajpheart.00793.2015

Besser, R. R., Ishahak, M., Mayo, V., Carbonero, D., Claure, I., & Agarwal, A. (2018). Engineered Microenvironments for Maturation of Stem Cell Derived Cardiac Myocytes. *Theranostics*, *8*(1), 124–140. https://doi.org/10.7150/thno.19441

Billman, G. E., & Kukielka, M. (2008). Novel transient outward and ultra-rapid delayed rectifier current antagonist, AVE0118, protects against ventricular fibrillation induced by myocardial ischemia. *Journal of Cardiovascular Pharmacology*, *51*(4), 352–8. https://doi.org/10.1097/FJC.0b013e31816586bd

Bizy, A., Guerrero-Serna, G., Hu, B., Ponce-Balbuena, D., Cicero Willis, B., Zarzoso, M., … Jalife, J. (2013). Myosin light chain 2-based selection of human iPSC-derived early ventricular cardiac myocytes. https://doi.org/10.1016/j.scr.2013.09.003

Blaauw, Y., Gögelein, H., Tieleman, R. G., van Hunnik, A., Schotten, U., & Allessie, M. A. (2004). “Early” Class III Drugs for the Treatment of Atrial Fibrillation. *Circulation*, *110*(13), 1717–1724. https://doi.org/10.1161/01.CIR.0000143050.22291.2E

Blazeski, A., Zhu, R., Hunter, D. W., Weinberg, S. H., Zambidis, E. T., & Tung, L. (2012). Cardiomyocytes derived from human induced pluripotent stem cells as models for normal and diseased cardiac electrophysiology and contractility. *Progress in Biophysics and Molecular Biology*, *110*(2–3), 166–177. https://doi.org/10.1016/J.PBIOMOLBIO.2012.07.013

Blinova, K., Stohlman, J., Vicente, J., Chan, D., Johannesen, L., Hortigon-Vinagre, M. P., … Strauss, D. G. (2017). Comprehensive translational assessment of human-induced pluripotent stem cell derived cardiomyocytes for evaluating drug-induced arrhythmias. *Toxicological Sciences*, *155*(1), 234–247. https://doi.org/10.1093/toxsci/kfw200

Blum, R. A., Ross, J. D., Brown, E. A., & Deweerth, S. P. (2007). An Integrated System for Simultaneous, Multichannel Neuronal Stimulation and Recording. *IEEE TRANSACTIONS ON CIRCUITS AND SYSTEMS-I: REGULAR PAPERS*, *54*(12). https://doi.org/10.1109/TCSI.2007.906071

Bock, G., Gebhart, M., Scharinger, A., Jangsangthong, W., Busquet, P., Poggiani, C., … Koschak, A. (2011). Functional properties of a newly identified C-terminal splice variant of Cav1.3 L-type Ca2+ channels. *The Journal of Biological Chemistry*, *286*(49), 42736–48. https://doi.org/10.1074/jbc.M111.269951

Bode, F., Kilborn, M., Karasik, P., & Franz, M. R. (2001). The Repolarization-Excitability Relationship in the Human Right Atrium Is Unaffected by Cycle Length, Recording Site and Prior Arrhythmias. https://doi.org/10.1016/S0735-1097(00)01189-X

Burashnikov, A., & Antzelevitch, C. (2003). Reinduction of Atrial Fibrillation Immediately After Termination of the Arrhythmia Is Mediated by Late Phase 3 Early Afterdepolarization–Induced Triggered Activity. *Circulation*, *107*(18), 2355–2360. https://doi.org/10.1161/01.CIR.0000065578.00869.7C

Burger, C., Gorbatyuk, O. S., Velardo, M. J., Peden, C. S., Williams, P., Zolotukhin, S., … Muzyczka, N. (2004). Recombinant AAV Viral Vectors Pseudotyped with Viral Capsids from Serotypes 1, 2, and 5 Display Differential Efficiency and Cell Tropism after Delivery to Different Regions of the Central Nervous System. *Molecular Therapy*, *10*(2), 302–317. https://doi.org/10.1016/J.YMTHE.2004.05.024

Burridge, P. W., Keller, G., Gold, J. D., & Wu, J. C. (2012). Production of de novo cardiomyocytes: human pluripotent stem cell differentiation and direct reprogramming. *Cell Stem Cell*, *10*(1), 16–28. https://doi.org/10.1016/j.stem.2011.12.013

Burridge, P. W., Matsa, E., Shukla, P., Lin, Z. C., Churko, J. M., Ebert, A. D., … Wu, J. C. (2014). Chemically defined generation of human cardiomyocytes. *Nature Methods*, *11*(8), 855–60. https://doi.org/10.1038/nmeth.2999

Campbell, F. R., S., E. G. D., & O'Shea, J. E. (1989). Effects of Vaagal Stimulation and Applied Acetylcholine on Pacemaker Potentials in the Guinea-pig Heart. *Journal of Physiology*, *415*, 57–68.

Canada, H. (2018). Brinavess Product Monograph, 1–33.

Cao, Y., Chen, H., Qiu, R., Hanna, M., Ma, E., Hjort, M., … Melosh, N. A. (2018). Universal intracellular biomolecule delivery with precise dosage control. *Science Advances*, *4*(10), eaat8131. https://doi.org/10.1126/sciadv.aat8131

Carmeliet, E. (2004). Intracellular Ca2+ concentration and rate adaptation of the cardiac action potential. *Cell Calcium*, *35*(6), 557–573. https://doi.org/10.1016/j.ceca.2004.01.010

Carrasco-Pozo, C., Pastene, E., Vergara, C., Zapata, M., Sandoval, C., & Gotteland, M. (2012). Stimulation of cytosolic and mitochondrial calcium mobilization by indomethacin in Caco-2 cells: Modulation by the polyphenols quercetin, resveratrol and rutin. *Biochimica et Biophysica Acta (BBA) - General Subjects*, *1820*(12), 2052–2061. https://doi.org/10.1016/J.BBAGEN.2012.09.015

Casillas-Espinosa, P. M., Hicks, A., Jeffreys, A., Snutch, T. P., O'Brien, T. J., & Powell, K. L. (2015). Z944, a Novel Selective T-Type Calcium Channel Antagonist Delays the Progression of Seizures in the Amygdala Kindling Model. *PLOS ONE*, *10*(8), e0130012. https://doi.org/10.1371/journal.pone.0130012

Chang, K. C., & Trayanova, N. A. (2016). Mechanisms of arrhythmogenesis related to calcium-driven alternans in a model of human atrial fibrillation. *Scientific Reports*, *6*(October), 36395. https://doi.org/10.1038/srep36395

Chen, T.-W., Wardill, T. J., Sun, Y., Pulver, S. R., Renninger, S. L., Baohan, A., … Kim, D. S. (2013a). Ultrasensitive fluorescent proteins for imaging neuronal activity. *Nature*, *499*(7458), 295–300. https://doi.org/10.1038/nature12354

Chen, T.-W., Wardill, T. J., Sun, Y., Pulver, S. R., Renninger, S. L., Baohan, A., … Kim, D. S. (2013b). Ultrasensitive fluorescent proteins for imaging neuronal activity. *Nature*, *499*(7458), 295–300. https://doi.org/10.1038/nature12354

Chen, Z., Xian, W., Bellin, M., Dorn, T., Tian, Q., Goedel, A., … Gepstein, L. (2016). Subtype-specific promoter-driven action potential imaging for precise disease modelling and drug testing in hiPSC-derived cardiomyocytes. *European Heart Journal*, *13*(11), 713–726. https://doi.org/10.1093/eurheartj/ehw189

Christ, T., Wettwer, E., Voigt, N., Hála, O., Radicke, S., Matschke, K., … Ravens, U. (2009). Pathology-specific effects of the IKur/Ito/IK,ACh blocker AVE0118 on ion channels in human chronic atrial fibrillation. *British Journal of Pharmacology*, *154*(8), 1619–1630. https://doi.org/10.1038/bjp.2008.209

Chua, S.-K., Chang, P.-C., Maruyama, M., Turker, I., Shinohara, T., Shen, M. J., … Chen, P.-S. (2011). Small-Conductance Calcium-Activated Potassium Channel and Recurrent Ventricular Fibrillation in Failing Rabbit Ventricles. *Circulation Research*, *108*(8), 971–979. https://doi.org/10.1161/CIRCRESAHA.110.238386

Colatsky, T., Fermini, B., Gintant, G., Pierson, J. B., Sager, P., Sekino, Y., … Stockbridge, N. (2016). The Comprehensive in Vitro Proarrhythmia Assay (CiPA) initiative — Update on progress. https://doi.org/10.1016/j.vascn.2016.06.002

Comtois, P., Kneller, J., & Nattel, S. (2005). Of circles and spirals: Bridging the gap between the leading circle and spiral wave concepts of cardiac reentry. *Europace*, *7*(SUPPL. 2), 10–20. https://doi.org/10.1016/j.eupc.2005.05.011

Corda, S., Samuel, J.-L., & Rappaport, L. (2000). Extracellular Matrix and Growth Factors During Heart Growth. *Heart Failure Reviews*, *5*(2), 119–130. https://doi.org/10.1023/A:1009806403194

Cotten, J. F. (2013). TASK-1 (KCNK3) and TASK-3 (KCNK9) Tandem Pore Potassium Channel Antagonists Stimulate Breathing in Isoflurane-Anesthetized Rats. *Anesthesia & Analgesia*, *116*(4), 810–816. https://doi.org/10.1213/ANE.0b013e318284469d

Crumb, W. J., Vicente, J., Johannesen, L., & Strauss, D. G. (2016). An evaluation of 30 clinical drugs against the comprehensive in vitro proarrhythmia assay (CiPA) proposed ion channel panel. *Journal of Pharmacological and Toxicological Methods*, *81*, 251–262. https://doi.org/10.1016/j.vascn.2016.03.009

Cyganek, L., Hasenfuss, G., Guan, K., Cyganek, L., Tiburcy, M., Sekeres, K., & Gerstenberg, K. (2018). Deep phenotyping of human induced pluripotent stem cell – derived atrial and ventricular cardiomyocytes Find the latest version : Deep phenotyping of human induced pluripotent stem cell – derived atrial and ventricular cardiomyocytes. *JCI Insight*, *3*(12), e99941. https://doi.org/10.1172/jci.insight.99941

Daily, N. J., Du, Z.-W., & Wakatsuki, T. (2017). High-Throughput Phenotyping of Human Induced Pluripotent Stem Cell-Derived Cardiomyocytes and Neurons Using Electric Field Stimulation and High-Speed Fluorescence Imaging. *ASSAY and Drug Development Technologies*, *15*(4), 178–188. https://doi.org/10.1089/adt.2017.781

Daily, N. J., Santos, R., Vecchi, J., Kemanli, P., & Wakatsuki, T. (2017). Calcium Transient Assays for Compound Screening with Human iPSC-derived Cardiomyocytes: Evaluating New Tools, *17*(1), 1–11. https://doi.org/10.1038/nm.2451.A

De Ferrari, G. M., Maier, L. S., Mont, L., Schwartz, P. J., Simonis, G., Leschke, M., … RAFFAELLO Investigators (see Online Supplementary Appendix for List of Participating Centers and Investigators). (2015). Ranolazine in the treatment of atrial fibrillation: Results of the dose-ranging RAFFAELLO (Ranolazine in Atrial Fibrillation Following An ELectricaL CardiOversion) study. *Heart Rhythm*, *12*(5), 872–8. https://doi.org/10.1016/j.hrthm.2015.01.021

de Groot, N. M. S., Kirchhof, C. J., van Gelder, I. C., Meeder, J. G., Balk, A. H. M. M., Wilde, A. A., & Simoons, M. L. (2010). Dronedarone in patients with atrial fibrillation. *Netherlands Heart Journal*, *18*(7–8), 370–373. https://doi.org/10.1007/BF03091794

Decher, N., Kiper, A. K., Rolfes, C., Schulze-Bahr, E., & Rinné, S. (2015). The role of acid-sensitive two-pore domain potassium channels in cardiac electrophysiology: focus on arrhythmias. *Pflügers Archiv - European Journal of Physiology*, *467*(5), 1055–1067. https://doi.org/10.1007/s00424-014-1637-5

Decher, N., Kumar, P., Gonzalez, T., Pirard, B., & Sanguinetti, M. C. (2006). Binding site of a novel Kv1.5 blocker: a "foot in the door" against atrial fibrillation. *Molecular Pharmacology*, *70*(4), 1204–11. https://doi.org/10.1124/mol.106.026203

Dempsey, G. T., Chaudhary, K. W., Atwater, N., Nguyen, C., Brown, B. S., McNeish, J. D., … Kralj, J. M. (2016). Cardiotoxicity screening with simultaneous optogenetic pacing, voltage imaging and calcium imaging. *Journal of Pharmacological and Toxicological Methods*, *81*, 240–250. https://doi.org/10.1016/j.vascn.2016.05.003

Devalla, H. D., Schwach, V., Ford, J. W., Milnes, J. T., El-Haou, S., Jackson, C., … Passier, R. (2015). Atrial-like cardiomyocytes from human pluripotent stem cells are a robust preclinical model for assessing atrial-selective pharmacology. *EMBO Molecular Medicine*, *7*(4), 394–410. https://doi.org/10.15252/emmm.201404757

Diness, J. G., Skibsbye, L., Jespersen, T., Bartels, E. D., Sørensen, U. S., Hansen, R. S., & Grunnet, M. (2011). Effects on atrial fibrillation in aged hypertensive rats by Ca 2+-activated K+ channel inhibition. *Hypertension*, *57*(6), 1129–1135. https://doi.org/10.1161/HYPERTENSIONAHA.111.170613

Diness, J. G., Skibsbye, L., Simó-Vicens, R., Santos, J. L., Lundegaard, P., Citerni, C., … Bentzen, B. H. (2017). Termination of vernakalant-resistant atrial fibrillation by inhibition of small-conductance Ca2+-Activated K+ channels in Pigs. *Circulation: Arrhythmia and Electrophysiology*, *10*(10). https://doi.org/10.1161/CIRCEP.117.005125

Diness, J. G., Sørensen, U. S., Nissen, J. D., Al-Shahib, B., Jespersen, T., Grunnet, M., & Hansen, R. S. (2010). Inhibition of small-conductance ca2+-activated k+channels terminates and protects against atrial fibrillation. *Circulation: Arrhythmia and Electrophysiology*, *3*(4), 380–390. https://doi.org/10.1161/CIRCEP.110.957407

Dittrich, H. C., Feld, G. K., Bahnson, T. D., Camm, A. J., Golitsyn, S., Katz, A., … Brown, A. M. (2015). COR-ART: A multicenter, randomized, double-blind, placebo-controlled dose-ranging study to evaluate single oral doses of vanoxerine for conversion of recent-onset atrial fibrillation or flutter to normal sinus rhythm. *Heart Rhythm*, *12*(6), 1105–12. https://doi.org/10.1016/j.hrthm.2015.02.014

Djurovic, S., Iversen, N., Jeansson, S., Hoover, F., & Christensen, G. (2004). Comparison of Nonviral Transfection and Adeno-Associated Viral Transduction on Cardiomyocytes. *Molecular Biotechnology*, *28*(1), 21–32. https://doi.org/10.1385/MB:28:1:21

Dobrev, D. (2017). Unique cardiomyocyte ultrastructure in atria: Role of T tubules in subcellular Ca2+ signaling and atrial arrhythmogenesis. *Heart Rhythm*, *14*(2), 282–283. https://doi.org/10.1016/j.hrthm.2016.10.013

Dobrev, D., Friedrich, A., Voigt, N., Jost, N., Wettwer, E., Christ, T., … Ravens, U. (2005). The G Protein–Gated Potassium Current $I_{K,ACh}$ Is Constitutively Active in Patients With Chronic Atrial Fibrillation. *Circulation*, *112*(24), 3697–3706. https://doi.org/10.1161/CIRCULATIONAHA.105.575332

Dorenkamp, M., Morguet, A. J., Sticherling, C., Behrens, S., & Zabel, M. (2013). Long-Term Prognostic Value of Restitution Slope in Patients with Ischemic and Dilated Cardiomyopathies. *PLoS ONE*, *8*(1), e54768. https://doi.org/10.1371/journal.pone.0054768

Dorian, P., & Mangat, I. (2003). *Quality of Life Variables in the Selection of Rate Versus Rhythm Control in Patients with Atrial Fibrillation: Observations from the Canadian Trial of Atrial Fibrillation*. *Cardiac Electrophysiology Review* (Vol. 7). Kluwer Academic Publishers. Retrieved from https://link.springer.com/content/pdf/10.1023/B:CEPR.0000012395.33292.cd.pdf

Dorian, P., Pinter, A., Mangat, I., Korley, V., Cvitkovic, S. S., & Beatch, G. N. (2007). The effect of vernakalant (RSD1235), an investigational antiarrhythmic agent, on atrial electrophysiology in humans. *Journal of Cardiovascular Pharmacology*, *50*(1), 35–40. https://doi.org/10.1097/FJC.0b013e3180547553

Du, Y., Zhang, X., Tu, D., Zhao, N., Liu, Y., Xiao, H., … Liao, Y. (2010). Molecular determinants of Kv1.5 channel block by diphenyl phosphine oxide-1. *Journal of Molecular and Cellular Cardiology*, *48*(6), 1111–20. https://doi.org/10.1016/j.yjmcc.2010.02.010

Dubois, N. C., Craft, A. M., Sharma, P., Elliott, D. a, Stanley, E. G., Elefanty, A. G., … Keller, G. (2011). SIRPA is a specific cell-surface marker for isolating cardiomyocytes derived from human pluripotent stem cells. *Nature Biotechnology*, *29*(11), 1011–1018. https://doi.org/10.1038/nbt.2005

Dull, T., Zufferey, R., Kelly, M., Mandel, R. J., Nguyen, M., Trono, D., & Naldini, L. (1998). *A Third-Generation Lentivirus Vector with a Conditional Packaging System Downloaded from*. *JOURNAL OF VIROLOGY* (Vol. 72). Retrieved from http://jvi.asm.org/

Dunlop, J., Bowlby, M., Peri, R., Vasilyev, D., & Arias, R. (2008). High-throughput electrophysiology: an emerging paradigm for ion-channel screening and physiology. *Nature Reviews Drug Discovery*, *7*(4), 358–368. https://doi.org/10.1038/nrd2552

Ellinor, P. T., Lunetta, K. L., Glazer, N. L., Pfeufer, A., Alonso, A., Chung, M. K., … Kääb, S. (2010). Common variants in KCNN3 are associated with lone atrial fibrillation. *Nature Genetics*, *42*(3), 240–244. https://doi.org/10.1038/ng.537

Elliott, D. A., Braam, S. R., Koutsis, K., Ng, E. S., Jenny, R., Lagerqvist, E. L., … Stanley, E. G. (2011). NKX2-5(eGFP/w) hESCs for isolation of human cardiac progenitors and cardiomyocytes. *Nature Methods*, *8*(12), 1037–40. https://doi.org/10.1038/nmeth.1740

Ellis, B. L., Hirsch, M. L., Barker, J. C., Connelly, J. P., Steininger, R. J., & Porteus, M. H. (2013). A survey of ex vivo/in vitro transduction efficiency of mammalian primary cells and cell lines with Nine natural adeno-associated virus (AAV1-9) and one engineered adeno-associated virus serotype. *Virology Journal*, *10*(1), 74. https://doi.org/10.1186/1743-422X-10-74

Espinoza, C. A., Mehra, S., & DeAntonio, H. (2016). Double Trouble: Concurrent Atrial Fibrillation and Ventricular Tachycardia. *Revista Española de Cardiología (English Edition)*, *69*(8), 779–780. https://doi.org/10.1016/j.rec.2015.12.026

FEDIDA, D., ORTH, P. M. R., CHEN, J. Y. C., LIN, S., PLOUVIER, B., JUNG, G., … BEATCH, G. N. (2005). The Mechanism of Atrial Antiarrhythmic Action of RSD1235. *Journal of Cardiovascular Electrophysiology*, *16*(11), 1227–1238. https://doi.org/10.1111/j.1540-8167.2005.50028.x

Fedida, D., Wible, B., Fermini, B., Faust, F., Nattel, S., & Brown, A. M. (1993). Identity of a Novel Delayed Rectifier Current From Human Heart With a Cloned K+ Channel Current. *Circulation Research*, *73*(1), 210–216.

Finnin, M. (2010). Vernakalant: A novel agent for the termination of atrial fibrillation. *American Journal of Health-System Pharmacy*, *67*(14), 1157–1164. https://doi.org/10.2146/ajhp080501

Flaherty, M. P., Kamerzell, T. J., & Dawn, B. (2012). Wnt Signaling and Cardiac Differentiation. *Progress in Molecular Biology and Translational Science*, *111*, 153–174. https://doi.org/10.1016/B978-0-12-398459-3.00007-1

Ford, J., Milnes, J., El Haou, S., Wettwer, E., Loose, S., Matschke, K., … Ravens, U. (2016). The positive frequency-dependent electrophysiological effects of the IKur inhibitor XEN-D0103 are desirable for the treatment of atrial fibrillation. *Heart Rhythm*, *13*(2), 555–64. https://doi.org/10.1016/j.hrthm.2015.10.003

Ford, J., Milnes, J., Wettwer, E., Christ, T., Rogers, M., Sutton, K., … Ravens, U. (2013). Human Electrophysiological and Pharmacological Properties of XEN-D0101. *Journal of Cardiovascular Pharmacology*, *61*(5), 408–415. https://doi.org/10.1097/FJC.0b013e31828780eb

Ford, J. W., & Milnes, J. T. (2008). New drugs targeting the cardiac ultra-rapid delayed-rectifier current (I Kur): rationale, pharmacology and evidence for potential therapeutic value. *Journal of Cardiovascular Pharmacology*, *52*(2), 105–20. https://doi.org/10.1097/FJC.0b013e3181719b0c

Franco, D., Markman, M. M. W., Wagenaar, G. T. M., Ya, J., Lamers, W. H., & Moorman, A. F. M. (1999). Myosin light chain 2a and 2v identifies the embryonic outflow tract myocardium in the developing rodent heart. *The Anatomical Record*, *254*(1), 135–146. https://doi.org/10.1002/(SICI)1097-0185(19990101)254:1<135::AID-AR17>3.0.CO;2-S

Franz, M. R. (2003). The Electrical Restitution Curve Revisited:. Steep or Flat Slope-Which is Better? *Journal of Cardiovascular Electrophysiology*, *14*(s10), S140–S147. https://doi.org/10.1046/j.1540.8167.90303.x

Franz, M. R., Jamal, S. M., & Narayan, S. M. (2012). The role of action potential alternans in the initiation of atrial fibrillation in humans: A review and future directions. *Europace*, *14*(SUPPL. 5), 58–64. https://doi.org/10.1093/europace/eus273

Gaborit, N., Le Bouter, S., Szuts, V., Varro, A., Escande, D., Nattel, S., & Demolombe, S. (2007). Regional and tissue specific transcript signatures of ion channel genes in the non-diseased human heart. *The Journal of Physiology*, *582*(2), 675–693. https://doi.org/10.1113/jphysiol.2006.126714

Ganesan, A. N., Shipp, N. J., Brooks, A. G., Kuklik, P., Lau, D. H., Lim, H. S., … Sanders, P. (2013). Long-term Outcomes of Catheter Ablation of Atrial Fibrillation: A Systematic Review and Meta-analysis. *Journal of the American Heart Association*, *2*(2). https://doi.org/10.1161/JAHA.112.004549

Gao, L., Kupfer, M. E., Jung, J. P., Yang, L., Zhang, P., Da Sie, Y., … Zhang, J. (2017). Myocardial Tissue Engineering with Cells Derived from Human-Induced Pluripotent Stem Cells and a Native-Like, High-Resolution, 3-Dimensionally Printed Scaffold. *Circulation Research*, *120*(8), 1318–1325. https://doi.org/10.1161/CIRCRESAHA.116.310277

Geiss, G. K., Bumgarner, R. E., Birditt, B., Dahl, T., Dowidar, N., Dunaway, D. L., … Dimitrov, K. (2008). Direct multiplexed measurement of gene expression with color-coded probe pairs. *Nature Biotechnology*, *26*(3), 317–325. https://doi.org/10.1038/nbt1385

Gentles, R. G., Grant-Young, K., Hu, S., Huang, Y., Poss, M. A., Andres, C., … Harden, D. G. (2008). Initial SAR studies on apamin-displacing 2-aminothiazole blockers of calcium-activated small conductance potassium channels. *Bioorganic & Medicinal Chemistry Letters*, *18*(19), 5316–5319. https://doi.org/10.1016/J.BMCL.2008.08.023

Gierten, J., Ficker, E., Bloehs, R., Schweizer, P. A., Zitron, E., Scholz, E., … Thomas, D. (2010). The human cardiac K2P3.1 (TASK-1) potassium leak channel is a molecular target for the class III antiarrhythmic drug amiodarone. *Naunyn-Schmiedeberg's Archives of Pharmacology*, *381*(3), 261–270. https://doi.org/10.1007/s00210-009-0454-4

Gogelein, H., Brendel, J., Steinmeyer, K., Strobing, C., Picard, N., Rampe, D., … Bleich, M. (2004). Effects of the atrial antiarrhythmic drug AVE0118 on cardiac ion channels. *Naunyn-Schmiedeberg's Archives of Pharmacology*, *370*(3), 183–192. https://doi.org/10.1007/s00210-004-0957-y

Goldhaber, J. I., Xie, L.-H., Duong, T., Motter, C., Khuu, K., & Weiss, J. N. (2005). Action Potential Duration Restitution and Alternans in Rabbit Ventricular Myocytes. *Circulation Research*, *96*(4), 459–466. https://doi.org/10.1161/01.res.0000156891.66893.83

Goldstein, S. A. N., Bockenhauer, D., O'Kelly, I., & Zilberberg, N. (2001). Potassium leak channels and the KCNK family of two-p-domain subunits. *Nature Reviews Neuroscience*, *2*(3), 175–184. https://doi.org/10.1038/35058574

Gonzá lez, W., Zúniga, L., Cid, L. P., Arévalo, B., Niemeyer, M. I., & Sepúlveda, F. V. (2013). An extracellular ion pathway plays a central role in the cooperative gating of a K2P K+ channel by extracellular pH. *Journal of Biological Chemistry*, *288*(8), 5984–5991. https://doi.org/10.1074/jbc.M112.445528

Greiser, M., Kerfant, B.-G., Williams, G. S. B., Voigt, N., Harks, E., Dibb, K. M., … Schotten, U. (2014). Tachycardia-induced silencing of subcellular Ca2+ signaling in atrial myocytes. *The Journal of Clinical Investigation*, *124*(11), 4759–4772. https://doi.org/10.1172/JCI70102

Gudbjartsson, D. F., Arnar, D. O., Helgadottir, A., Gretarsdottir, S., Holm, H., Sigurdsson, A., … Stefansson, K. (2007). Variants conferring risk of atrial fibrillation on chromosome 4q25. *Nature*, *448*(7151), 353–357. https://doi.org/10.1038/nature06007

Gupta, T., Khera, S., Kolte, D., Aronow, W. S., & Iwai, S. (2015). Antiarrhythmic properties of ranolazine: A review of the current evidence. *International Journal of Cardiology*, *187*, 66–74. https://doi.org/10.1016/j.ijcard.2015.03.324

Haïssaguerre, M., Jaïs, P., Shah, D. C., Takahashi, A., Hocini, M., Quiniou, G., … Clémenty, J. (1998). Spontaneous Initiation of Atrial Fibrillation by Ectopic Beats Originating in the Pulmonary Veins. *New England Journal of Medicine*, *339*(10), 659–666. https://doi.org/10.1056/NEJM199809033391003

Harleton, E., Besana, A., Chandra, P., Danilo, P., Rosen, T. S., Rosen, M. R., … Feinmark, S. J. (2015). TASK-1 current is inhibited by phosphorylation during human and canine chronic atrial fibrillation. *American Journal of Physiology-Heart and Circulatory Physiology*, *308*(2), H126–H134. https://doi.org/10.1152/ajpheart.00614.2014

Haugaard, M. M., Hesselkilde, E. Z., Pehrson, S., Carstensen, H., Flethøj, M., Præstegaard, K. F., … Jespersen, T. (2015). Pharmacologic inhibition of small-conductance calcium-activated potassium (SK) channels by NS8593 reveals atrial antiarrhythmic potential in horses. *Heart Rhythm*, *12*(4), 825–835. https://doi.org/10.1016/J.HRTHM.2014.12.028

Hawwa, N., & Menon, V. (2013). Ranolazine: Clinical Applications and Therapeutic Basis. *American Journal of Cardiovascular Drugs*, *13*(1), 5–16. https://doi.org/10.1007/s40256-012-0003-2

Herron, T. J., Lee, P., & Jalife, J. (2012). Optical imaging of voltage and calcium in cardiac cells & tissues. *Circulation Research*, *110*(4), 609–623. https://doi.org/10.1161/CIRCRESAHA.111.247494

Himmel, H. M. (2013). Drug-induced functional cardiotoxicity screening in stem cell-derived human and mouse cardiomyocytes: Effects of reference compounds. *Journal of Pharmacological and Toxicological Methods*, *68*(1), 97–111. https://doi.org/10.1016/j.vascn.2013.05.005

Hirschi, K. K., Li, S., & Roy, K. (2014). Induced pluripotent stem cells for regenerative medicine. *Annual Review of Biomedical Engineering*, *16*, 277–94. https://doi.org/10.1146/annurev-bioeng-071813-105108

Hochbaum, D. R., Zhao, Y., Farhi, S. L., Klapoetke, N., Werley, C. A., Kapoor, V., … Cohen, A. E. (2014). All-optical electrophysiology in mammalian neurons using engineered microbial rhodopsins. *Nature Methods*, *11*(8), 825–33. https://doi.org/10.1038/nmeth.3000

Hohnloser, S. H., Kuck, K.-H., & Lilienthal, J. (2000). Rhythm or rate control in atrial fibrillation—Pharmacological Intervention in Atrial Fibrillation (PIAF): a randomised trial. *The Lancet*, *356*(9244), 1789–1794. https://doi.org/10.1016/S0140-6736(00)03230-X

Hortigon-Vinagre, M. P., Zamora, V., Burton, F. L., Green, J., Gintant, G. A., & Smith, G. L. (2017). The Use of Ratiometric Fluorescence Measurements of the Voltage Sensitive Dye Di-4-ANEPPS to Examine Action Potential Characteristics and Drug Effects on Human Induced Pluripotent Stem Cell-Derived Cardiomyocytes. https://doi.org/10.1093/toxsci/kfw171

Horváth, A., Lemoine, M. D., Löser, A., Mannhardt, I., Flenner, F., Uzun, A. U., … Christ, T. (2018). Low Resting Membrane Potential and Low Inward Rectifier Potassium Currents Are Not Inherent Features of hiPSC-Derived Cardiomyocytes. *Stem Cell Reports*, *10*(3), 822–833. https://doi.org/10.1016/J.STEMCR.2018.01.012

Hosseini, R., Benton, D. C. H., Dunn, P. M., Jenkinson, D. H., & Moss, G. W. J. (2001). SK3 is an important component of K+ channels mediating the afterhyperpolarization in cultured rat SCG neurones. *Journal of Physiology*, *535*(2), 323–334. https://doi.org/10.1111/j.1469-7793.2001.00323.x

Hou, J. H., Kralj, J. M., Douglass, A. D., Engert, F., & Cohen, A. E. (2014). Simultaneous mapping of membrane voltage and calcium in zebrafish heart in vivo reveals chamber-specific developmental transitions in ionic currents. *Frontiers in Physiology*, *5 AUG*(September), 1–10. https://doi.org/10.3389/fphys.2014.00344

Hsueh, C.-H., Chang, P.-C., Hsieh, Y.-C., Reher, T., Chen, P.-S., & Lin, S.-F. (2013). Proarrhythmic effect of blocking the small conductance calcium activated potassium channel in isolated canine left atrium. *Heart Rhythm*, *10*(6), 891–898. https://doi.org/10.1016/j.hrthm.2013.01.033

Huang, H.-L., Hsing, H.-W., Lai, T.-C., Chen, Y.-W., Lee, T.-R., Chan, H.-T., … Chan, H.-L. (2010). *Trypsin-induced proteome alteration during cell subculture in mammalian cells*. *Journal of Biomedical Science* (Vol. 17). https://doi.org/10.1186/1423-0127-17-36

Investigators, T. A. F. F. I. of R. M. (AFFIRM). (2002). A Comparison of Rate Control and Rhythm Control in Patients with Atrial Fibrillation. *New England Journal of Medicine*, *347*(23), 1825–1833. https://doi.org/10.1056/NEJMoa021328

Ishida, H., Genka, C., Nakazawa, H., Seguchi, H., Kadono, T., Hirota, Y., … Tanaami, T. (2005). Difference in Propagation of Ca2+ Release in Atrial and Ventricular Myocytes. *The Japanese Journal of Physiology*, *55*(2), 81–91. https://doi.org/10.2170/jjphysiol.r2077

Jaiswal, A., & Goldbarg, S. (2014). Dofetilide induced torsade de pointes: Mechanism, risk factors and management strategies. *Indian Heart Journal*, *66*, 640–648. https://doi.org/10.1016/j.ihj.2013.12.021

Jans, D., Callewaert, G., Krylychkina, O., Hoffman, L., Gullo, F., Prodanov, D., & Braeken, D. (2017). Action potential-based MEA platform for in vitro screening of drug-induced cardiotoxicity using human iPSCs and rat neonatal myocytes. *Journal of Pharmacological and Toxicological Methods*, 1–0. https://doi.org/10.1016/j.vascn.2017.05.003

January, C. T., Wann, L. S., Alpert, J. S., Calkins, H., Cigarroa, J. E., Cleveland, J. C., … Yancy, C. W. (2014). 2014 AHA/ACC/HRS Guideline for the Management of Patients With Atrial Fibrillation: Executive Summary. *Journal of the American College of Cardiology*, *64*(21), 2246–2280. https://doi.org/10.1016/j.jacc.2014.03.021

Jin, L., Han, Z., Platisa, J., Wooltorton, J. R. A., Cohen, L. B., & Pieribone, V. A. (2012). Single Action Potentials and Subthreshold Electrical Events Imaged in Neurons with a Fluorescent Protein Voltage Probe. *Neuron*, *75*(5), 779–785. https://doi.org/10.1016/j.neuron.2012.06.040

Josowitz, R., Lu, J., Falce, C., D'Souza, S. L., Wu, M., Cohen, N., … Gelb, B. D. (2014). Identification and Purification of Human Induced Pluripotent Stem Cell-Derived Atrial-Like Cardiomyocytes Based on Sarcolipin Expression. *PLoS ONE*, *9*(7), e101316. https://doi.org/10.1371/journal.pone.0101316

Katayama, H., Yamamoto, A., Mizushima, N., Yoshimori, T., & Miyawaki, A. (2008). GFP-like Proteins Stably Accumulate in Lysosomes. *Cell Structure and Function*, *33*(1), 1–12. https://doi.org/10.1247/csf.07011

Kim, B.-S., Kim, Y.-H., Hwang, G.-S., Pak, H.-N., Lee, S. C., Shim, W. J., … Ro, Y. M. (2002). Action potential duration restitution kinetics in human atrial fibrillation. *Journal of the American College of Cardiology*, *39*(8), 1329–1336. https://doi.org/10.1016/S0735-1097(02)01760-6

Kim, K. H., Kim, D., Park, J. Y., Jung, H. J., Cho, Y.-H., Kim, H. K., … Kwon, H. J. (2015). NNC 55-0396, a T-type Ca2+ channel inhibitor, inhibits angiogenesis via suppression of hypoxia-inducible factor-1α signal transduction. *Journal of Molecular Medicine*, *93*(5), 499–509. https://doi.org/10.1007/s00109-014-1235-1

Kiper, A. K., Rinné, S., Rolfes, C., Ramírez, D., Seebohm, G., Netter, M. F., … Decher, N. (2015). Kv1.5 blockers preferentially inhibit TASK-1 channels: TASK-1 as a target against atrial fibrillation and obstructive sleep apnea? *Pflugers Archiv European Journal of Physiology*, *467*(5), 1081–1090. https://doi.org/10.1007/s00424-014-1665-1

Kisselbach, L., Merges, M., Bossie, A., & Boyd, A. (2009). CD90 expression on human primary cells and elimination of contaminating fibroblasts from cell cultures. *Cytotechnology*, *59*(1), 31–44. https://doi.org/10.1007/s10616-009-9190-3

Koch, B., Nijmeijer, B., Kueblbeck, M., Cai, Y., Walther, N., & Ellenberg, J. (2018). Generation and validation of homozygous fluorescent knock-in cells using CRISPR–Cas9 genome editing. *Nature Protocols*, *13*(6), 1465–1487. https://doi.org/10.1038/nprot.2018.042

Kovacs, R. J., & Bailey, J. C. (1985). Effects of acetylcholine on action potential characteristics of atrial and ventricular myocardium after bilateral cervical vagotomy in the cat. *Circulation Research*, *56*(4), 613–620. https://doi.org/10.1161/01.RES.56.4.613

LACERDA, A. E., KURYSHEV, Y. A., YAN, G.-X., WALDO, A. L., & BROWN, A. M. (2010). Vanoxerine: Cellular Mechanism of a New Antiarrhythmic. *Journal of Cardiovascular Electrophysiology*, *21*(3), 301–310. https://doi.org/10.1111/j.1540-8167.2009.01623.x

Lagrutta, A., Wang, J., Fermini, B., & Salata, J. J. (2006). Novel, potent inhibitors of human Kv1.5 K+ channels and ultrarapidly activating delayed rectifier potassium current. *The Journal of Pharmacology and Experimental Therapeutics*, *317*(3), 1054–63. https://doi.org/10.1124/jpet.106.101162

Laksman, Z., Wauchop, M., Lin, E., Protze, S., Lee, J., Yang, W., … Backx, P. H. (2017). Modeling Atrial Fibrillation using Human Embryonic Stem Cell- Derived Atrial Tissue. https://doi.org/10.1038/s41598-017-05652-y

Lee, J. H., Protze, S. I., Laksman, Z., Backx, P. H., & Keller, G. M. (2017). Human Pluripotent Stem Cell-Derived Atrial and Ventricular Cardiomyocytes Develop from Distinct Mesoderm Populations. *Cell Stem Cell*, *21*(2), 179–194.e4. https://doi.org/10.1016/j.stem.2017.07.003

Lee, T.-S., Kaku, T., Takebayashi, S., Uchino, T., Miyamoto, S., Hadama, T., … Ono, K. (2006). Actions of Mibefradil, Efonidipine and Nifedipine Block of Recombinant T- and L-Type Ca²⁺ Channels with Distinct Inhibitory Mechanisms. *Pharmacology*, *78*(1), 11–20. https://doi.org/10.1159/000094900

Lei, M., Wu, L., Terrar, D. A., & Huang, C. L.-H. (2018). Modernized Classification of Cardiac Antiarrhythmic Drugs. *Circulation*, *138*(17), 1879–1896. https://doi.org/10.1161/CIRCULATIONAHA.118.035455

Lemme, M., Ulmer, B. M., Lemoine, M. D., Zech, A. T. L., Flenner, F., Ravens, U., … Eschenhagen, T. (2018). Atrial-like Engineered Heart Tissue: An In Vitro Model of the Human Atrium. *Stem Cell Reports*, *11*(6), 1378–1390. https://doi.org/10.1016/j.stemcr.2018.10.008

Lentz, T. B., Gray, S. J., & Samulski, R. J. (2011). Viral Vectors for Gene Delivery to the Central Nervous System. https://doi.org/10.1016/j.nbd.2011.09.014

Leyton-Mange, J. S., Mills, R. W., Macri, V. S., Jang, M. Y., Butte, F. N., Ellinor, P. T., & Milan, D. J. (2014). Rapid cellular phenotyping of human pluripotent stem cell-derived cardiomyocytes using a genetically encoded fluorescent voltage sensor. *Stem Cell Reports*, *2*(2), 163–170. https://doi.org/10.1016/j.stemcr.2014.01.003

Lian, X., Hsiao, C., Wilson, G., Zhu, K., Hazeltine, L. B., Azarin, S. M., … Palecek, S. P. (2012). Robust cardiomyocyte differentiation from human pluripotent stem cells via temporal modulation of canonical Wnt signaling. *Proceedings of the National Academy of Sciences of the United States of America*, *109*(27), E1848-57. https://doi.org/10.1073/pnas.1200250109

Lian, X., Zhang, J., Azarin, S. M., Zhu, K., Hazeltine, L. B., Bao, X., … Palecek, S. P. (2013). Directed cardiomyocyte differentiation from human pluripotent stem cells by modulating Wnt/β-catenin signaling under fully defined conditions. *Nature Protocols*, *8*, 162–75. https://doi.org/10.1038/nprot.2012.150

Liau, B., Jackman, C. P., Li, Y., & Bursac, N. (2017). Developmental stage-dependent effects of cardiac fibroblasts on function of stem cell-derived engineered cardiac tissues. *Scientific Reports*, *7*(1), 42290. https://doi.org/10.1038/srep42290

Limberg, S. H., Netter, M. F., Rolfes, C., Rinné, S., Schlichthörl, G., Zuzarte, M., … Decher, N. (2011). TASK-1 channels may modulate action potential duration of human atrial cardiomyocytes. *Cellular Physiology and Biochemistry*, *28*(4), 613–624. https://doi.org/10.1159/000335757

Lin, C.-Y., Lin, Y.-J., Lo, L.-W., Chen, Y.-Y., Chong, E., Chang, S.-L., … Chen, S.-A. (2015). Factors predisposing to ventricular proarrhythmia during antiarrhythmic drug therapy for atrial fibrillation in patients with structurally normal heart. *Heart Rhythm*, *12*(7), 1490–1500. https://doi.org/10.1016/J.HRTHM.2015.04.018

Lin, E., Craig, C., Lamothe, M., Sarunic, M. V, Beg, M. F., & Tibbits, G. F. (2015). Construction and use of a zebrafish heart voltage and calcium optical mapping system, with integrated electrocardiogram and programmable electrical stimulation. *American Journal of Physiology. Regulatory, Integrative and Comparative Physiology*, *308*(9), R755-68. https://doi.org/10.1152/ajpregu.00001.2015

Lip, G. Y. H., Fauchier, L., Freedman, S. B., Van Gelder, I., Natale, A., Gianni, C., … Lane, D. A. (2016). Atrial fibrillation. *Nature Reviews Disease Primers*, *2*, 16016. https://doi.org/10.1038/nrdp.2016.16

Liu, Q., Jiang, C., Xu, J., Zhao, M., Bortle, K. Van, & Cheng, X. (2018). Genome-Wide Temporal Profiling of Transcriptome and Open- Chromatin of Early Cardiomyocyte Differentiation Derived From hiPSCs and hESCs, *121*(May 2017), 376–391. https://doi.org/10.1161/CIRCRESAHA.116.310456.Genome-Wide

Liu, Z., Williams, R. B., & Rosen, B. D. (2013). The potential contribution of ranolazine to Torsade de Pointe. *Journal of Cardiovascular Disease Research*, *4*(3), 187–190. https://doi.org/10.1016/j.jcdr.2013.08.005

Livak, K. J., & Schmittgen, T. D. (2001). Analysis of relative gene expression data using real-time quantitative PCR and the 2-ΔΔCT method. *Methods*, *25*(4), 402–408. https://doi.org/10.1006/meth.2001.1262

Lloyd-Jones, D. M., Wang, T. J., Leip, E. P., Larson, M. G., Levy, D., Vasan, R. S., … Benjamin, E. J. (2004). Lifetime Risk for Development of Atrial Fibrillation. *Circulation*, *110*(9).

Lu, H. R., Hortigon-Vinagre, M. P., Zamora, V., Kopljar, I., De Bondt, A., Gallacher, D. J., & Smith, G. (2017). Application of optical action potentials in human induced pluripotent stem cells-derived cardiomyocytes to predict drug-induced cardiac arrhythmias. https://doi.org/10.1016/j.vascn.2017.05.001

Machida, T., Hashimoto, N., Kuwahara, I., Ogino, Y., Matsuura, J., Yamamoto, W., … Nakaya, H. (2011). Effects of a highly selective acetylcholine-activated K+ channel blocker on experimental atrial fibrillation. *Circulation: Arrhythmia and Electrophysiology*, *4*(1), 94–102. https://doi.org/10.1161/CIRCEP.110.951608

Magnani, J. W., Rienstra, M., Lin, H., Sinner, M. F., Lubitz, S. A., McManus, D. D., … Benjamin, E. J. (2011). Atrial Fibrillation. *Circulation*, *124*(18), 1982–1993. https://doi.org/10.1161/CIRCULATIONAHA.111.039677

Marczenke, M., Piccini, I., Mengarelli, I., Fell, J., Röpke, A., Seebohm, G., … Greber, B. (2017). Cardiac subtype-specific modeling of Kv1.5 ion channel deficiency using human pluripotent stem cells. *Frontiers in Physiology*, *8*(JUL), 1–11. https://doi.org/10.3389/fphys.2017.00469

Mathur, A., Loskill, P., Shao, K., Huebsch, N., Hong, S. G., Marcus, S. G., … Healy, K. E. (2015). Human iPSC-based cardiac microphysiological system for drug screening applications. *Scientific Reports*, *5*, 1–7. https://doi.org/10.1038/srep08883

McCain, M. L., & Parker, K. K. (2011). Mechanotransduction: the role of mechanical stress, myocyte shape, and cytoskeletal architecture on cardiac function. *Pflügers Archiv - European Journal of Physiology*, *462*(1), 89–104. https://doi.org/10.1007/s00424-011-0951-4

Milnes, J. T., El-haou, S., Loose, S., Jackson, C., Tang, R., Ford, J., & Ravens, U. (2011). Abstract 20199: In the Absence of Muscarinic-Activation, Inhibition of Kir3.1/3.4 and Kir3.4/3.4, but Not Kir3.1/3.4-Alone Prolongs Repolarisation of Atrial Tissue from Patients with Atrial Fibrillation, *706*, 261057.

Milone, M. C., & O'Doherty, U. (2018). Clinical use of lentiviral vectors. *Leukemia*, *32*(7), 1529–1541. https://doi.org/10.1038/s41375-018-0106-0

Minkenberg, B., Wheatley, M., & Yang, Y. (2017). CRISPR/Cas9-Enabled Multiplex Genome Editing and Its Application. *Progress in Molecular Biology and Translational Science*, *149*, 111–132. https://doi.org/10.1016/BS.PMBTS.2017.05.003

Miyaoka, Y., Chan, A. H., Judge, L. M., Yoo, J., Huang, M., Nguyen, T. D., … Conklin, B. R. (2014). Isolation of single-base genome-edited human iPS cells without antibiotic selection. *Nature Methods*, *11*(3), 291–3. https://doi.org/10.1038/nmeth.2840

Miyauchi, Y., Zhou, S., Okuyama, Y., Miyauchi, M., Hayashi, H., Hamabe, A., … Karagueuzian, H. S. (2003). Altered atrial electrical restitution and heterogeneous sympathetic hyperinnervation in hearts with chronic left ventricular myocardial infarction: Implications for atrial fibrillation. *Circulation*, *108*(3), 360–366. https://doi.org/10.1161/01.CIR.0000080327.32573.7C

Molina, C. E., Llach, A., Herraiz-Martínez, A., Tarifa, C., Barriga, M., Wiegerinck, R. F., … Hove-Madsen, L. (2016). Prevention of adenosine A2A receptor activation diminishes beat-to-beat alternation in human atrial myocytes. *Basic Research in Cardiology*, *111*(1), 5. https://doi.org/10.1007/s00395-015-0525-2

Nakai, J., Ohkura, M., & Imoto, K. (2001). A high signal-to-noise Ca(2+) probe composed of a single green fluorescent protein. *Nature Biotechnology*, *19*(2), 137–41. https://doi.org/10.1038/84397

Narayan, S. M., Kazi, D., Krummen, D. E., & Rappel, W.-J. (2008). Repolarization and Activation Restitution Near Human Pulmonary Veins and Atrial Fibrillation Initiation: A Mechanism for the Initiation of Atrial Fibrillation by Premature Beats. *Journal of the American College of Cardiology*, *52*(15), 1222–1230. https://doi.org/10.1016/J.JACC.2008.07.012

Narayana, S. K., Woods, D. R., & Boos, C. J. (2011). Management of amiodarone-related thyroid problems. https://doi.org/10.1177/2042018811398516

Nattel, S., Burstein, B., & Dobrev, D. (2008). Atrial remodeling and atrial fibrillation: mechanisms and implications. *Circulation. Arrhythmia and Electrophysiology*, *1*(1), 62–73. https://doi.org/10.1161/CIRCEP.107.754564

Nozaki, Y., Honda, Y., Watanabe, H., Saiki, S., Koyabu, K., Itoh, T., … Kunimatsu, T. (2016). CSAHi study: Validation of multi-electrode array systems (MEA60/ 2100) for prediction of drug-induced proarrhythmia using human iPS cell-derived cardiomyocytes -assessment of inter-facility and cells lot- to-lot-variability. *Regulatory Toxicology and Pharmacology*, *77*, 75–86. https://doi.org/10.1016/j.yrtph.2016.02.007

Nunes, S. S., Miklas, J. W., Liu, J., Aschar-Sobbi, R., Xiao, Y., Zhang, B., … Radisic, M. (2013). Biowire: a platform for maturation of human pluripotent stem cell–derived cardiomyocytes. *Nature Methods*, *10*(8), 781–787. https://doi.org/10.1038/nmeth.2524

O'Donohoe, P. B., Huskens, N., Turner, P. J., Pandit, J. J., & Buckler, K. J. (2018). A1899, PK-THPP, ML365, and Doxapram inhibit endogenous TASK channels and excite calcium signaling in carotid body type-1 cells. *Physiological Reports*, *6*(19), e13876. https://doi.org/10.14814/phy2.13876

O'Reilly, D. J., Hopkins, R. B., Healey, J. S., Dorian, P., Sauriol, L., Tarride, J. E., … Goeree, R. A. (2013). The Burden of Atrial Fibrillation on the Hospital Sector in Canada. *Canadian Journal of Cardiology*, *29*(2), 229–235. https://doi.org/10.1016/j.cjca.2012.03.023

Opolski, G., Torbicki, A., Kosior, D. A., Szulc, M., Wozakowska-Kapłon, B., Kołodziej, P., & Achremczyk, P. (2004). Rate Control vs Rhythm Control in Patients With Nonvalvular Persistent Atrial Fibrillation: The Results of the Polish How to Treat Chronic Atrial Fibrillation (HOT CAFE) Study. *Chest*, *126*(2), 476–486. https://doi.org/10.1378/CHEST.126.2.476

Özgen, N., Dun, W., Sosunov, E. A., Anyukhovsky, E. P., Hirose, M., Duffy, H. S., … Rosen, M. R. (2008). Early electrical remodeling in rabbit pulmonary vein results from trafficking of intracellular SK2 channels to membrane sites. *Cardiovascular Research*, *75*(4).

Packer, D. L., Mark, D. B., Robb, R. A., Monahan, K. H., Bahnson, T. D., Poole, J. E., … Lee, K. L. (2019). Effect of Catheter Ablation vs Antiarrhythmic Drug Therapy on Mortality, Stroke, Bleeding, and Cardiac Arrest Among Patients With Atrial Fibrillation. *JAMA*. https://doi.org/10.1001/jama.2019.0693

Pappone, C., Augello, G., Sala, S., Gugliotta, F., Vicedomini, G., Gulletta, S., … Santinelli, V. (2006). A Randomized Trial of Circumferential Pulmonary Vein Ablation Versus Antiarrhythmic Drug Therapy in Paroxysmal Atrial Fibrillation. *Journal of the American College of Cardiology*, *48*(11), 2340–2347. https://doi.org/10.1016/j.jacc.2006.08.037

Park, F., & Kay, M. A. (2001). Modified HIV-1 Based Lentiviral Vectors Have an Effect on Viral Transduction Efficiency and Gene Expression in Vitro and in Vivo. *Molecular Therapy*, *4*(3), 164–173. https://doi.org/10.1006/MTHE.2001.0450

Pasqualini, F. S., Sheehy, S. P., Agarwal, A., Aratyn-Schaus, Y., & Parker, K. K. (2015). Structural phenotyping of stem cell-derived cardiomyocytes. *Stem Cell Reports*, *4*(3), 340–7. https://doi.org/10.1016/j.stemcr.2015.01.020

Pavri, B. B., Greenberg, H. E., Kraft, W. K., Lazarus, N., Lynch, J. J., Salata, J. J., … Bloomfield, D. (2012). MK-0448, a Specific Kv1.5 Inhibitor. *Circulation: Arrhythmia and Electrophysiology*, *5*(6), 1193–1201. https://doi.org/10.1161/CIRCEP.111.969782

Penugonda, N., Mohmand-Borkowski, A., & Burke, J. F. (2011). Dronedarone for atrial fibrillation: How does it compare with amiodarone? *Cleveland Clinic Journal of Medicine*, *78*(3), 179–185. https://doi.org/10.3949/ccjm.78a.10049

Pérez Koldenkova, V., & Nagai, T. (2013). Genetically encoded Ca2 + indicators: Properties and evaluation. *Biochimica et Biophysica Acta (BBA) - Molecular Cell Research*, *1833*(7), 1787–1797. https://doi.org/10.1016/J.BBAMCR.2013.01.011

Podd, S. J., Freemantle, N., Furniss, S. S., & Sulke, N. (2016). First clinical trial of specific I_{KACh} blocker shows no reduction in atrial fibrillation burden in patients with paroxysmal atrial fibrillation: pacemaker assessment of BMS 914392 in patients with paroxysmal atrial fibrillation. *Europace*, *18*(3), 340–346. https://doi.org/10.1093/europace/euv263

Poulet, C., Wettwer, E., Grunnet, M., Jespersen, T., Fabritz, L., Matschke, K., … Ravens, U. (2015). Late sodium current in human atrial cardiomyocytes from patients in sinus rhythm and atrial fibrillation. *PLoS ONE*, *10*(6). https://doi.org/10.1371/journal.pone.0131432

Protze, S. I., Liu, J., Nussinovitch, U., Ohana, L., Backx, P. H., Gepstein, L., & Keller, G. M. (2016). Sinoatrial node cardiomyocytes derived from human pluripotent cells function as a biological pacemaker. *Nature Publishing Group*. https://doi.org/10.1038/nbt.3745

Qi, X.-Y., Diness, J. G., Brundel, B. J. J. M., Zhou, X.-B., Naud, P., Wu, C.-T., … Nattel, S. (2013). Role of Small-Conductance Calcium-Activated Potassium Channels in Atrial Electrophysiology and Fibrillation in the Dog. *Circulation*, *129*(4), 430–440. https://doi.org/10.1161/circulationaha.113.003019

Qian, Y., Piatkevich, K. D., Mc Larney, B., Abdelfattah, A. S., Mehta, S., Murdock, M. H., … Campbell, R. E. (2019). A genetically encoded near-infrared fluorescent calcium ion indicator. *Nature Methods*, *16*(2), 171–174. https://doi.org/10.1038/s41592-018-0294-6

Qu, Z., Weiss, J. N., & Garfinkel, A. (1999). Cardiac electrical restitution properties and stability of reentrant spiral waves: a simulation study. *Am J Physiol*, *276*(1 Pt 2), H269-83. Retrieved from http://ajpheart.physiology.org/cgi/content/full/276/1/H269

Rajamohan, D., Kalra, S., Duc Hoang, M., George, V., Staniforth, A., Russell, H., … Denning, C. (2016). Automated Electrophysiological and Pharmacological Evaluation of Human Pluripotent Stem Cell-Derived Cardiomyocytes. *Stem Cells and Development*, *25*(6), 439–452. https://doi.org/10.1089/scd.2015.0253

Ravens, U. (2017). Atrial-selective K + channel blockers: potential antiarrhythmic drugs in atrial fibrillation? . *Canadian Journal of Physiology and Pharmacology*, *95*(11), 1313–1318. https://doi.org/10.1139/cjpp-2017-0024

Ribeiro, M. C., Tertoolen, L. G., Guadix, J. A., Bellin, M., Kosmidis, G., D'Aniello, C., … Passier, R. (2015). Functional maturation of human pluripotent stem cell derived cardiomyocytes in vitro – Correlation between contraction force and electrophysiology. *Biomaterials*, *51*, 138–150. https://doi.org/10.1016/J.BIOMATERIALS.2015.01.067

Richard;, V. L. M. N., Mangoni, M. E., Nargeot, J., & Richard, S. (2001). Inhibition of T-Type and L-Type Calcium Channels by Mibefradil: Physiologic and Pharmacologic Bases of Cardiovascular Effects. *Journal of Cardiovascular Pharmacology*, *37*(6), 649–661. Retrieved from http://www.ncbi.nlm.nih.gov/pubmed/11392461

Richards, M. A., Clarke, J. D., Saravanan, P., Voigt, N., Dobrev, D., Eisner, D. A., … Dibb, K. M. (2011). Transverse tubules are a common feature in large mammalian atrial myocytes including human. *American Journal of Physiology-Heart and Circulatory Physiology*, *301*(5), H1996–H2005. https://doi.org/10.1152/ajpheart.00284.2011

Robertson, C., Tran, D. D., & George, S. C. (2013). Concise Review: Maturation Phases of Human Pluripotent Stem Cell-Derived Cardiomyocytes. *STEM CELLS*, *31*(5), 829–837. https://doi.org/10.1002/stem.1331

Roden, D., & Willerson, J. T. (2012). Cardiovascular Drugs. *Circulation*, *102*(5), 415–415. https://doi.org/10.1161/01.cir.97.5.415

Rossier, M. F., Ertel, E. A., Vallotton, M. B., Capponi, A. M., Flockerzi, V., & Hofmann, F. (1998). Inhibitory action of mibefradil on calcium signaling and aldosterone synthesis in bovine adrenal glomerulosa cells. *The Journal of Pharmacology and Experimental Therapeutics*, *287*(3), 824–31. Retrieved from http://www.ncbi.nlm.nih.gov/pubmed/9864260

Roy, D., Pratt, C. M., Torp-Pedersen, C., Wyse, D. G., Toft, E., Juul-Moller, S., … Camm, A. J. (2008). Vernakalant hydrochloride for rapid conversion of atrial fibrillation: A phase 3, randomized, placebo-controlled trial. *Circulation*, *117*(12), 1518–1525. https://doi.org/10.1161/CIRCULATIONAHA.107.723866

Roy, D., Rowe, B. H., Stiell, I. G., Coutu, B., Ip, J. H., Phaneuf, D., … Beatch, G. N. (2004). A randomized, controlled trial of RSD1235, a novel anti-arrhythmic agent, in the treatment of recent onset atrial fibrillation. *Journal of the American College of Cardiology*, *44*(12), 2355–2361. https://doi.org/10.1016/j.jacc.2004.09.021

Roy, D., Talajic, M., Nattel, S., Wyse, D. G., Dorian, P., Lee, K. L., … Waldo, A. L. (2008). Rhythm Control versus Rate Control for Atrial Fibrillation and Heart Failure. *New England Journal of Medicine*, *358*(25), 2667–2677. https://doi.org/10.1056/NEJMoa0708789

Sakuma, T., Barry, M. A., & Ikeda, Y. (2012). Lentiviral vectors: basic to translational. *The Biochemical Journal*, *443*(3), 603–18. https://doi.org/10.1042/BJ20120146

Sanford, L., & Palmer, A. (2017). Recent Advances in Development of Genetically Encoded Fluorescent Sensors. *Methods in Enzymology*, *589*, 1–49. https://doi.org/10.1016/BS.MIE.2017.01.019

Santini, M., & Ricci, R. (2001). Atrial fibrillation coexisting with ventricular tachycardia: a challenge for dual chamber defibrillators. *Heart (British Cardiac Society)*, *86*(3), 253–4. https://doi.org/10.1136/HEART.86.3.253

Sarrias, A., Villuendas, R., Bisbal, F., Pereferrer, D., Rueda, F., Serra, J., … Bayés-Genís, A. (2015). From Atrial Fibrillation to Ventricular Fibrillation and Back. *Circulation*, *132*(21), 2035–2036. https://doi.org/10.1161/CIRCULATIONAHA.115.018891

Schmidt, C., Wiedmann, F., Schweizer, P. A., Becker, R., Katus, H. A., & Thomas, D. (2012). Novel electrophysiological properties of dronedarone: inhibition of human cardiac two-pore-domain potassium (K2P) channels. *Naunyn-Schmiedeberg's Archives of Pharmacology*, *385*(10), 1003–1016. https://doi.org/10.1007/s00210-012-0780-9

Schmidt, C., Wiedmann, F., Voigt, N., Zhou, X.-B., Heijman, J., Lang, S., … Thomas, D. (2015). Upregulation of K_{2P} 3.1 K^+ Current Causes Action Potential Shortening in Patients With Chronic Atrial Fibrillation. *Circulation*, *132*(2), 82–92. https://doi.org/10.1161/CIRCULATIONAHA.114.012657

Schreiber, D., Rostock, T., Fröhlich, M., Sultan, A., Servatius, H., Hoffmann, B. A., … Steven, D. (2015). Five-Year Follow-Up After Catheter Ablation of Persistent Atrial Fibrillation Using the Stepwise Approach and Prognostic Factors for Success. *Circulation: Arrhythmia and Electrophysiology*, *8*(2), 308–317. https://doi.org/10.1161/CIRCEP.114.001672

Shafaattalab, S., Li, A. Y., Lin, E., Stevens, C. M., Dewar, L. J., Lynn, F. C., … Tibbits, G. F. (2019). In vitro analyses of suspected arrhythmogenic thin filament variants as a cause of sudden cardiac death in infants. *Proceedings of the National Academy of Sciences of the United States of America*, 201819023. https://doi.org/10.1073/pnas.1819023116

Shaheen, N., Shiti, A., Huber, I., Shinnawi, R., Arbel, G., Gepstein, A., … Gepstein, L. (2018). Human Induced Pluripotent Stem Cell-Derived Cardiac Cell Sheets Expressing Genetically Encoded Voltage Indicator for Pharmacological and Arrhythmia Studies. *Stem Cell Reports*, *10*(6), 1879–1894. https://doi.org/10.1016/J.STEMCR.2018.04.006

Sharma, A., Burridge, P. W., Mckeithan, W. L., Serrano, R., Shukla, P., Sayed, N., … Wu, J. C. (2017). High-throughput screening of tyrosine kinase inhibitor cardiotoxicity with human induced pluripotent stem cells.

Shattock, M. J., Park, K. C., Yang, H.-Y., Lee, A. W. C., Niederer, S., MacLeod, K. T., & Winter, J. (2017). Restitution slope is principally determined by steady-state action potential duration. *Cardiovascular Research*, *113*(7), 817–828. https://doi.org/10.1093/cvr/cvx063

Shcheglovitov, A., Zhelay, T., Vitko, Y., Osipenko, V., Perez-Reyes, E., Kostyuk, P., & Shuba, Y. (2005). Contrasting the effects of nifedipine on subtypes of endogenous and recombinant T-type Ca2+ channels. *Biochemical Pharmacology*, *69*(5), 841–854. https://doi.org/10.1016/J.BCP.2004.11.024

Shen, Y., Lai, T., & Campbell, R. E. (2015). Red fluorescent proteins (RFPs) and RFP-based biosensors for neuronal imaging applications. *Neurophotonics*, *2*(3), 31203. https://doi.org/10.1117/1.NPh.2.3.031203

Shinnawi, R., Huber, I., Maizels, L., Shaheen, N., Gepstein, A., Arbel, G., … Gepstein, L. (2015). Monitoring human-induced pluripotent stem cell-derived cardiomyocytes with genetically encoded calcium and voltage fluorescent reporters. *Stem Cell Reports*, *5*(4), 582–596. https://doi.org/10.1016/j.stemcr.2015.08.009

Shunmugam, S. R., Sugihara, C., Freemantle, N., Round, P., Furniss, S., & Sulke, N. (2018). A double-blind, randomised, placebo-controlled, cross-over study assessing the use of XEN-D0103 in patients with paroxysmal atrial fibrillation and implanted pacemakers allowing continuous beat-to-beat monitoring of drug efficacy. *Journal of Interventional Cardiac Electrophysiology*, *51*(3), 191–197. https://doi.org/10.1007/s10840-018-0318-2

Simó-Vicens, R., Kirchhoff, J. E., Dolce, B., Abildgaard, L., Speerschneider, T., Sørensen, U. S., … Bentzen, B. H. (2017). A new negative allosteric modulator, AP14145, for the study of small conductance calcium-activated potassium (KCa2) channels. *British Journal of Pharmacology*, *174*(23), 4396–4408. https://doi.org/10.1111/bph.14043

Singh, S. N., Tang, X. C., Singh, B. N., Dorian, P., Reda, D. J., Harris, C. L., … Ezekowitz, M. D. (2006). Quality of Life and Exercise Performance in Patients in Sinus Rhythm Versus Persistent Atrial Fibrillation: A Veterans Affairs Cooperative Studies Program Substudy. *Journal of the American College of Cardiology*, *48*(4), 721–730. https://doi.org/10.1016/J.JACC.2006.03.051

Skibsbye, L., Poulet, C., Diness, J. G., Bentzen, B. H., Yuan, L., Kappert, U., … Jespersen, T. (2014). Small-conductance calcium-activated potassium (SK) channels contribute to action potential repolarization in human atria. *Cardiovascular Research*, *103*(1), 156–167. https://doi.org/10.1093/cvr/cvu121

Smith, A. S. T., Macadangdang, J., Leung, W., Laflamme, M. A., & Kim, D. H. (2017). Human iPSC-derived cardiomyocytes and tissue engineering strategies for disease modeling and drug screening. *Biotechnology Advances*, *35*(1), 77–94. https://doi.org/10.1016/j.biotechadv.2016.12.002

Sorgente, A., Chierchia, G.-B., de Asmundis, C., Sarkozy, A., Capulzini, L., & Brugada, P. (2011). Complications of atrial fibrillation ablation: when prevention is better than cure. *Europace*, *13*(11), 1526–1532. https://doi.org/10.1093/europace/eur209

St-Pierre, F., Marshall, J. D., Yang, Y., Gong, Y., Schnitzer, M. J., & Lin, M. Z. (2014a). High-fidelity optical reporting of neuronal electrical activity with an ultrafast fluorescent voltage sensor. *Nature Neuroscience*, *17*(6), 884–9. https://doi.org/10.1038/nn.3709

St-Pierre, F., Marshall, J. D., Yang, Y., Gong, Y., Schnitzer, M. J., & Lin, M. Z. (2014b). High-fidelity optical reporting of neuronal electrical activity with an ultrafast fluorescent voltage sensor. *Nature Neuroscience*, *17*(6), 884–9. https://doi.org/10.1038/nn.3709

Stabile, G., Bertaglia, E., Senatore, G., De Simone, A., Zoppo, F., Donnici, G., … Vitale, D. F. (2006). Catheter ablation treatment in patients with drug-refractory atrial fibrillation: a prospective, multi-centre, randomized, controlled study (Catheter Ablation For The Cure Of Atrial Fibrillation Study)†. *European Heart Journal*, *27*(2), 216–221. https://doi.org/10.1093/eurheartj/ehi583

Strøbaek, D., Hougaard, C., Johansen, T. H., Sørensen, U. S., Nielsen, E. Ø., Nielsen, K. S., … Christophersen, P. (2006). Inhibitory gating modulation of small conductance Ca2+-activated K+ channels by the synthetic compound (R)-N-(benzimidazol-2-yl)-1,2,3,4-tetrahydro-1-naphtylamine (NS8593) reduces afterhyperpolarizing current in hippocampal CA1 neurons. *Molecular Pharmacology*, *70*(5), 1771–82. https://doi.org/10.1124/mol.106.027110

Strøbaek, D., Jørgensen, T. D., Christophersen, P., Ahring, P. K., & Olesen, S. P. (2000). Pharmacological characterization of small-conductance Ca(2+)-activated K(+) channels stably expressed in HEK 293 cells. *British Journal of Pharmacology*, *129*(5), 991–9. https://doi.org/10.1038/sj.bjp.0703120

Sun, B., Wei, J., Zhong, X., Guo, W., Yao, J., Wang, R., … Chen, S. R. W. (2018). The cardiac ryanodine receptor, but not sarcoplasmic reticulum Ca2+-ATPase, is a major determinant of Ca2+ alternans in intact mouse hearts. *Journal of Biological Chemistry*, jbc.RA118.003760. https://doi.org/10.1074/JBC.RA118.003760

Takahashi, A., Camacho, P., Lechleiter, J. D., & Herman, B. (1999). Measurement of Intracellular Calcium. *Physiological Reviews*, *79*(4), 1089–1125. https://doi.org/10.1152/physrev.1999.79.4.1089

Takahashi, K., Tanabe, K., Ohnuki, M., Narita, M., Ichisaka, T., Tomoda, K., & Yamanaka, S. (2007). Induction of Pluripotent Stem Cells from Adult Human Fibroblasts by Defined Factors. *Cell*, *131*(5), 861–872. https://doi.org/10.1016/J.CELL.2007.11.019

Tang, Y.-R., Yang, W.-W., Wang, Y., Gong, Y.-Y., Jiang, L.-Q., & Lin, L. (2015). Estrogen Regulates the Expression of Small-Conductance Ca²⁺-Activated K⁺ Channels in Colonic Smooth Muscle Cells. *Digestion*, *91*(3), 187–196. https://doi.org/10.1159/000371544

Tiburcy, M., Hudson, J. E., Balfanz, P., Schlick, S., Meyer, T., Liao, M. C., … Gepstein, L. (2017). Defined Engineered Human Myocardium With Advanced Maturation for Applications in Heart Failure Modeling and Repair. *Circulation*, *135*(19), 1832–1847. https://doi.org/10.1161/circulationaha.116.024145

Tohyama, S., Hattori, F., Sano, M., Hishiki, T., Nagahata, Y., Matsuura, T., … Fukuda, K. (2013). Distinct Metabolic Flow Enables Large-Scale Purification of Mouse and Human Pluripotent Stem Cell-Derived Cardiomyocytes. *Stem Cell*, *12*, 127–137. https://doi.org/10.1016/j.stem.2012.09.013

Tse, G., Wong, S. T., Tse, V., Lee, Y. T., Lin, H. Y., & Yeo, J. M. (2016). Cardiac dynamics: Alternans and arrhythmogenesis. *Journal of Arrhythmia*, *32*(5), 411–417. https://doi.org/10.1016/j.joa.2016.02.009

Tsutsui, H., Karasawa, S., Okamura, Y., & Miyawaki, A. (2008). Improving membrane voltage measurements using FRET with new fluorescent proteins. *Nature Methods*, *5*(8), 683–5. https://doi.org/10.1038/nmeth.1235

Tu, C., Chao, B. S., & Wu, J. C. (2018). Strategies for Improving the Maturity of Human Induced Pluripotent Stem Cell-Derived Cardiomyocytes. *Circulation Research*, *123*(5), 512–514. https://doi.org/10.1161/CIRCRESAHA.118.313472

Tuteja, D., Rafizadeh, S., Timofeyev, V., Wang, S., Zhang, Z., Li, N., … Chiamvimonvat, N. (2010). Cardiac small conductance Ca2+-activated K+ channel subunits form heteromultimers via the coiled-coil domains in the C termini of the channels. *Circulation Research*, *107*(7), 851–859. https://doi.org/10.1161/CIRCRESAHA.109.215269

Tuteja, D., Xu, D., Timofeyev, V., Lu, L., Sharma, D., Zhang, Z., … Chiamvimonvat, N. (2005). Differential expression of small-conductance Ca2+-activated K+ channels SK1, SK2, and SK3 in mouse atrial and ventricular myocytes. *American Journal of Physiology - Heart and Circulatory Physiology*, *289*(6).

Uosaki, H., Fukushima, H., Takeuchi, A., Matsuoka, S., Nakatsuji, N., Yamanaka, S., & Yamashita, J. K. (2011). Efficient and Scalable Purification of Cardiomyocytes from Human Embryonic and Induced Pluripotent Stem Cells by VCAM1 Surface Expression. *PLoS ONE*, *6*(8), e23657. https://doi.org/10.1371/journal.pone.0023657

van den Berg, C. W., Okawa, S., Chuva de Sousa Lopes, S. M., van Iperen, L., Passier, R., Braam, S. R., … Mummery, C. L. (2015). Transcriptome of human foetal heart compared with cardiomyocytes from pluripotent stem cells. *Development (Cambridge, England)*, 3231–3238. https://doi.org/10.1242/dev.123810

Veevers, J., Farah, E. N., Corselli, M., Witty, A. D., Palomares, K., Vidal, J. G., … Evans, S. M. (2018). Stem Cell Reports Resource Cell-Surface Marker Signature for Enrichment of Ventricular Cardiomyocytes Derived from Human Embryonic Stem Cells. https://doi.org/10.1016/j.stemcr.2018.07.007

Veldkamp, M. W., Geuzebroek, G. S. C., Baartscheer, A., Verkerk, A. O., Schumacher, C. A., Suarez, G. G., … Coronel, R. (2018a). Neurokinin-3 receptor activation selectively prolongs atrial refractoriness by inhibition of a background K+ channel. *Nature Communications*, *9*(1), 4357. https://doi.org/10.1038/s41467-018-06530-5

Veldkamp, M. W., Geuzebroek, G. S. C., Baartscheer, A., Verkerk, A. O., Schumacher, C. A., Suarez, G. G., … Coronel, R. (2018b). Neurokinin-3 receptor activation selectively prolongs atrial refractoriness by inhibition of a background K+ channel. *Nature Communications*, *9*(1), 4357. https://doi.org/10.1038/s41467-018-06530-5

Verkerk, A. O., Geuzebroek, G. S. C., Veldkamp, M. W., & Wilders, R. (2012). Effects of acetylcholine and noradrenalin on action potentials of isolated rabbit sinoatrial and atrial myocytes. *Frontiers in Physiology*, *3 MAY*(May), 1–9. https://doi.org/10.3389/fphys.2012.00174

Verkerk, A. O., Veerman, C. C., Zegers, J. G., Mengarelli, I., Bezzina, C. R., & Wilders, R. (2017). Patch-clamp recording from human induced pluripotent stemcell-derived cardiomyocytes: Improving action potential characteristics throughdynamic clamp. *International Journal of Molecular Sciences*, *18*(9). https://doi.org/10.3390/ijms18091873

Walfridsson, H., Anfinsen, O. G., Berggren, A., Frison, L., Jensen, S., Linhardt, G., … Carlsson, L. (2015). Is the acetylcholine-regulated inwardly rectifying potassium current a viable antiarrhythmic target? Translational discrepancies of AZD2927 and A7071 in dogs and humans. *Europace*, *17*(3), 473–482. https://doi.org/10.1093/europace/euu192

Wang, Y., Tang, S., Harvey, K. E., Salyer, A. E., Li, T. A., Rantz, E. K., … Hockerman, G. H. (2018). Molecular Determinants of the Differential Modulation of Cav1.2 and Cav1.3 by Nifedipine and FPL 64176. *Molecular Pharmacology*, *94*(3), 973–983. https://doi.org/10.1124/mol.118.112441

Wang, Z., Fermini, B., & Nattel, S. (1995). Effects of flecainide, quinidine, and 4-aminopyridine on transient outward and ultrarapid delayed rectifier currents in human atrial myocytes. *The Journal of Pharmacology and Experimental Therapeutics*, *272*(1), 184–96. Retrieved from http://www.ncbi.nlm.nih.gov/pubmed/7815332

Watanabe, M. a, & Koller, M. L. (2002). Mathematical analysis of dynamics of cardiac memory and accommodation: theory and experiment. *American Journal of Physiology. Heart and Circulatory Physiology*, *282*(4), H1534-47. https://doi.org/10.1152/ajpheart.00351.2001

Wazni, O. M., Marrouche, N. F., Martin, D. O., Verma, A., Bhargava, M., Saliba, W., … Natale, A. (2005). Radiofrequency Ablation vs Antiarrhythmic Drugs as First-line Treatment of Symptomatic Atrial Fibrillation. *JAMA*, *293*(21), 2634. https://doi.org/10.1001/jama.293.21.2634

Wettwer, E., Christ, T., Endig, S., Rozmaritsa, N., Matschke, K., Lynch, J. J., … Ravens, U. (2013). The new antiarrhythmic drug vernakalant: Ex vivo study of human atrial tissue from sinus rhythm and chronic atrial fibrillation. *Cardiovascular Research*, *98*(1), 145–154. https://doi.org/10.1093/cvr/cvt006

Wettwer, E., Hála, O., Christ, T., Heubach, J. F., Dobrev, D., Knaut, M., … Ravens, U. (2004). Role of IKur in controlling action potential shape and contractility in the human atrium: Influence of chronic atrial fibrillation. *Circulation*, *110*(16), 2299–2306. https://doi.org/10.1161/01.CIR.0000145155.60288.71

Wijffels, M. C. E. F., Kirchhof, C. J. H. J., Dorland, R., & Allessie, M. A. (1995). Atrial Fibrillation Begets Atrial Fibrillation. *Circulation*, *92*(7), 1954–1968. https://doi.org/10.1161/01.CIR.92.7.1954

Wold, W. S. M., & Toth, K. (2013). Adenovirus vectors for gene therapy, vaccination and cancer gene therapy. *Current Gene Therapy*, *13*(6), 421–33. Retrieved from http://www.ncbi.nlm.nih.gov/pubmed/24279313

Wu, J., Abdelfattah, A. S., Miraucourt, L. S., Kutsarova, E., Ruangkittisakul, A., Zhou, H., … Campbell, R. E. (2014). A long Stokes shift red fluorescent Ca2+ indicator protein for two-photon and ratiometric imaging. *Nature Communications*, *5*(May), 5262. https://doi.org/10.1038/ncomms6262

Wu, J., Prole, D. L., Shen, Y., Lin, Z., Gnanasekaran, A., Liu, Y., … Campbell, R. E. (2014). Red fluorescent genetically encoded Ca2+ indicators for use in mitochondria and endoplasmic reticulum. *The Biochemical Journal*, *464*(1), 13–22. https://doi.org/10.1042/BJ20140931

Wu, R., & Patwardhan, A. (2004). Restitution of Action Potential Duration During Sequential Changes in Diastolic Intervals Shows Multimodal Behavior. https://doi.org/10.1161/01.RES.0000119322.87051.A9

Wulff, H., Kolski-Andreaco, A., Sankaranarayanan, A., Sabatier, J.-M., & Shakkottai, V. (2007). Modulators of small- and intermediate-conductance calcium-activated potassium channels and their therapeutic indications. *Current Medicinal Chemistry*, *14*(13), 1437–57. Retrieved from http://www.ncbi.nlm.nih.gov/pubmed/17584055

Wyse, D. G., Van Gelder, I. C., Ellinor, P. T., Go, A. S., Kalman, J. M., Narayan, S. M., … Rienstra, M. (2014). Lone Atrial Fibrillation. *Journal of the American College of Cardiology*, *63*(17), 1715–1723. https://doi.org/10.1016/j.jacc.2014.01.023

Xu, X. Q., Soo, S. Y., Sun, W., & Zweigerdt, R. (2009). Global Expression Profile of Highly Enriched Cardiomyocytes Derived from Human Embryonic Stem Cells. *Stem Cells*, *27*(9), 2163–2174. https://doi.org/10.1002/stem.166

Yang, H. H., & St-Pierre, F. (2016). Genetically Encoded Voltage Indicators: Opportunities and Challenges. https://doi.org/10.1523/JNEUROSCI.1095-16.2016

Yang, X., Pabon, L., & Murry, C. E. (2014). Engineering Adolescence. *Circulation Research*, *114*(3), 511–523. https://doi.org/10.1161/CIRCRESAHA.114.300558

Yue, D. T., & Marban, E. (1988). A novel cardiac potassium channel that is active and conductive at depolarized potentials. *Pflügers Archiv European Journal of Physiology*, *413*(2), 127–133. https://doi.org/10.1007/BF00582522

Zeng, H., Roman, M. I., Lis, E., Lagrutta, A., & Sannajust, F. (2016). Use of FDSS/µCell imaging platform for preclinical cardiac electrophysiology safety screening of compounds in human induced pluripotent stem cell-derived cardiomyocytes. *Journal of Pharmacological and Toxicological Methods*, *81*, 217–222. https://doi.org/10.1016/j.vascn.2016.05.009

Zhang, Q., Jiang, J., Han, P., Yuan, Q., Zhang, J., Zhang, X., … Ma, Y. (2011). Direct differentiation of atrial and ventricular myocytes from human embryonic stem cells by alternating retinoid signals. *Cell Research*, *21*(4), 579–587. https://doi.org/10.1038/cr.2010.163

Zhang, X.-D., Lieu, D. K., & Chiamvimonvat, N. (2015). Small-conductance Ca2+-activated K+ channels and cardiac arrhythmias. *Heart Rhythm*, *12*(8), 1845–1851. https://doi.org/10.1016/J.HRTHM.2015.04.046

Zhang, Z., He, Y., Tuteja, D., Xu, D., Timofeyev, V., Zhang, Q., … Chiamvimonvat, N. (2005). Functional Roles of $Ca_v1.3(\alpha_{1D})$ Calcium Channels in Atria. *Circulation*, *112*(13), 1936–1944. https://doi.org/10.1161/CIRCULATIONAHA.105.540070

Zhong, X., Sun, B., Vallmitjana, A., Mi, T., Guo, W., Ni, M., … Chen, S. R. W. (2016). Suppression of ryanodine receptor function prolongs Ca2+ release refractoriness and promotes cardiac alternans in intact hearts. *The Biochemical Journal*, *473*(21), 3951–3964. https://doi.org/10.1042/BCJ20160606

Zhong, X., Vallmitjana, A., Sun, B., Xiao, Z., Guo, W., Wei, J., … Wayne Chen, S. R. (2018). Reduced expression of cardiac ryanodine receptor protects against stress-induced ventricular tachyarrhythmia, but increases the susceptibility to cardiac alternans. *The Biochemical Journal*, *475*(1), 169–183. https://doi.org/10.1042/BCJ20170631

Zou, B., Flaherty, D. P., Simpson, D. S., Maki, B. E., Miller, M. R., Shi, J., … Li, M. (2010). *ML365: Development of Bis-Amides as Selective Inhibitors of the KCNK3/TASK1 Two Pore Potassium Channel*. *Probe Reports from the NIH Molecular Libraries Program*. Retrieved from http://www.ncbi.nlm.nih.gov/pubmed/24479195

Zufferey, R., Dull, T., Mandel, R. J., Bukovsky, A., Quiroz, D., Naldini, L., & Trono, D. (1998). *Self-Inactivating Lentivirus Vector for Safe and Efficient In Vivo Gene Delivery*. *JOURNAL OF VIROLOGY* (Vol. 72). Retrieved from http://jvi.asm.org/

Zylbergold, P., Ramakrishnan, N., & Hébert, T. E. (2010). The role of G proteins in assembly and function of Kir3 inwardly rectifying potassium channels. *Channels*, *4*(5), 411–421. https://doi.org/10.4161/chan.4.5.13327

Appendix A.

S1S2 Protocol

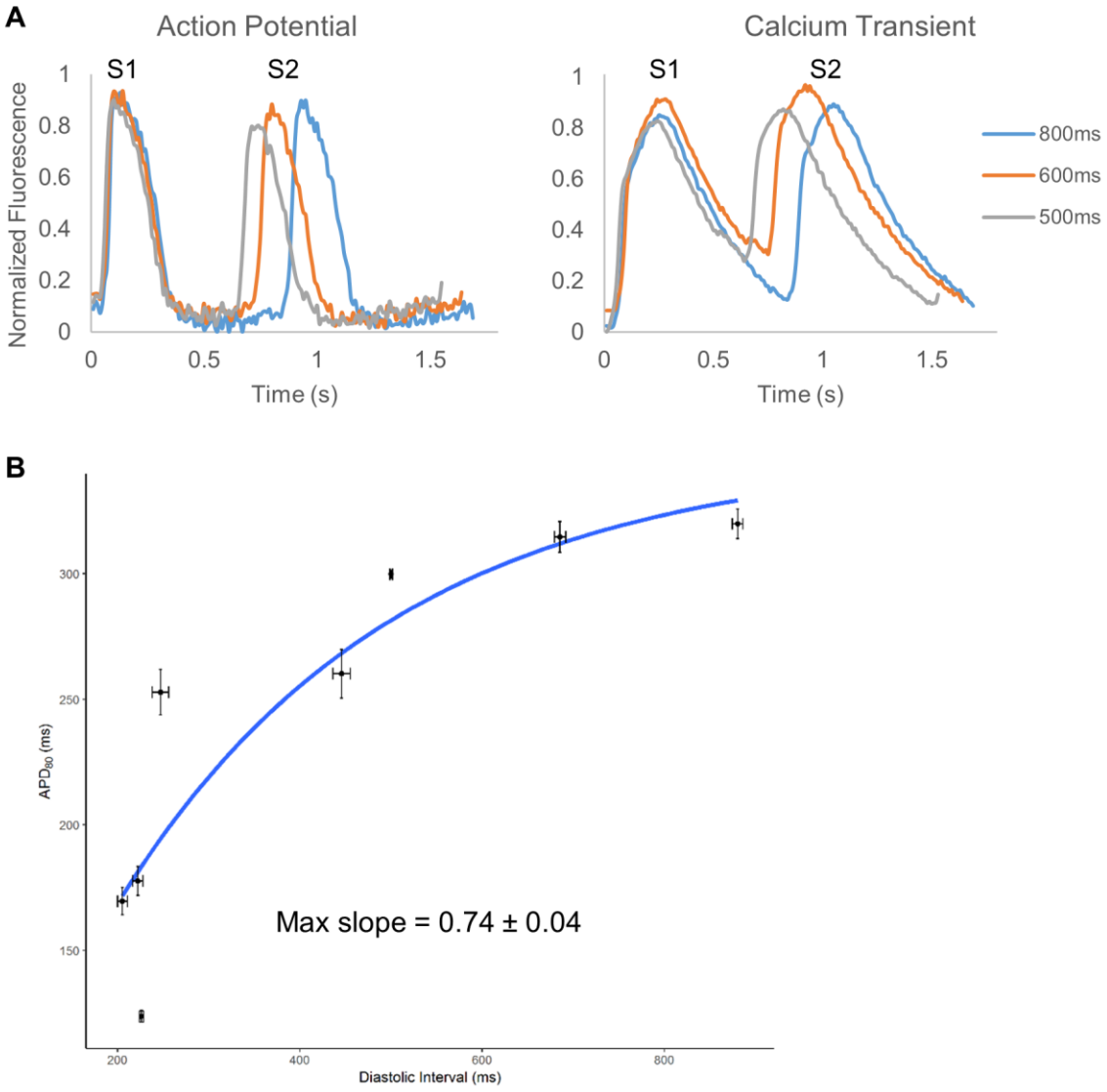

Figure A.1. S1S2 protocol tested in hiPSC-vCMs.
A) Representative traces of action potential and calcium transient under S1S2 protocol. Five S1 stimuli were delivered at an interval 1000 ms before the single S2 stimuli delivered at the interval as indicated in the figure legend. The protocol continues with progressively shortening of the S1-S2 interval until failure to capture electrical stimulus. B) The electrical restitution curve of hiPSC-vCMs obtained through S1S2 protocol. The maximum slope of the curve (0.74 ± 0.04) was smaller to that obtained from variable rate protocol (1.26 ± 0.08). Data were presented as mean ± SEM. n = 3 from 3 differentiation batches.

Appendix B.

Analysis of Atrial-Selective Pharmacology

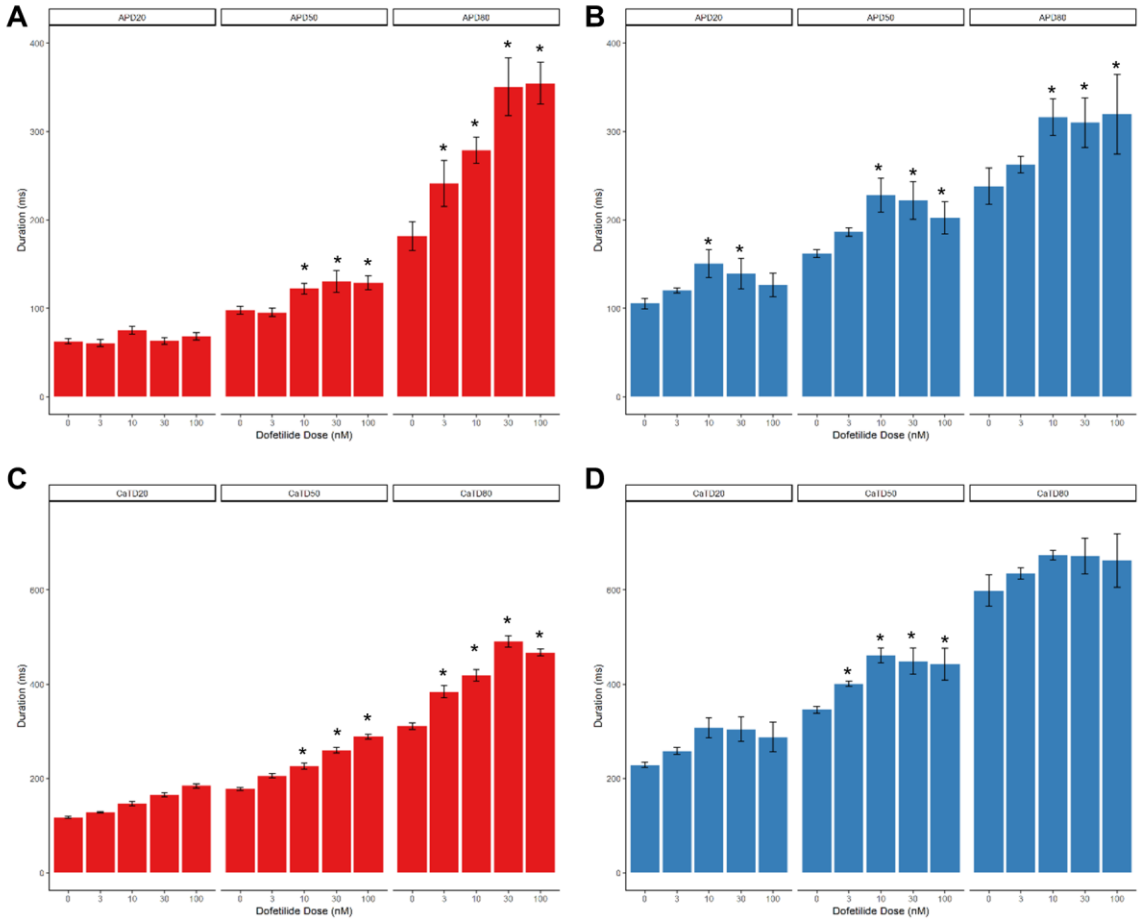

Figure B.1. **The effects of dofetilide on hiPSC-aCMs (A: APD; B: CaTD) and hiPSC-vCMs (C: APD; D: CaTD).**

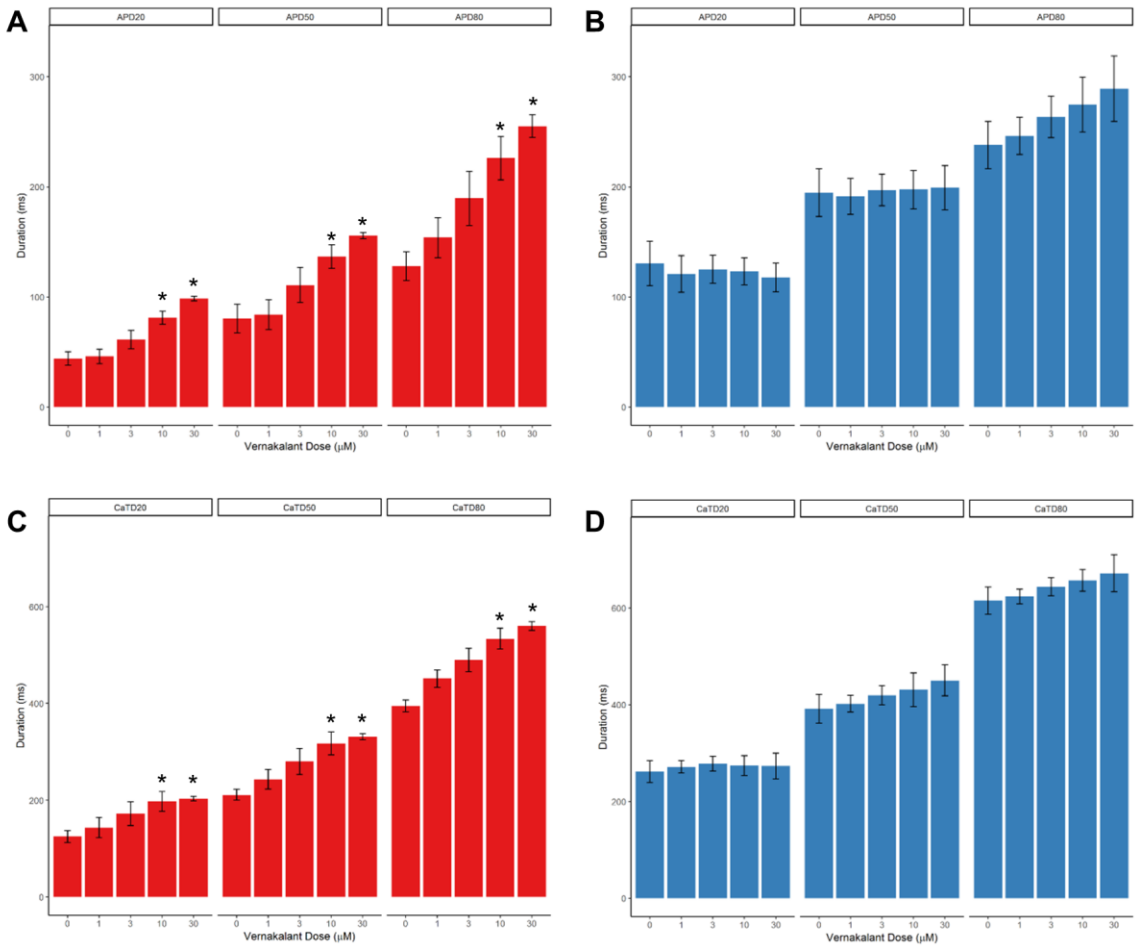

Figure B.2. The effects of vernakalant on hiPSC-aCMs (A: APD; C: CaTD) and hiPSC-vCMs (B: APD; D: CaTD).

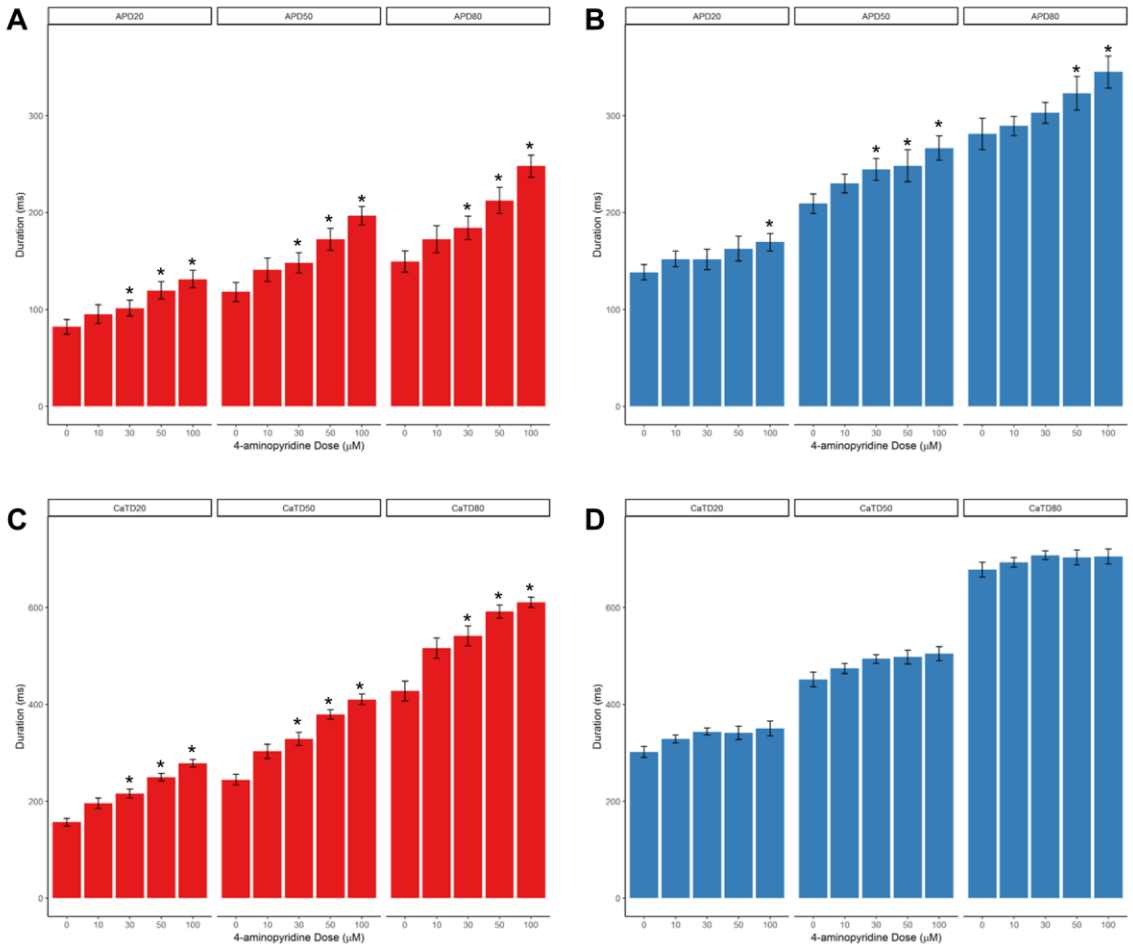

Figure B.3. The effects of 4-aminopyridine on hiPSC-aCMs (A: APD; C: CaTD) and hiPSC-vCMs (B: APD; D: CaTD).

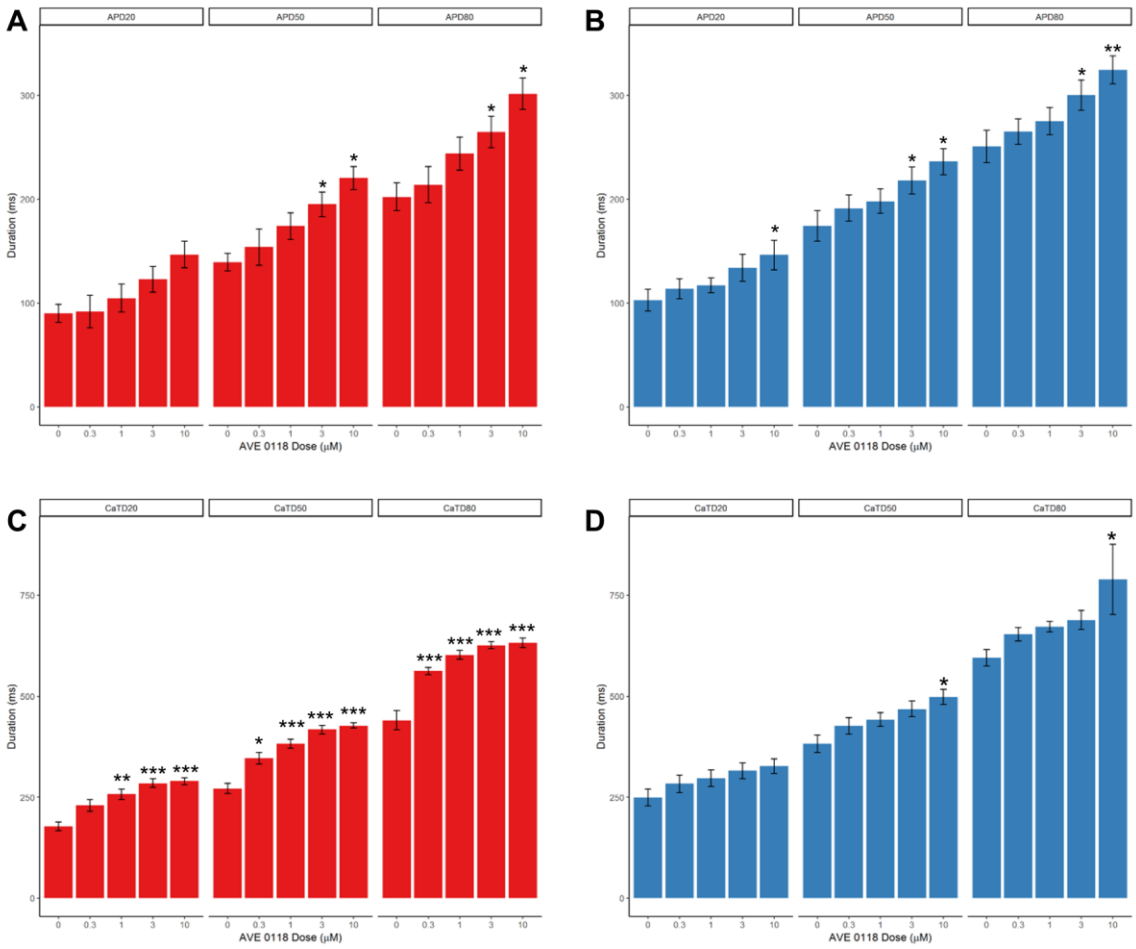

Figure B.4. The effects of AVE 0118 on hiPSC-aCMs (A: APD; C: CaTD) and hiPSC-vCMs (B: APD; D: CaTD).

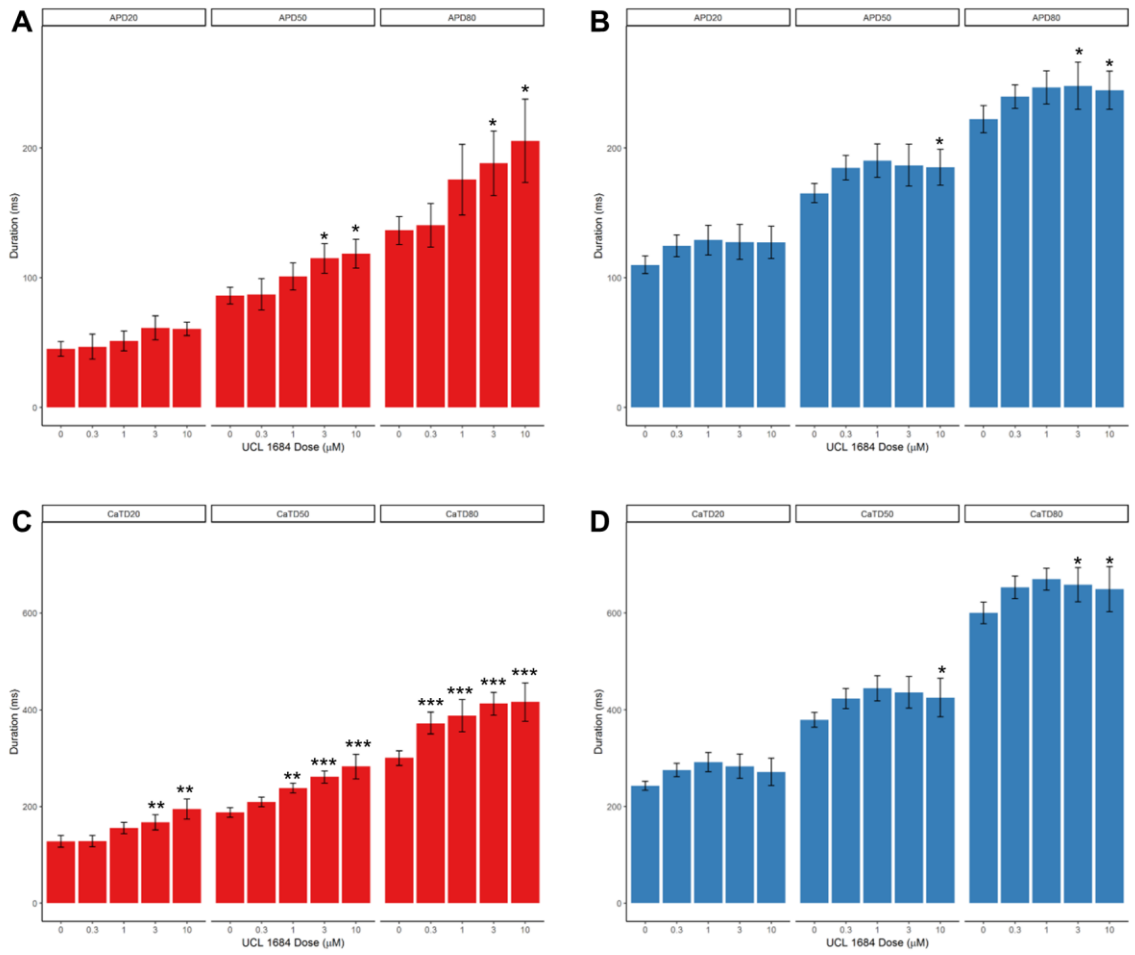

Figure B.5. The effects of UCL 1684 on hiPSC-aCMs (A: APD; C: CaTD) and hiPSC-vCMs (B: APD; D: CaTD).

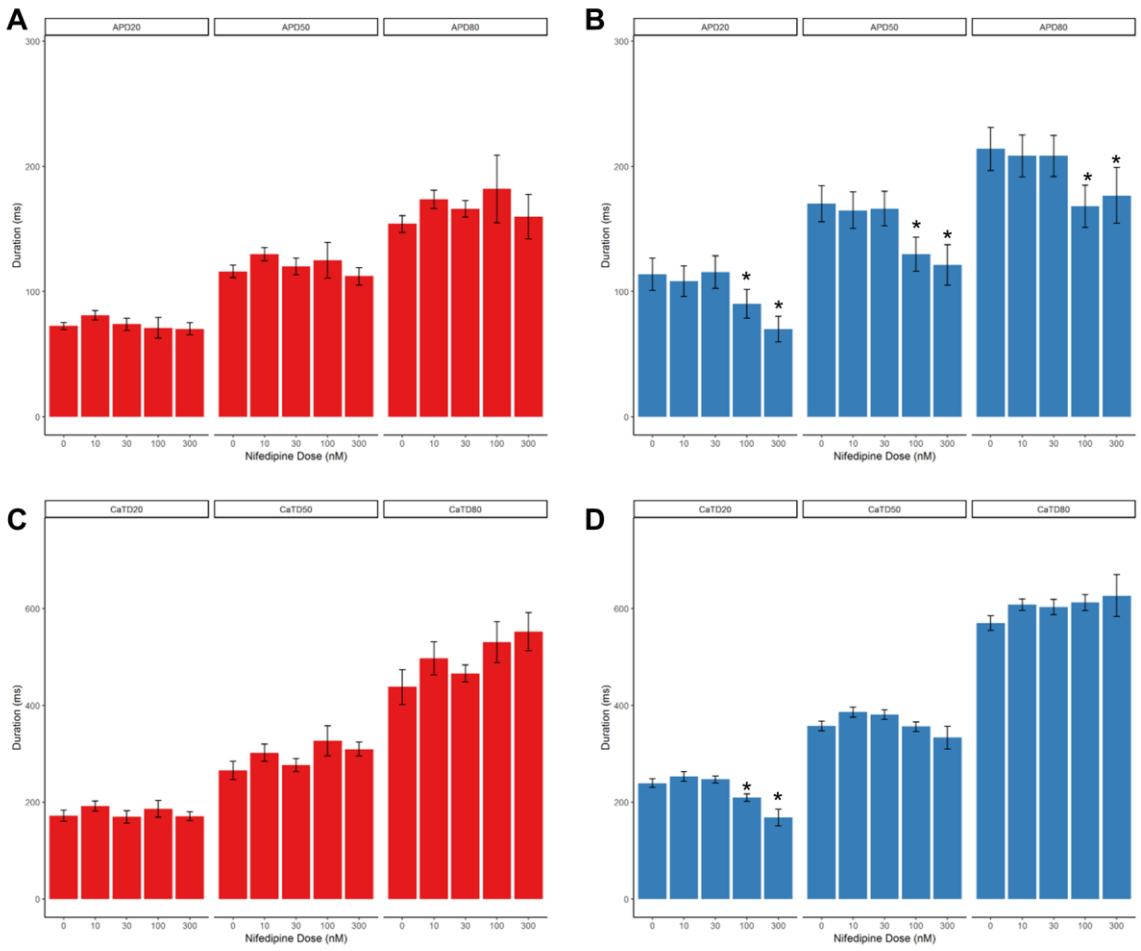

Figure B.6. The effects of nifedipine on hiPSC-aCMs (A: APD; C: CaTD) and hiPSC-vCMs (B: APD; D: CaTD).